Quantum Noise Cancellation beyond the Standard Quantum Limit in Hybrid Optomechanical Systems

A THESIS SUBMITTED IN FULFILMENT OF THE REQUIREMENTS

FOR THE DEGREE OF DOCTOR OF PHILOSOPHY

by

Alolika Roy

Thesis Supervisor

Prof. Amarendra Kumar Sarma

Department of Physics

INDIAN INSTITUTE OF TECHNOLOGY GUWAHATI

July 8, 2026

Dedicated to my Parents.

Declaration

I hereby declare that the work presented in the thesis entitled "Quantum Noise Cancellation beyond the Standard Quantum Limit in Hybrid Optomechanical Systems" has been carried out by me under the supervision of Prof. Amarendra Kumar Sarma at the Department of Physics, Indian Institute of Technology Guwahati, India. This thesis has not been submitted anywhere else for any degree. The work presented in the thesis is entirely my own unless referenced to the contrary.

Signature: Alolika Roy

Date: 08.07.2026

Alolika Roy

Roll No. 196121002

Department of Physics

IIT Guwahati

Guwahati, India.

r.alolika@iitg.ac.in

Certificate

It is certified that the work contained in the thesis entitled "Quantum Noise Cancellation beyond the Standard Quantum Limit in Hybrid Optomechanical Systems" by Ms. Alolika Roy (Roll No. 196121002), a Ph.D. student in the Department of Physics, Indian Institute of Technology Guwahati, is carried out under my supervision and has not been submitted elsewhere for the award of any other degree.

Amarendra Kumar Sarma 08/07/2026

Prof. Amarendra Kumar Sarma

Department of Physics

IIT Guwahati

Guwahati, India.

aksarma@iitg.ac.in

Acknowledgements

I would like to express my deepest gratitude to my thesis supervisor, Prof. Amarendra Kumar Sarma, for his invaluable guidance, constant encouragement, and thoughtful mentorship throughout my Ph.D. journey. His insight, patience, and high standards shaped not only this work but also my approach to research and scientific writing. I consider myself fortunate to have pursued my doctoral studies under his supervision.

I sincerely thank the members of my Doctoral Committee for their time, guidance, and constructive suggestions at various stages of my research. I am grateful to Dr. Pankaj Mishra (DC Chairperson) for his careful evaluation and supportive direction. I also thank Dr. Kanhaiya Pandey (Former DC Chairperson) for his guidance during the earlier phase of my doctoral work. My sincere appreciation goes to Prof. Bhupen Deka and Dr. Arif Warsi Laskar for their valuable comments and encouragement, which helped improve the clarity and depth of this thesis.

I acknowledge the Department of Physics, Indian Institute of Technology Guwahati, for providing a stimulating academic environment and necessary institutional support. I am thankful to the Quantum Optics and Quantum Technology research group for offering a vibrant platform to learn, discuss, and grow as a researcher. I also gratefully acknowledge the financial support provided through the UGC fellowship, which enabled me to pursue my doctoral studies.

I would like to acknowledge the facilities and resources that supported my work, including the theoretical laboratory infrastructure and the availability of a dedicated desktop for computations and writing. I also thank the technical staff and supporting personnel who helped maintain a smooth research environment.

I am grateful to my lab colleagues and group members who made my research journey enriching. At first I would like to specially thank those whom I met during my Ph.D. and who contributed to a collaborative and supportive atmosphere: Dr. Dipti Kanika Mahato, Dr. Sampreet Kalita, Dr. Roson Nongthombam, Pooja Kumari Gupta, Urmimala Dewan, Gaurav Bonde, Aman Verma, and Puja Kumari. Their discussions, help, and companionship made many challenging phases manageable. I also express my sincere appreciation to the former members of our group Dr. Ambaresh Sahoo, Dr. Shubhadeep Chakrabarty, Dr. A. H. M. Abdelaziz, Dr. Jyoti Prasad Deka , Dr. Koijam Monica Devi , Dr. Bijita Sarma, Dr. Koushik Paul, Dr. Samit Kumar Gupta, Dr. Parvendra Kumar and Dr. Manirupa Saha whose earlier contributions and works have been a continuing source of reference and inspiration for me, even though I did not have the opportunity to meet all of them personally.

I would like to express my heartfelt gratitude to my parents for their unconditional love, sacrifices, and unwavering support throughout my academic journey. Their belief in me has been my strongest source of motivation, especially during difficult times. I also offer a special note of thanks to my spouse, Dr. Ankur Singha for his constant encouragement, insightful suggestions, and steady emotional support throughout my Ph.D. journey. His presence and faith in my work made this long journey lighter and more meaningful. Without his immense support, my PhD journey would have been difficult. I am also thankful to my sister Aditi di, brother-in-law Rajib da and nephew Ved, my uncle and aunt. I am also grateful to my in-law's family and friends, Amori di, Apsara di, Gupta da, Mukesh, Sutapa, Kumarendra, Hemanta, Kaushik, Ansuma, jutika, Barnali baidew and Pranabjyoti bhindew for the encouragement and love throughout the journey. I would also like to convey my thanks to Dr. Vipul Arora Sir and Shreya Madam as mentors in research, in the journey of life , as well as in the spiritual path.

My warm thanks also go to my friends at the hostel who added warmth and joy to my daily life and helped me through stressful days with their companionship Amalika, Gargi, Esha, Pooja, Saraswati, Sonali, Priyanka, Lipika. Their friendship made my hectic routine feel less overwhelming and reminded me, time and again, of the importance of kindness and support.

My sincere gratitude goes to my teachers who taught me in my school, college, university and here in IIT for teaching and sharing their immense knowledge, from whom I learned and still learn.

Finally, I acknowledge B.D. College, Patna, where I joined last year, for providing a professional environment and support as I balanced academic responsibilities with the final phase of my doctoral work.

To everyone who contributed directly or indirectly to this thesis, I offer my sincere thanks. Any remaining errors are solely my responsibility.

Abstract

Cavity optomechanics is a leading platform for precision sensing in which mechanical motion is read out via its interaction with an electromagnetic cavity field, enabling the detection of extremely small forces and displacements. In continuous measurements, quantum fluctuations of the probe enforce a trade-off between measurement imprecision and radiation-pressure backaction, giving rise to the Standard Quantum Limit (SQL) that constrains achievable force and displacement sensitivities. This thesis investigates coherent quantum noise cancelation (CQNC) as a route to surpass SQL by engineering destructive interference of backaction noise.

We develop the theoretical framework of linearized cavity optomechanics, derive the relevant noise spectra, and formulate the matching conditions required for broadband cancelation. Building on this analysis, we explore and compare multiple hybrid CQNC platforms in which the mechanical resonator is coupled to an auxiliary degree of freedom (e.g., an additional cavity mode, an effective negative-mass oscillator, or an electromechanical/microwave subsystem). We further assess how realistic imperfections including optical loss, finite auxiliary bandwidth, detuning, and parameter mismatch degrade cancelation and set practical limits on achievable sensitivity.

Overall, this work clarifies design trade-offs and identifies experimentally relevant regimes for backaction reduction and beyond-SQL force sensing, with potential relevance to precision metrology applications such as force microscopy and next-generation optomechanical sensors.

List of Publications

Journal Publications

1. A. Roy and A. K. Sarma, “Overcoming the standard quantum limit with an electro–optomechanical hybrid system for enhanced force sensing,” Phys. Rev. A **111**, 013509 (2025).

2. A. Roy and A. K. Sarma, “Force Sensing Beyond the Standard Quantum Limit in a Hybrid Optomechanical Platform ,” (accepted in Journal of Optical Society of America B (JOSA-B)) arXiv:2512.20081, (2025)

3. A. Roy and A. K. Sarma, “Quantum Noise Suppression Beyond the Standard Quantum Limit in a Hybrid Magnonic Optomechanical System” (under review in Phys. Rev. A) arXiv:2604.16136

Conference / Symposium / Workshop Attended

1. OPTICS 2026: Global Summit on Lasers, Optics and Photonics, International Conference, (Webinar), 23rd April, 2026: Oral Presentation.

2. Spark 2025: Symposium on Physics, National Conference, (North Lakhimpur University), 31 October-1 November, 2025: Oral Presentation.

3. Frontiers in Optics and teraHertz Photonics, , Symposium, (IEEE, IIT Guwahati), 13 May, 2024: participation.

4. Introduction to Machine Learning with Python, Workshop, (EEE, IIT Guwahati), 25-26 March, 2023: Participation.

Contents

List of Figures

List of Tables

Chapter 1

Introduction

Precision measurement has made significant progress in physics, from tests of fundamental interactions to the development of modern quantum technologies. Many of the most profound discoveries in science have emerged not merely from theoretical insight but also from the ability to measure physical quantities with great accuracy. A recent example would be gravitational-wave detection, where laser interferometers of many kilometers have achieved displacement sensitivities far below nuclear length scales and enabled direct observations of compact-binary mergers [2, 21]. Precision measurement opens up a broad range of applications in areas such as condensed matter physics, nanoscale metrology, emerging quantum technologies, etc., where the detection of extremely small forces, displacements, fields, or mass changes can reveal new quantum phenomena or enable novel quantum devices [29, 20].

In sensing whether it is a force, acceleration, pressure, magnetic field, or mass change, the quantity of interest is ultimately encoded in the dynamics of a mechanical degree of freedom. Mechanical resonators, therefore, serve as natural transducers between an external physical signal and a measurable observable. At micro and nanoscales, mechanical oscillators can be engineered with extremely high quality factors, allowing them to store energy for long periods of time and respond sensitively to weak perturbations. Their resonant nature provides an inherent signal enhancement near the mechanical resonance, where the mechanical susceptibility is large, while micro- and nano-fabrication enables wide tunability of mass, frequency, and geometry [4, 36].

To read such small mechanical motions, one requires a probe that is both sensitive and controllable. Optical and microwave fields are suitable for this role because they can couple to the mechanical motion with minimal dissipation while providing high bandwidth, low noise detection. For example, in optical interferometry one converts tiny displacements into measurable phase shifts, and microwave circuits can map this tiny motion to changes in cavity amplitude or resonance frequency with a near-quantum limited sensitivity [20, 62].

An important realization of such an optical readout is provided by cavity optomechanics. An optomechanical cavity system consisting of a mechanical resonator coupled to an optical cavity so that the resonance frequency of the cavity depends on the position of the mechanical oscillator. Therefore, the light that circulates in the cavity reads the mechanical motion and also imposes forces on it through radiation pressure or dynamical backaction [4, 36, 10]. So, optomechanics provides a readout mechanism and a control handle that make optomechanics a versatile framework for converting tiny mechanical motion into measurable electromagnetic signals with a high degree of control. In addition, by adjusting the detuning of the drive, the resonator can be cooled to its quantum ground state, change its effective stiffness through the optical spring effect, or drive it to amplification and self-oscillation [43, 69]. Ground state cooling has already been demonstrated to establish cavity optomechanics as a leading platform for quantum limited measurement [62, 17].

Despite these remarkable advances, quantum sensing encounters fundamental and practical limitations imposed by noise. The origin of noise can be either classical or quantum in nature. In practice, in an optomechanical system, the measurement is affected by thermal fluctuations, dissipation, environmental vibrations, and technical noise from lasers, electronics, detection systems, etc. Thermal noise which arises from coupling to a finite temperature environment can dominate mechanical motion unless the resonator is cooled or engineered for very low dissipation [4, 10]. Additional noises arise from optical absorption heating, laser frequency noise, and cavity detuning instability, and these can degrade the ideal quantum-limited performance if not carefully controlled [4, 38].

Beyond technical noise sources, quantum mechanics itself sets fundamental limits on measurement sensitivity. In a continuous measurement, the probe field carries unavoidable quantum fluctuations, which limit how accurately the signal can be inferred. At the same time, the measurement process disturbs the system being observed. In optomechanical displacement detection, these two fundamental noise contributions are: (i) measurement imprecision, arising from photon shot noise in the detected light, and (ii) measurement backaction, arising from radiation-pressure force fluctuations associated with photon number noise [15, 20, 12]. These noise sources are not independent; rather, they are linked by quantum uncertainty relations and by general noise constraints that govern linear quantum detectors [20, 29].

A central illustration of this trade-off is the Standard Quantum Limit (SQL) for continuous position measurements. The SQL expresses the fact that increasing the probe power reduces the imprecision noise, since the signal is measured more accurately, but simultaneously enhances radiation-pressure fluctuations, which drive the mechanical element more strongly. For a coherent probe, and in the absence of intentionally engineered quantum correlations, there is therefore an optimal measurement strength at which the total added noise is minimized. This minimum defines the SQL and serves as a natural benchmark for precision measurements [15, 12, 20]. For this reason, the SQL plays a central role in optomechanics and gravitational-wave detection, where it provides a standard reference point for assessing measurement performance [21, 35, 29].

Although the SQL represents an important benchmark, it is not an absolute quantum boundary. A variety of quantum-engineering strategies can circumvent it by modifying the balance between imprecision and backaction, or by introducing useful correlations between them. One major example is the injection of squeezed light, which reduces shot noise in the measured quadrature and has become an established technique in large-scale interferometers, improving sensitivity without requiring excessively high circulating optical power [1, 30, 15, 35]. More generally, frequency-dependent squeezing and variational readout exploit correlations between imprecision and backaction in a frequency-selective way, allowing the quantum-noise spectrum to be reshaped and the SQL to be surpassed over chosen bandwidths [35, 21, 20]. In cavity optomechanics, related ideas include backaction-evading measurements and two-tone driving schemes, which enable the readout of a single mechanical quadrature while introducing less disturbance to the conjugate one [4, 20].

Although these approaches can significantly improve sensitivity, they do not eliminate the fundamental competition between measurement imprecision and radiation-pressure backaction. In most cases, they work by redistributing quantum noise, exploiting correlations, or reducing noise in a particular quadrature or frequency window, rather than removing the origin of backaction itself. This limitation has motivated the development of strategies that aim to suppress the backaction contribution directly. One of the most important proposals in this direction is Coherent Quantum Noise Cancellation (CQNC) [64, 70, 44, 3, 58, 44, 56].

The basic idea of CQNC is to introduce an additional dynamical degree of freedom whose response to the measurement backaction is designed to oppose that of the mechanical oscillator. More precisely, the auxiliary system is engineered so that the motion it produces in response to the same backaction force has the same magnitude but opposite sign in to that of the ordinary radiation-pressure-driven mechanical motion. When this matching is achieved, the two backaction pathways interfere destructively in the detected signal, so that the backaction noise is canceled at the level of the measurement output rather than merely reduced by modified readout conditions [64, 20].

Several physical realizations of this idea have been proposed. The auxiliary response may be provided, for example, by an additional optical mode, a microwave circuit, or an effective negative-mass oscillator. The essential requirement is that the susceptibility of this auxiliary system should reproduce the mechanical susceptibility with the opposite sign over the frequency range of interest [64, 20]. In that case, the radiation-pressure backaction acting through the two channels can ideally cancel.

Under perfect matching conditions, CQNC can strongly suppress radiation-pressure noise over a broad bandwidth. This is especially attractive because it changes the usual balance between imprecision and backaction: if the backaction term is canceled, then the probe strength can in principle be increased to reduce shot-noise-limited imprecision without paying the standard penalty of enhanced radiation-pressure fluctuations. In this way, CQNC provides a route to force or displacement sensing beyond the Standard Quantum Limit, while remaining fully consistent with the general principles of quantum measurement theory [64, 20].

Goal of this thesis. The central aim of this thesis is to investigate optomechanical sensing beyond the Standard Quantum Limit through the framework of coherent quantum noise cancellation, with particular emphasis on the role of hybrid auxiliary platforms. The thesis examines how different hybrid implementations realize CQNC and compares the underlying physical mechanisms and susceptibility-matching conditions required for cancellation. It further studies how realistic nonidealities, such as unequal dissipation rates, linewidths, detuning, and coupling mismatch, constrain performance. By developing this analysis across three distinct hybrid architectures, the thesis progresses from a first concrete realization of CQNC to its realization in platforms offering different forms of controllability and tunability, and finally to its robustness under more experimentally relevant conditions. Taken together, these studies help identify the broader design principles of hybrid backaction cancellation and clarify their relevance for beyond-SQL sensing[64, 21, 29, 4, 38].

1.1 Basic Concepts of Cavity Optomechanics

The most basic and widely studied setting in optomechanics consists of an optical cavity coupled to a mechanical resonator. This interaction forms the foundation of optomechanical sensing where mechanical motion changes the optical resonance frequency, while the intracavity light field exerts radiation-pressure forces back on the mechanical element. This mutual interaction is the physical origin of both precision displacement readout and the quantum noise processes discussed throughout this thesis.

For concreteness, consider a Fabry–Pérot cavity of length L with one movable mirror, or more generally with an effective mechanical coordinate x that shifts the cavity resonance frequency $\omega_c(x)$. For small displacements, the resonance frequency can be expanded to first order as

$$\omega_c(x) \simeq \omega_c + Gx, \qquad G \equiv \frac{\partial \omega_c}{\partial x}, \tag{1.1}$$

where G characterizes the cavity-frequency shift per unit displacement.

The mechanical element is modeled as a harmonic oscillator with effective mass m, resonance frequency ω_m, and damping rate γ_m. Its position operator is written in terms of bosonic

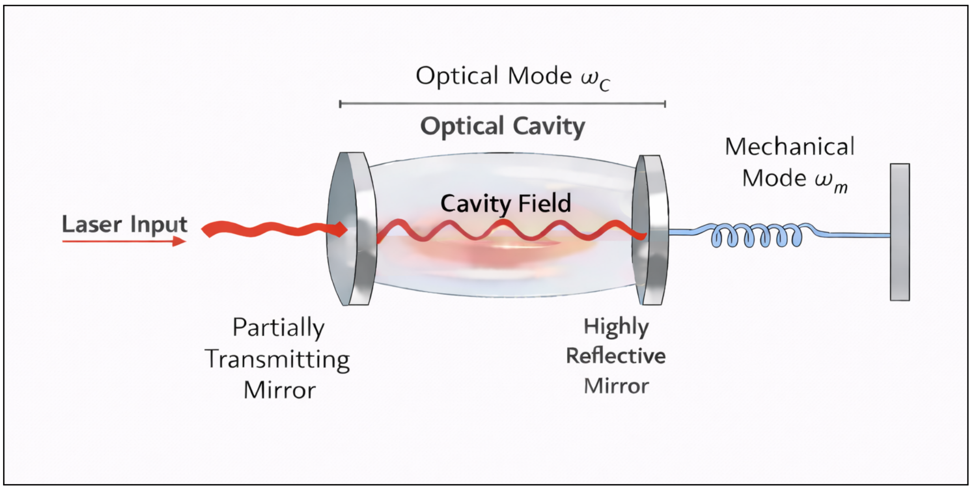

Figure 1.1: Standard cavity optomechanical setup: a Fabry–Pérot cavity with a movable mirror acting as the mechanical element.

annihilation and creation operators b and $b^\dagger$ as

$$x = x_{\text{zpf}}(b + b^\dagger), \qquad x_{\text{zpf}} = \sqrt{\frac{\hbar}{2m\omega_m}}, \tag{1.2}$$

where x_{zpf} denotes the zero-point fluctuation amplitude.

Because the cavity frequency depends on x, fluctuations of the mechanical oscillator modulate the optical field inside the cavity. Conversely, fluctuations in the intracavity photon number produce a radiation-pressure force that acts on the mechanical resonator. This bidirectional coupling underlies both the control of mechanical motion, such as cooling and amplification, and the transduction of displacement into optical signals for sensing applications [4].

1.1.1 Hamiltonian of cavity optomechanics

A quantum description of cavity optomechanics is obtained by quantizing both the optical cavity mode and the mechanical resonator. Let a ($a^\dagger$) denote the annihilation (creation) operator of the cavity mode with resonance frequency ω_c, and let b ($b^\dagger$) denote the corresponding operators for the mechanical mode of frequency ω_m. The standard optomechanical Hamiltonian is then

$$H = \hbar\omega_c a^\dagger a + \hbar\omega_m b^\dagger b - \hbar g_0 a^\dagger a(b + b^\dagger) + H_{\text{drive}}, \tag{1.3}$$

where H_{drive} describes the coherent driving of the cavity by an external laser field.

The first two terms represent the free energies of the optical and mechanical modes. The third term describes the radiation-pressure interaction: the intracavity photon number $a^\dagger a$ couples to the mechanical displacement quadrature $(b + b^\dagger)$. Physically, this interaction arises because the cavity resonance frequency depends on the mirror position. As a result, mechanical motion changes the optical resonance, while fluctuations in the photon number exert a force on the mechanics.

The coupling strength

$$g_0 = G x_{\text{zpf}} \tag{1.4}$$

is called the single-photon optomechanical coupling. It measures the shift of the cavity resonance frequency caused by the mechanical zero-point motion and therefore quantifies the intrinsic strength of the interaction at the level of a single intracavity photon. In many experimental systems, g_0 is relatively small. Nevertheless, by strongly driving the cavity and thereby increasing the intracavity photon number, the effective interaction can be greatly enhanced, making optomechanical effects observable and useful for precision sensing [4, 10].

1.1.2 Linearized optomechanics

In most experiments, the cavity is driven by a strong coherent laser at frequency ω_L. It is therefore convenient to move to a frame rotating at the drive frequency and introduce the detuning

$$\Delta \equiv \omega_L - \omega_c, \tag{1.5}$$

where, with this convention, $\Delta > 0$ corresponds to blue detuning.

Under strong driving, the cavity field acquires a large steady-state coherent amplitude α, and the mechanical resonator may also acquire a static coherent displacement β. One therefore decomposes the operators into steady-state amplitudes and fluctuations,

$$a = \alpha + \delta a, \qquad b = \beta + \delta b, \tag{1.6}$$

where δa and δb represent the quantum fluctuations around the classical steady state. In the following, for notational simplicity, we drop the δ and use a and b directly for the fluctuation operators.

Substituting this decomposition into the full Hamiltonian and retaining only terms up to quadratic order in the fluctuations yields the linearized Hamiltonian

$$H_{\text{lin}} \simeq -\hbar\Delta\, a^\dagger a + \hbar\omega_m b^\dagger b - \hbar\left(G_{\text{lin}}a + G_{\text{lin}}^* a^\dagger\right)(b + b^\dagger), \tag{1.7}$$

with the drive-enhanced optomechanical coupling

$$G_{\text{lin}} \equiv g_0\alpha. \tag{1.8}$$

Constant terms, as well as linear terms in the fluctuations, vanish when the expansion is carried out about the steady-state solution.

This linearized description forms the standard theoretical framework of quantum optomechanics. It is sufficient for describing most phenomena relevant to continuous measurements and sensing, including dynamical backaction, optomechanical cooling and amplification, and the emergence of the Standard Quantum Limit [4, 20].

1.1.3 Quantum Langevin equations and susceptibilities

To describe dissipation and fluctuations, the linearized dynamics must be supplemented by damping and noise terms. This leads to the quantum Langevin equations for the cavity and mechanical fluctuation operators. For the cavity mode, with energy decay rate κ, and the mechanical mode, with damping rate γ_m, the equations of motion are

$$\dot{a} = \left(i\Delta - \frac{\kappa}{2}\right)a + iG_{\text{lin}}(b + b^\dagger) + \sqrt{\kappa}\, a_{\text{in}}, \tag{1.9}$$

$$\dot{b} = \left(-i\omega_m - \frac{\gamma_m}{2}\right)b + i\left(G_{\text{lin}}^* a + G_{\text{lin}} a^\dagger\right) + \sqrt{\gamma_m}\, b_{\text{in}}. \tag{1.10}$$

Here a_{in} denotes the optical input noise, which may correspond to vacuum noise or more general quantum states of light such as squeezed input, while b_{in} describes the thermal noise associated with the mechanical environment.

These equations are often analyzed most conveniently in the frequency domain, where the response of each mode can be expressed in terms of a susceptibility. To illustrate the general idea, consider a linear equation of motion of the form

$$\dot{u} = \left(-i\Omega_0 - \frac{\Gamma}{2}\right)u + f(t). \tag{1.11}$$

In the frequency domain, the response takes the form

$$u(\omega) = \chi(\omega) f(\omega), \tag{1.12}$$

where

$$\chi(\omega) = \frac{1}{\Gamma/2 - i(\omega - \Omega_0)} \tag{1.13}$$

is the susceptibility, up to the chosen Fourier-transform convention.

For the optical cavity, the corresponding bare cavity susceptibility is

$$\chi_c(\omega) = \frac{1}{\kappa/2 - i(\omega + \Delta)}. \tag{1.14}$$

This quantity characterizes how the intracavity field responds to external driving and fluctuations at frequency ω.

For the mechanical resonator, it is often more intuitive to work directly with the displacement x instead of the annihilation operator b. The bare mechanical susceptibility is then

$$\chi_m(\omega) = \frac{1}{m\left(\omega_m^2 - \omega^2 - i\gamma_m\omega\right)}, \tag{1.15}$$

which relates an applied force to the resulting displacement response.

In force detection, this susceptibility provides the linear force-to-displacement relationship where an external force $F_{\text{ext}}(\omega)$ produces

$$x(\omega) = \chi_m(\omega) F_{\text{ext}}(\omega) \tag{1.16}$$

provided optomechanical dynamical backaction is negligible. Once the cavity field is coupled to the mechanics, however, the radiation-pressure interaction modifies this bare response. The mechanical oscillator then acquires an effective susceptibility that includes optical spring and damping effects, and it is precisely this modified response that gives rise to the quantum-noise trade-offs underlying the Standard Quantum Limit.

1.1.4 Input–output relation and measured quadratures

So far, we have described the internal dynamics of the cavity and mechanical modes in terms of their susceptibilities and fluctuation operators. To connect this description with an actual measurement, one must relate the intracavity field to the optical field leaving the cavity, since

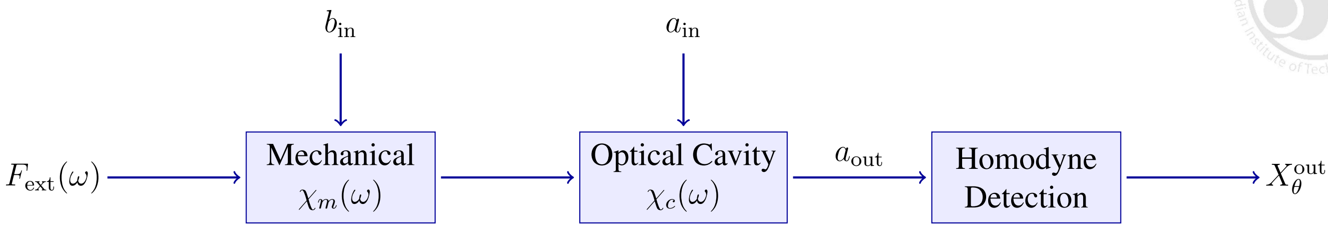

Figure 1.2: Block diagram of an optomechanical sensing chain. An external force drives the mechanical resonator, whose response is governed by the mechanical susceptibility $\chi_m(\omega)$. The resulting motion modulates the cavity field, characterized by the optical susceptibility $\chi_c(\omega)$, and the outgoing light is measured by homodyne detection of the quadrature X_θ^{out}. Mechanical bath noise b_{in} and optical input noise a_{in} enter as the principal noise sources.

it is this outgoing field that is experimentally detected.

In the standard input–output formalism, the output field operator is related to the input field and the intracavity fluctuation operator by

$$a_{\text{out}} = a_{\text{in}} - \sqrt{\kappa}\, a, \tag{1.17}$$

where a_{in} and a_{out} denote the incoming and outgoing optical fields, respectively. This relation shows that fluctuations of the intracavity field are directly imprinted onto the output light. Since the intracavity field is itself coupled to the mechanical motion, the output field carries information about the mechanical displacement and any external force acting on the resonator.

Experimentally, this information is commonly extracted by homodyne detection, in which the output field is interfered with a strong local oscillator and a chosen field quadrature is measured. The detected output quadrature is

$$X_\theta^{\text{out}}(\omega) = \frac{1}{\sqrt{2}}\left(e^{-i\theta} a_{\text{out}}(\omega) + e^{i\theta} a_{\text{out}}^\dagger(\omega)\right), \tag{1.18}$$

where the local-oscillator phase θ selects which quadrature is measured. In an ideal homodyne setup, the photocurrent is proportional to $X_\theta^{\text{out}}(\omega)$, up to detector gain and efficiency. The fluctuations of this photocurrent, characterized by its noise spectral density, determine the ultimate sensitivity of the measurement.

The discussion above establishes how a mechanical signal is transduced into an optical observable. However, the optomechanical interaction does more than simply transfer information from mechanics to light. Because the cavity field also exerts radiation-pressure forces on the resonator, the measurement process modifies the mechanical dynamics themselves. This effect is central to both optomechanical control and the quantum limits of sensing, and it is therefore discussed next.

1.2 Optomechanical Dynamics Relevant to Sensing

In an optomechanical device, the optical field serves not only as a probe of mechanical motion but also as an active dynamical agent. Through radiation pressure, fluctuations of the intracavity light field feed back onto the mechanical resonator and alter its response. This phenomenon is known as *dynamical backaction* and plays a central role in optomechanical sensing.

The physical origin of dynamical backaction is the finite response time of the cavity. When the cavity is driven off resonance, mechanical motion shifts the cavity frequency and thereby modulates the intracavity field. Because the cavity reacts with a delay determined by its linewidth κ, the resulting radiation-pressure force is generally not exactly in phase with the motion. This phase lag causes the optical force to act either as an additional damping mechanism or as an amplifying drive, depending on the detuning.

In the resolved-sideband regime, $\omega_m \gg \kappa$, these effects become particularly transparent. Driving the cavity close to the red sideband, $\Delta \simeq -\omega_m$, leads to optical cooling, meaning that the effective mechanical damping is increased. By contrast, driving near the blue sideband, $\Delta \simeq +\omega_m$, amplifies the motion and can eventually drive the system into parametric instability [4].

A compact description of this cavity-induced modification is obtained through the optical self-energy $\Sigma(\omega)$, which renormalizes the bare mechanical susceptibility [4, 20, 43] according to

$$\chi_{m,\mathrm{eff}}^{-1}(\omega) = \chi_m^{-1}(\omega) + \Sigma(\omega). \tag{1.19}$$

Here $\Sigma(\omega)$ depends on the drive-enhanced optomechanical coupling G_{lin} and on the cavity susceptibility $\chi_c(\omega)$. Its real part gives rise to the optical spring effect, namely a shift in the mechanical resonance frequency, while its imaginary part modifies the effective mechanical damping.

From the viewpoint of sensing, dynamical backaction has both beneficial and limiting consequences. On the one hand, optical damping and the optical spring effect can be used to stabilize the resonator, engineer its response, and shape the measurement bandwidth. On the other hand, the same radiation-pressure interaction also introduces fluctuating forces that act as measurement backaction noise [14]. Thus, the sensitivity of an optomechanical detector is determined not only by how efficiently mechanical motion is converted into an optical signal, but also by how strongly the act of measurement perturbs the mechanical system.

For this reason, a description based only on the equations of motion is not sufficient to assess sensing performance. What ultimately matters is the competition between signal transduction, thermal fluctuations, measurement imprecision, and radiation-pressure backaction. This naturally motivates a reformulation of the problem in terms of noise spectra and estimation theory, which leads directly to the concept of the Standard Quantum Limit.

1.2.1 Displacement and force sensing

In a typical optomechanical sensor, the physical quantity to be measured acts on the mechanical resonator as an external force, acceleration, or some equivalent perturbation. The resonator converts this disturbance into a displacement, which is then read out optically and serves as the observable carrier of the signal. In the frequency domain, the mechanical motion may be written as

$$x(\omega) = \chi_{m,\text{eff}}(\omega)\Big[F_{\text{sig}}(\omega) + F_{\text{th}}(\omega) + F_{\text{ba}}(\omega)\Big], \tag{1.20}$$

where $\chi_{m,\text{eff}}(\omega)$ is the effective mechanical susceptibility including dynamical backaction, $F_{\text{sig}}(\omega)$ is the external signal force to be estimated, $F_{\text{th}}(\omega)$ is the thermal Langevin force from the environment, and $F_{\text{ba}}(\omega)$ denotes the radiation-pressure backaction force arising from optical fluctuations.

The role of the optical cavity is to convert this mechanical displacement into a measurable optical signal. As discussed in the input–output description, the output quadrature $X_\theta^{\text{out}}(\omega)$ carries information about the displacement $x(\omega)$ through the optomechanical interaction. The sensing task is therefore to infer either the displacement itself or, equivalently, the external force that generated it, from the detected optical field.

A natural linear estimator for the displacement is

$$\hat{x}_{\text{est}}(\omega) = \frac{1}{\mathcal{G}(\omega)} X_\theta^{\text{out}}(\omega), \tag{1.21}$$

where $\mathcal{G}(\omega)$ is the effective transduction gain, determined by the cavity detuning [12, 15, 20], linewidth, optomechanical coupling, and the chosen homodyne angle. Physically, $\mathcal{G}(\omega)$ quantifies how efficiently mechanical motion is mapped onto the measured optical quadrature.

In an ideal noise-free measurement, the estimator $\hat{x}_{\text{est}}(\omega)$ would reproduce the true displacement exactly. In practice, however, it also contains contributions from optical shot noise, thermal fluctuations, and radiation-pressure backaction. The sensitivity of the sensor is therefore determined not only by the signal response encoded in $\mathcal{G}(\omega)$, but by the total noise referred back to the displacement or, equivalently, to the applied force. This noise-referred viewpoint provides the natural framework for quantifying measurement sensitivity and for identifying the conditions under which the Standard Quantum Limit emerges. The overall sensing chain is illustrated schematically in Fig. 1.3: an external signal first drives the mechanical resonator, whose displacement is then transduced to the optical output phase quadrature, while fluctuations of the optical amplitude generate radiation-pressure backaction on the mechanical element and feed measurement noise back into the sensing process.

1.2.2 Noise in optomechanical sensing: classical and quantum origins

Because both the mechanical resonator and the optical readout are subject to fluctuations, the inferred displacement $\hat{x}_{\text{est}}(\omega)$ inevitably contains noise in addition to the true signal. A convenient way to characterize this limitation is through the added displacement-noise spectral density $S_{xx}^{\text{add}}(\omega)$, or equivalently through the corresponding force-referred noise [70, 20, 4],

$$S_{FF}^{\text{add}}(\omega) = \frac{S_{xx}^{\text{add}}(\omega)}{|\chi_{m,\text{eff}}(\omega)|^2}. \tag{1.22}$$

It is useful to distinguish between classical and quantum noise sources. Classical noise [4, 20, 14, 43], such as thermal fluctuations of the mechanical environment or technical laser noise, arises from imperfect isolation and experimental nonidealities. In principle, such noise can be reduced through improved engineering, cryogenic cooling, or better stabilization. Quantum noise, by contrast, is intrinsic to the measurement process itself and originates from the

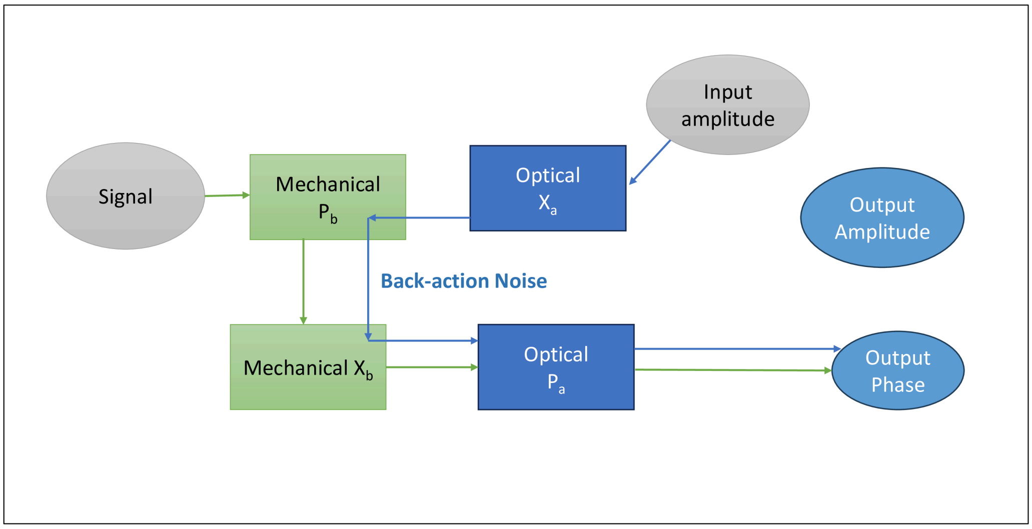

Figure 1.3: Schematic signal and noise pathways in a standard optomechanical measurement. An external signal drives the mechanical resonator, whose displacement is transduced to the optical phase output and used for estimation. At the same time, fluctuations in the optical amplitude quadrature generate radiation-pressure backaction on the mechanical element, thereby introducing measurement backaction into the sensing chain.

quantization of the optical and mechanical degrees of freedom. In optomechanical sensing, the two most important quantum noise contributions are measurement imprecision and radiation-pressure backaction.

Measurement imprecision: shot noise. Even in the absence of all technical noise, the optical probe field exhibits unavoidable vacuum fluctuations. These fluctuations appear in the detected output as photon shot noise [4, 20, 3, 14, 38, 43, 70, 41, 41, 44, 58, 11, 9] and limit how precisely the mechanical displacement can be inferred from the measured optical signal. In homodyne detection, the measured field quadrature is represented by non-commuting operators, so a perfectly stable mean field is still accompanied by irreducible fluctuations required by quantum mechanics. Equivalently, vacuum fluctuations entering the unused port of the detection setup contribute noise that cannot be removed in standard coherent probing [20, 15, 4].

When referred back to the mechanical displacement, these optical fluctuations give rise to the imprecision-noise contribution $S_{xx}^{\mathrm{imp}}(\omega)$. For a coherent input state, the vacuum contribution to the output quadrature spectrum is approximately flat over the frequency range of interest

$$S^{\mathrm{out}}_{X_\theta X_\theta}(\omega)\big|_{\mathrm{vac}} \simeq \frac{1}{2}, \tag{1.23}$$

up to convention-dependent factors such as single-sided versus double-sided spectral densities and the detector efficiency. Converting this optical noise into an equivalent displacement noise using the transduction gain $\mathcal{G}(\omega)$ yields

$$S^{\mathrm{imp}}_{xx}(\omega) = \frac{S^{\mathrm{out}}_{X_\theta X_\theta}(\omega)}{|\mathcal{G}(\omega)|^2}. \tag{1.24}$$

This expression makes clear that stronger transduction reduces the imprecision noise. In many relevant operating regimes, the gain scales approximately as $\mathcal{G}(\omega) \propto \sqrt{n_c}$, where n_c is the intracavity photon number, so that

$$S^{\mathrm{imp}}_{xx}(\omega) \propto \frac{1}{n_c}. \tag{1.25}$$

Thus, shot-noise-limited imprecision decreases as the probe power is increased.

Radiation-pressure backaction. The same optical field that carries information about the mechanical motion also exerts a fluctuating force on the resonator. Since each intracavity photon carries momentum, fluctuations in photon number lead to fluctuations in the radiation-pressure force. These force fluctuations constitute radiation pressure backaction [4, 20, 3, 14, 38, 43, 70, 41, 41, 44, 58, 11, 27, 46, 63, 51]. Like shot noise, this is not a technical imperfection but a direct consequence of the quantum nature of the electromagnetic field. The same vacuum fluctuations responsible for shot noise also produce photon-number fluctuations, which now act back on the mechanics through the amplitude quadrature of the cavity field.

Within the linearized description, the radiation-pressure force operator can be written schematically as

$$\hat{F}_{\mathrm{ba}}(\omega) = \hbar G_{\mathrm{lin}}\, \hat{X}_0(\omega), \tag{1.26}$$

where $G_{\mathrm{lin}} = g_0\sqrt{n_c}$ is the drive-enhanced optomechanical coupling and $\hat{X}_0$ denotes the intracavity amplitude quadrature associated with photon-number fluctuations [4, 20]. Even for a perfectly coherent drive, vacuum fluctuations entering the cavity generate fluctuations of $\hat{X}_0$ and therefore a stochastic force acting on the mechanical resonator.

The corresponding backaction force-noise spectral density is

$$S_{FF}^{\mathrm{ba}}(\omega) = \hbar^2 G_{\mathrm{lin}}^2 \, S_{X_0X_0}(\omega). \tag{1.27}$$

For a coherent vacuum-limited input, the intracavity amplitude fluctuations are determined by vacuum noise filtered by the cavity susceptibility,

$$S_{X_0X_0}(\omega) \sim \kappa \, |\chi_c(\omega)|^2, \qquad \chi_c(\omega) = \left[\frac{\kappa}{2} - i(\Delta + \omega)\right]^{-1}, \tag{1.28}$$

so that, up to convention-dependent factors of order unity,

$$S_{FF}^{\mathrm{ba}}(\omega) \propto \hbar^2 G_{\mathrm{lin}}^2 \, \kappa \, |\chi_c(\omega)|^2. \tag{1.29}$$

This fluctuating force drives the mechanical resonator through its effective susceptibility, producing an equivalent displacement noise

$$S_{xx}^{\mathrm{ba}}(\omega) = |\chi_{m,\mathrm{eff}}(\omega)|^2 S_{FF}^{\mathrm{ba}}(\omega). \tag{1.30}$$

Since $G_{\mathrm{lin}}^2 \propto n_c$, one obtains the characteristic scaling

$$S_{FF}^{\mathrm{ba}}(\omega) \propto n_c, \qquad S_{xx}^{\mathrm{ba}}(\omega) \propto n_c, \tag{1.31}$$

showing that radiation-pressure backaction increases with probe power.

We therefore arrive at a central feature of continuous optomechanical measurement that the two fundamental quantum-noise contributions scale in opposite ways with measurement strength. Increasing probe power suppresses the imprecision noise, but at the same time it enhances radiation-pressure backaction. The competition between these two effects gives rise to the Standard Quantum Limit [3, 14, 38, 43, 70].

1.2.3 Standard Quantum Limit (SQL)

The Standard Quantum Limit (SQL) arises from the fundamental competition between the two quantum-noise sources discussed above [3, 14, 38, 43, 70] i.e. measurement imprecision in the optical readout and radiation-pressure backaction acting on the mechanical resonator. These are not independent technical imperfections, but two complementary consequences of the same underlying quantum fluctuations of the optical field.

Increasing the optical probe power improves the precision of the readout because the rel-

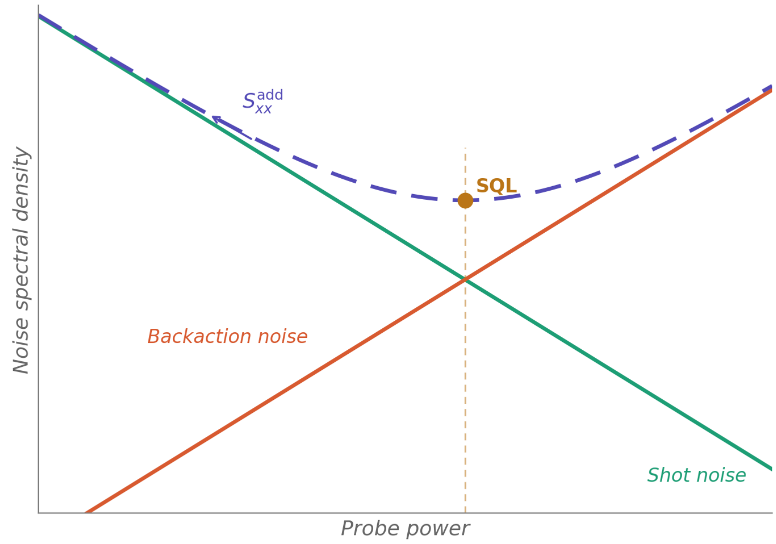

Figure 1.4: Schematic imprecision-backaction tradeoff as a function of probe power. The shot noise decreases with increasing power, whereas the backaction contribution increases. Their sum exhibits a minimum, which defines the SQL operating point in the absence of engineered correlations.

ative contribution of shot noise is reduced. At the same time, however, a stronger intracavity field produces larger photon-number fluctuations and therefore stronger radiation-pressure force fluctuations acting on the mechanics. As a result, any attempt to suppress one contribution by increasing the measurement strength necessarily enhances the other.

If no correlations are deliberately engineered between imprecision and backaction, there exists an optimal probe strength at which the total added noise is minimized. This minimum defines the SQL for continuous position measurement. The SQL should therefore be understood not as a limitation of experimental quality alone, but as a direct consequence of the quantum nature of measurement itself.

This viewpoint is particularly important in optomechanics. It shows why simply increasing laser power, improving the cavity finesse, or cooling the mechanical resonator cannot by themselves eliminate the SQL. To go beyond this limit, one must employ genuinely quantum strategies, such as creating useful imprecision–backaction correlations or directly suppressing the backaction contribution.

To make the origin of the SQL more explicit, it is useful to examine the scaling of the individual noise contributions with measurement strength.

1.2.4 Origin of the SQL: shot noise-backaction trade-off

In an ideal continuous measurement based on coherent light and without engineered correlations, the two dominant quantum-noise contributions scale oppositely with the optical probe power P:

$$S_{xx}^{\text{imp}}(\omega) \propto \frac{1}{P}, \qquad S_{FF}^{\text{ba}}(\omega) \propto P. \tag{1.32}$$

The first relation reflects the reduction of shot-noise imprecision at higher probe power, while the second expresses the increase of radiation-pressure force noise.

The total added displacement noise is therefore

$$S_{xx}^{\text{add}}(\omega) = S_{xx}^{\text{imp}}(\omega) + |\chi_{m,\text{eff}}(\omega)|^2 \, S_{FF}^{\text{ba}}(\omega), \tag{1.33}$$

where the second term is the backaction force noise referred to displacement through the effective mechanical susceptibility.

Because the imprecision contribution decreases with increasing P, while the backaction contribution increases, their sum possesses a minimum at a finite optimal probe power. This optimal operating point defines the SQL for continuous displacement measurement.

A widely used heuristic expression for the SQL in displacement sensing is

$$S_{xx}^{\text{SQL}}(\omega) \sim \hbar \, |\chi_{m,\text{eff}}(\omega)|, \tag{1.34}$$

up to numerical factors that depend on spectral-density conventions and on the precise detection scheme. For force sensing, the corresponding SQL is often written as

$$S_{FF}^{\text{SQL}}(\omega) \sim \frac{\hbar}{|\chi_{m,\text{eff}}(\omega)|}. \tag{1.35}$$

These expressions make clear that the SQL is shaped by the mechanical response itself. Near the mechanical resonance, the susceptibility becomes large, which enhances the response to an external force. However, the same large susceptibility also amplifies the displacement produced by radiation-pressure backaction. In this sense, the SQL reflects a fundamental balance between signal amplification and measurement-induced disturbance.

1.2.5 SQL as a practical benchmark in optomechanical sensors

In real optomechanical experiments, approaching the SQL requires much more than optimizing the nominal measurement strength. Technical noise sources such as laser frequency noise, amplitude noise, detector noise, and mechanical vibrations must be suppressed to a level below the fundamental quantum contributions. In addition, the resonator must either be cooled sufficiently or possess a sufficiently large $\omega_m Q$ product so that thermal noise does not dominate the measurement band.

The SQL should therefore be regarded not as a single universal number, but as a frequency-dependent benchmark determined by the mechanical susceptibility, cavity linewidth, detuning, optical power, and readout method. It represents the best sensitivity achievable with conventional coherent probing in the absence of deliberately engineered quantum correlations.

In this thesis, the SQL serves as the central reference point for evaluating performance. Our aim is not merely to optimize probe power or cooling, but to investigate strategies that directly suppress or coherently cancel radiation-pressure backaction while preserving high measurement precision. This viewpoint naturally motivates the study of Coherent Quantum Noise Cancellation, which forms the central theme of the following chapters.

1.3 Beyond the SQL: Quantum-Enhanced Sensing Strategies

Surpassing the Standard Quantum Limit requires going beyond the simplest measurement scenario, namely coherent probing in which measurement imprecision and radiation-pressure backaction remain uncorrelated. A range of quantum-enhanced sensing strategies has been developed to overcome this limitation, each modifying the measurement noise budget in a different way. Some methods reduce the noise of the measured optical quadrature, others evade backaction for selected observables, and others engineer correlations or interference pathways that suppress the backaction contribution itself. In this section, we briefly review the main conceptual routes beyond the SQL and thereby place Coherent Quantum Noise Cancellation in its broader context.

1.3.1 Squeezed light injection

One of the most direct ways to improve measurement sensitivity is to replace the coherent optical probe with a squeezed state of light [8, 19, 37, 40, 44, 45, 67]. In a squeezed state, the quantum uncertainty of one field quadrature is reduced below the vacuum level at the expense of enhanced fluctuations in the conjugate quadrature. If the squeezing is aligned with the measured quadrature, the readout noise can be suppressed below the usual shot-noise floor, thus reducing the imprecision contribution [15, 20, 44].

In its simplest form, squeezed-light injection improves sensitivity by lowering the optical readout noise without changing the basic measurement principle. More generally, frequency-dependent squeezing allows the squeezed quadrature to vary with analysis frequency, making it possible to improve performance over a broader bandwidth. Such techniques are now routinely used in large-scale interferometric detectors and are also highly relevant in cavity-optomechanical sensing architectures.

1.3.2 Backaction-evading measurements

A conceptually different strategy is provided by backaction-evading (BAE) measurements [27, 46, 63, 51]. For a harmonic oscillator, it is possible in an idealized setting to measure a single mechanical quadrature that behaves as a quantum non-demolition observable. In such a scheme, the measurement backaction is redirected into the conjugate quadrature, while the measured quadrature remains, in principle, undisturbed.

In practice, BAE protocols are often implemented using two-tone driving schemes that selectively couple the optical field to a single rotating mechanical quadrature. This can strongly suppress backaction on the measured observable and thereby surpass the usual SQL for that quadrature. However, the advantage is typically limited to a restricted bandwidth and requires careful phase control and stable matching of the drives [4]. For this reason, BAE measurements are highly powerful but often intrinsically narrowband.

1.3.3 Quantum noise cancellation

A third route is quantum noise cancellation. In contrast to squeezing, which primarily reduces measurement imprecision, and backaction-evading schemes, which avoid backaction for a selected observable, the goal here is to suppress the backaction contribution itself. This is achieved by engineering destructive interference in the backaction pathway, so that the measurement remains sensitive to the signal while the radiation-pressure noise is canceled.

Among these approaches, *Coherent Quantum Noise Cancellation* (CQNC) is particularly appealing [70, 44, 3, 58, 44, 56]. The central idea is to introduce an auxiliary dynamical pathway that produces an equal-and-opposite response to the measurement backaction, thereby canceling the radiation-pressure noise coherently at the output [64]. Because this cancellation can, in principle, be arranged over a broad frequency range, CQNC is especially attractive for force sensing and broadband displacement sensing in regimes where radiation-pressure noise is the dominant limitation. For this reason, CQNC forms the central focus of this thesis.

1.4 Coherent Quantum Noise Cancellation (CQNC): A Route Beyond the SQL

1.4.1 Motivation and core idea

In a standard optomechanical position measurement, radiation-pressure backaction arises because fluctuations in the intracavity photon number generate a fluctuating force on the mechanical resonator. At the level of the mechanical dynamics, this backaction force is indistinguishable from an externally applied signal force as both are filtered by the same mechanical susceptibility and both are subsequently encoded in the measured optical output. Consequently, backaction becomes a fundamental limitation precisely in the regime where the mechanical susceptibility is largest and the sensor is most responsive.

Coherent Quantum Noise Cancellation (CQNC) was proposed as a way to overcome this limitation by introducing an auxiliary dynamical pathway whose response to the same optical fluctuations is equal in magnitude but opposite in sign to the ordinary backaction pathway [64, 70, 44, 3, 58, 44, 56]. The objective is therefore not merely to reduce measurement noise, but to cancel the radiation-pressure contribution itself through destructive interference. A key insight of Tsang and Caves [64] is that such cancellation can be achieved through coherent interactions, or equivalently coherent feedforward, without relying on measurement-based feedback. Under suitable matching conditions, this cancellation can in principle persist over a broad frequency range, which distinguishes CQNC from more narrowband backaction-evading strategies.

1.4.2 Negative-mass oscillator as the canonical auxiliary system

The clearest theoretical realization of CQNC employs an auxiliary oscillator with an effective negative mass, commonly referred to as a negative-mass oscillator (NMO). The defining property of this auxiliary mode is that its susceptibility has the opposite sign to that of an ordinary positive-mass mechanical oscillator over the frequency range of interest. If the same radiation-pressure fluctuations couple both to the physical resonator and to this auxiliary mode, then the resulting responses can interfere destructively in the measurement record.

Radiation-pressure fluctuations drive the mechanical resonator in the usual way. The same fluctuations also drive the auxiliary negative-mass mode, but because this mode responds with the opposite sign, its contribution can subtract the backaction-induced motion from the measured output. If the readout is arranged appropriately, the true external signal remains accessible while the radiation-pressure-noise contribution is suppressed.

This perspective makes clear that CQNC is neither a post-processing technique nor a reinterpretation of the detected data. Rather, it is a modification of the sensor dynamics themselves. The cancellation occurs because the detector is engineered so that two distinct noise pathways interfere destructively before they appear in the final measured observable.

1.4.3 CQNC condition and matching requirements

Backaction cancellation in CQNC is not automatic. It requires careful matching of response functions, coupling strengths, and relative phases between the physical mechanical pathway and the auxiliary pathway. In the idealized limit, one seeks conditions under which the backaction contribution to the displacement estimator $\hat{x}_{\mathrm{est}}$ or to the inferred signal force $\hat{F}_{\mathrm{sig}}$ vanishes over the frequency band of interest.

Schematically, the measured output quadrature may be written as

$$X_\theta^{\mathrm{out}}(\omega) = \underbrace{\mathcal{G}(\omega)\, x(\omega)}_{\text{signal transduction}} + \underbrace{X_{\mathrm{imp}}(\omega)}_{\text{imprecision}} + \underbrace{\mathcal{B}(\omega)\, F_{\mathrm{ba}}(\omega)}_{\text{backaction pathway}}, \tag{1.36}$$

where $\mathcal{G}(\omega)$ denotes the signal transduction gain, $X_{\mathrm{imp}}(\omega)$ is the imprecision noise, and $\mathcal{B}(\omega)F_{\mathrm{ba}}(\omega)$ represents the backaction contribution reaching the output. CQNC seeks to engineer an auxiliary contribution $X_{\mathrm{aux}}(\omega)$ such that

$$\mathcal{B}(\omega)\, F_{\mathrm{ba}}(\omega) + X_{\mathrm{aux}}(\omega) \approx 0 \qquad \text{over the relevant bandwidth.} \tag{1.37}$$

In practice, this requires at least two essential conditions. First, the auxiliary response must closely match the mechanical response, up to an overall sign, across the frequency range of interest. Second, the relative phase between the two pathways must be controlled with sufficient precision to maintain destructive interference in the presence of loss, detuning errors, and parameter drift. These requirements are demanding, and they explain why much of the CQNC literature focuses not only on the basic principle but also on physically realizable architectures capable of approximating the required negative-mass response with adequate robustness.

1.4.4 Beyond-SQL sensing through coherent cancellation

If the backaction pathway is successfully canceled, then the total added noise is no longer constrained by the usual imprecision–backaction trade-off. Instead, the sensitivity is limited primarily by the remaining imprecision noise together with residual auxiliary noise, internal loss, and imperfect matching. In the ideal limit, the probe power can therefore be increased to reduce imprecision without incurring the standard radiation-pressure penalty, thereby enabling sensitivity beyond the SQL over the frequency range in which cancellation holds.

Importantly, this does not violate quantum mechanics. CQNC does not eliminate all quantum fluctuations from the measurement. Rather, it modifies the detector dynamics so that a particular quantum-noise pathway—namely radiation-pressure backaction—is coherently can-

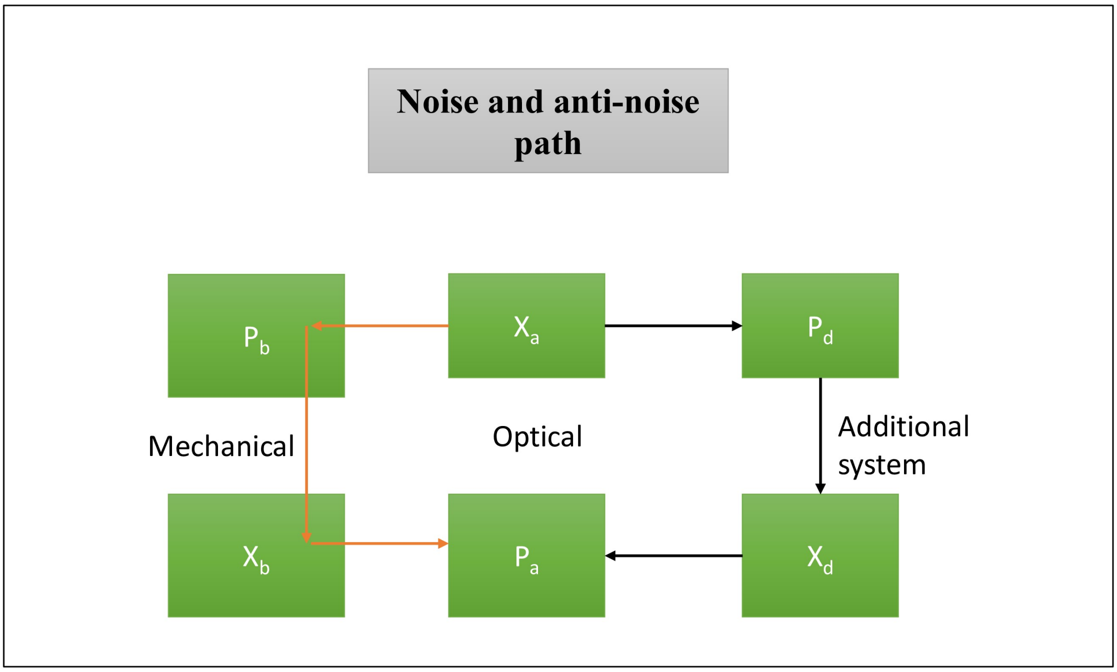

Figure 1.5: Anti-noise

Figure 1.6: Conceptual illustration of coherent quantum noise cancellation. Radiation-pressure fluctuations reach the detector output through two pathways: the ordinary mechanical pathway and an auxiliary pathway with opposite response, such as an effective negative-mass oscillator. Under suitable matching conditions, these two pathways interfere destructively, suppressing the backaction contribution in the measured signal.

celed by interference with an auxiliary response. The total noise remains subject to general quantum constraints, but the usual SQL associated with standard coherent probing can be surpassed because the measurement architecture itself has been changed.

CQNC was originally introduced by Tsang and Caves as a general coherent-control strategy for optomechanical sensing [64]. Subsequent work has explored more concrete implementations, including all-optical realizations of effective negative-mass oscillators, cascaded schemes, and related hybrid platforms designed to approximate the ideal matching conditions required for broadband cancellation [56]. More recent studies continue to address the main practical challenges of CQNC, including realistic dissipation, finite bandwidth, detector inefficiency, and the identification of experimentally feasible auxiliary systems.

1.5 Scope and Structure of the Thesis

This thesis is organized around the study of coherent quantum noise cancellation in three hybrid optomechanical platforms. After establishing the general optomechanical and measurement-theoretic framework in this chapter, the remainder of the thesis examines CQNC in an electro-optomechanical system, an optomechanical system coupled to an ensemble of quantum dots, and a hybrid cavity magnomechanical system. These three platforms are considered in order to examine how the same backaction-cancellation principle can be implemented through different auxiliary subsystems, each with its own physical advantages and operating constraints. In this way, the thesis progresses from establishing whether CQNC can be realized in a concrete hybrid setting to exploring how the mechanism carries over to other platforms with distinct features such as strong light-matter coupling, tunability, and robustness under realistic imperfections.

The remainder of the thesis is organized as follows.

- **Chapter 2** studies coherent quantum noise cancellation in a hybrid electro-optomechanical system. In this architecture, a superconducting qubit coupled to the mechanical resonator provides the auxiliary response required for backaction suppression. We show that when the backaction contribution from the electromechanical subsystem is equal in magnitude and opposite in sign to that of the optomechanical subsystem, near-perfect backaction evasion can be achieved, leading to enhanced sensitivity.

- **Chapter 3** investigates a hybrid quantum-dot-assisted optomechanical platform, in which an ensemble of quantum dots is coupled to the intracavity optical mode while an intra-cavity OPA modifies the optical quadratures. Quantum-dot ensemble provides a solid-state light-matter auxiliary subsystem with collective optical response, thereby allowing the backaction-cancellation mechanism to be explored in a hybrid setting different from the electro-optomechanical case. Our analysis shows that this hybrid architecture can achieve strong backaction suppression, surpass the SQL over a broad frequency range. We further analyze the role of the intracavity optical parametric amplifier and show that increasing the OPA gain allows optimal noise reduction to be reached at lower input laser power.

- **Chapter 4** considers an OPA-assisted cavity magnomechanical system, where the intracavity optical field is coupled to a magnon mode. This platform is particularly attractive for CQNC because the magnon mode provides a tunable auxiliary response that can be used to suppress radiation-pressure backaction beyond the more restrictive setting of single-quadrature backaction evasion. After deriving the linearized quantum Langevin equations and transforming them to the frequency domain, we obtain the CQNC condition and show how the magnon-induced susceptibility can be used to cancel radiation-pressure backaction. The results demonstrate broadband sub-SQL sensitivity, reduced optimal operating power with increasing OPA gain, and robustness against realistic imperfections such as coupling mismatch and unequal dissipation rates.

- **Chapter 5** summarizes the main conclusions of the thesis and discusses the broader implications, limitations, and possible future directions of hybrid CQNC-based sensing architectures.

Chapter 2

Enhanced Force Sensing in an Electro-Optomechanical Hybrid System[1]

2.1 Introduction

In this chapter, we investigate force sensing in the hybrid electro-optomechanical system introduced in Ref. [47], which consists of an optical cavity, a mechanical resonator, and a superconducting qubit. This platform is particularly interesting because it provides a direct interface between optical, mechanical, and electrical degrees of freedom within a single device. In the proposal of the previous article [47], the system was studied mainly in the context of ground-state cooling of the mechanical mode. This already indicates that the hybrid architecture offers a high degree of controllability and can strongly modify the mechanical response through the auxiliary electromechanical subsystem. Motivated by this, we explore here a different domain, whether the same platform can be used for precision force sensing beyond the Standard Quantum Limit through coherent quantum noise cancellation.

The system is especially appealing for this purpose because the mechanical resonator couples simultaneously to two distinct subsystems, the optical cavity, which provides the measurement channel, and the superconducting qubit, which acts as an auxiliary degree of freedom. The optical cavity allows the external force signal to be transduced into a measurable optical

[1]This work is published in Phys. Rev. A 111, 013509 (2025)

output, while the electromechanical coupling to the qubit introduces an additional response pathway. If this auxiliary pathway is engineered appropriately, its response to measurement backaction can counteract the standard optomechanical backaction. In this way, the hybrid architecture provides a natural setting for implementing backaction suppression while retaining optical readout of the signal.

In addition to the hybrid electromechanical coupling, we include an intracavity optical parametric amplifier (OPA), which modifies the optical quadratures and provides an additional handle for reducing the measurement-added noise. We show that the combined action of the auxiliary electromechanical subsystem and the OPA can significantly enhance the force sensitivity of the device. When the effective electromechanical response matches the optomechanical backaction pathway with opposite sign, the radiation-pressure backaction can be cancelled. This leads to strong suppression of the added-force noise and enables sensitivity beyond the Standard Quantum Limit over a broad frequency range. We further find that increasing the OPA gain shifts the optimal operating point toward lower input laser power, thereby making low-power, high-sensitivity operation possible within this framework.

The chapter is organized as follows: Section 2.2 introduces the hybrid electro-optomechanical model and its Hamiltonian. Section 2.3 derives the linearized quantum Langevin equations and their frequency-domain solution. Section 2.4 formulates the force-sensing protocol and obtains the condition for coherent backaction cancellation. Section 2.5 presents the numerical results for the added-force noise spectral density and compares the hybrid CQNC scheme with the standard optomechanical case. Finally, Section 2.6 summarizes the main conclusions of the chapter.

2.2 The System

We consider a hybrid electro-optomechanical system consisting of an optical cavity, a mechanical resonator, and a superconducting Cooper-pair-box (CPB) qubit, as shown schematically in Fig. 2.1. The optical cavity, with resonance frequency ω_c, is driven by a laser of frequency ω_L and input power P_L, while the mechanical resonator of frequency Ω forms the central element of the setup. On the optical side, the cavity field couples to the mechanical motion through the standard radiation-pressure interaction. On the electrical side, the same mechanical resonator couples to the superconducting qubit through a displacement-dependent capacitance $C_x(x)$. Because the mechanical motion changes this capacitance, it modulates the electrostatic energy of the CPB circuit and thereby generates an electromechanical interaction.

The mechanical resonator therefore serves as an interface between the optical and electrical sectors of the hybrid device. This is the key feature of the present system, the optical cavity provides the readout channel for force detection, whereas the qubit introduces an auxiliary response pathway through the electromechanical coupling. In addition, an intracavity optical parametric amplifier (OPA) is included in the cavity in order to modify the optical quadratures and provide an additional control parameter for reducing the overall measurement-added noise.

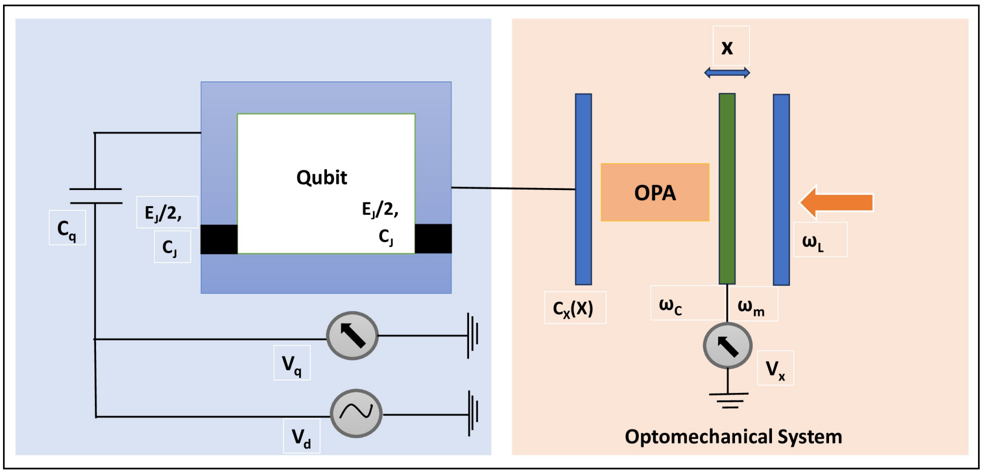

Figure 2.1: Schematic diagram of the hybrid electro-optomechanical system. The CPB is biased by voltages V_q and V_x, and driven by the voltage V_d. The total capacitance of the qubit is $C_\Sigma(x) = 2C_J + C_q + C_x(x)$, where the displacement-dependent capacitance $C_x(x)$ couples the qubit to the mechanical resonator.

The dynamics of the hybrid system can then be described by the following Hamiltonian.

$$H = H_{OM} + H_{OPA} + H_L + H_Q, \tag{2.1}$$

where the different contributions are described below.

The optomechanical part is

$$H_{OM} = \hbar\Omega\hat{b}^\dagger\hat{b} - \hbar\Delta_c\hat{a}^\dagger\hat{a} + \hbar g_0\hat{a}^\dagger\hat{a}\,(\hat{b}^\dagger + \hat{b}), \tag{2.2}$$

which describes the standard cavity-optomechanical interaction. The first term corresponds to the mechanical mode, the second to the optical cavity mode, and the third to the radiation pressure coupling of strength g_0. Here $\Delta_c = \omega_L - \omega_c$ denotes the cavity detuning, while $\hat{a}$ ($\hat{a}^\dagger$) and $\hat{b}$ ($\hat{b}^\dagger$) are the annihilation (creation) operators of the optical and mechanical modes, respectively.

The intracavity OPA is described by

$$H_{OPA} = i\hbar\mathcal{G}(\hat{a}^{\dagger 2}e^{i\theta} - \hat{a}^2 e^{i\theta}), \tag{2.3}$$

where $\mathcal{G}$ is the parametric gain and θ is the pump phase [58]. Choosing $\theta = 0$ simplifies this term to

$$H_{OPA} = i\hbar\mathcal{G}(\hat{a}^{\dagger 2} - \hat{a}^2). \tag{2.4}$$

The coherent cavity drive is represented by

$$H_L = i\hbar E_L(\hat{a}^\dagger - \hat{a}), \tag{2.5}$$

where

$$E_L = \sqrt{\frac{P_L\kappa}{\hbar\omega_L}}. \tag{2.6}$$

The electromechanical contribution, written in the drive frame of the qubit and under the rotating-wave approximation, is

$$H_Q = -\hbar\frac{\Delta_q}{2}\sigma_z + \frac{1}{2}\hbar\Omega_R\sigma_x + \hbar G(\hat{b}^\dagger + \hat{b})\sigma_z, \tag{2.7}$$

where Ω_R is the qubit drive amplitude, Δ_q is the qubit detuning, and G is the electromechanical coupling strength. The operators σ_x and σ_z are the corresponding Pauli matrices. The Pauli matrices σ_x, σ_z, σ^+ and σ^- satisfy

$$[\sigma_z, \sigma^+] = 2\sigma^+, \qquad [\sigma_z, \sigma^-] = -2\sigma^-, \qquad [\sigma^-, \sigma^+] = \sigma_z, \tag{2.8}$$

with $\sigma_x = \sigma^+ + \sigma^-$.

In the low-excitation regime of the qubit [57, 18, 26, 39], one has

$$\sigma_z \simeq \langle\sigma_z\rangle \simeq -1, \tag{2.9}$$

so that σ^+ and σ^- may be approximated as bosonic operators satisfying

$$[\sigma^-, \sigma^+] = 1. \tag{2.10}$$

In this limit, one introduces bosonic annihilation and creation operators $\hat{d}$ and $\hat{d}^\dagger$ through

$$\sigma_- = \hat{d}, \qquad \sigma_+ = \hat{d}^\dagger. \tag{2.11}$$

The Hamiltonian then takes the form (see Appendix A)

$$\begin{aligned} H =& \Delta_q \hat{d}^\dagger \hat{d} + \frac{1}{2}\Omega'_R(\hat{d}^\dagger + \hat{d}) + \frac{\hbar\Omega}{2}(\hat{x}^2 + \hat{p}^2) \\ &- \hbar\Delta_c \hat{a}^\dagger \hat{a} + \hbar g_0 \alpha(\hat{a}^\dagger + \hat{a})\hat{X}_b + i\hbar\mathcal{G}(\hat{a}^{\dagger 2} - \hat{a}^2) \\ &+ G\bar{d}\hat{X}_b(\hat{d}^\dagger + \hat{d}) + 2G\bar{X}_b \hat{d}^\dagger \hat{d} + i\hbar E_L(\hat{a}^\dagger - \hat{a}). \end{aligned} \tag{2.12}$$

Here, $\hat{x}$ and $\hat{p}$ denote the dimensionless position and momentum quadratures, respectively [4].

Since the cavity is strongly driven and the qubit is only weakly excited, the relevant dynamics for force sensing are those of small fluctuations around the classical steady state. The system can therefore be analyzed within the linearized quantum Langevin framework, which we develop in the next section.

2.3 Linearized dynamics and frequency-domain solution

In the linearized approach, each system operator is written as a steady-state mean value plus a small quantum fluctuation,

$$\hat{A} = \bar{A} + \delta\hat{A}, \tag{2.13}$$

where $\bar{A}$ is the mean-field value and $\delta\hat{A}$ denotes the corresponding fluctuation operator. Keeping only terms up to first order in the fluctuations yields a set of linear quantum Langevin equations.

For convenience, we introduce amplitude and phase quadratures for the optical, mechanical, and qubit modes,

$$\hat{x}_A = \frac{\hat{A} + \hat{A}^\dagger}{\sqrt{2}}, \qquad \hat{p}_A = i\frac{\hat{A}^\dagger - \hat{A}}{\sqrt{2}}, \tag{2.14}$$

where $\hat{A} = \hat{a}, \hat{b}, \hat{d}$. The corresponding input-noise operators are denoted by

$$A^{in} = \hat{a}^{in}, \hat{b}^{in}, \hat{d}^{in}, \tag{2.15}$$

and satisfy the standard correlations [66, 7, 23, 70]

$$\langle \hat{a}_{in}(t)\hat{a}^{\dagger}_{in}(t')\rangle = \delta(t-t'), \tag{2.16}$$

$$\langle \hat{b}_{in}(t)\hat{b}^{\dagger}_{in}(t')\rangle = \delta(t-t'), \tag{2.17}$$

$$\langle \hat{d}_{in}(t)\hat{d}^{\dagger}_{in}(t')\rangle = \delta(t-t'). \tag{2.18}$$

Their quadratures are defined as

$$\hat{X}^{in}_{A} = \frac{\hat{A}^{in} + \hat{A}^{in\dagger}}{\sqrt{2}}, \qquad \hat{P}^{in}_{A} = i\frac{\hat{A}^{in\dagger} - \hat{A}^{in}}{\sqrt{2}}. \tag{2.19}$$

With these definitions, the linearized quantum Langevin equations are

$$\dot{\hat{x}}_a = \left(-\frac{\kappa}{2} + 2\mathcal{G}\right)\hat{x}_a + \sqrt{\kappa}\,\hat{x}^{in}_a, \tag{2.20}$$

$$\dot{\hat{p}}_a = -\left(\frac{\kappa}{2} + 2\mathcal{G}\right)\hat{p}_a - \sqrt{2}g_0\alpha\,\hat{x}_b + \sqrt{\kappa}\,\hat{p}^{in}_a, \tag{2.21}$$

$$\dot{\hat{x}}_b = \Omega\hat{p}_b, \tag{2.22}$$

$$\begin{aligned}\dot{\hat{p}}_b = &-\Omega\hat{x}_b - \sqrt{2}g_0\alpha\,\hat{x}_a - \gamma_m\hat{p}_b + \sqrt{\gamma_m}(f_{th} + f_{ext})\\ &- \sqrt{2}G\bar{d}\,\hat{x}_d,\end{aligned} \tag{2.23}$$

$$\dot{\hat{x}}_d = \Delta_q\hat{p}_d + 2G\bar{x}\,\hat{p}_d - \frac{\Gamma}{2}\hat{x}_d + \sqrt{\Gamma}\,\hat{x}^{in}_d, \tag{2.24}$$

$$\begin{aligned}\dot{\hat{p}}_d = &-\Delta_q\hat{x}_d - 2\sqrt{2}G\bar{d}\,\hat{x}_b - 2G\bar{x}_b\hat{x}_d + 2\Omega_R\bar{d}\,\hat{x}_d\\ &- \frac{\Gamma}{\sqrt{2}}\hat{p}_d + \sqrt{\Gamma}\,\hat{p}^{in}_d.\end{aligned} \tag{2.25}$$

Here, $\bar{x}$ and $\bar{d}$ denote the steady-state values, while γ_m, κ, and Γ are the mechanical damping rate, cavity decay rate, and qubit dephasing rate, respectively. The force f_{th} represents the Brownian thermal noise acting on the mechanical mode, whereas f_{ext} is the external force to be measured.

To study the linear response of the system [4], it is convenient to transform the dynamics from the time domain to the frequency domain using the Fourier convention

$$O(\omega) = \frac{1}{\sqrt{2\pi}}\int dt\, O(t)e^{-i\omega t}. \tag{2.26}$$

The linearized equations can then be written in terms of frequency-dependent response functions as

$$\hat{X}_b(\omega) = \chi_m\left\{-g\hat{X}_a(\omega) + \sqrt{\gamma_m}\big(F_{th}(\omega) + F_{ext}(\omega)\big) - G'\hat{X}_d(\omega)\right\}, \tag{2.27}$$

$$\hat{P}_b(\omega) = \frac{i\omega}{\Omega}\hat{X}_b(\omega), \tag{2.28}$$

$$\hat{X}_a(\omega) = \sqrt{\kappa}\lambda_+\hat{X}_a^{in}(\omega), \tag{2.29}$$

$$\begin{aligned}\hat{P}_a(\omega) = {} & g^2\chi_m\lambda_-\lambda_+\sqrt{\kappa}\,\hat{X}_a^{in}(\omega) \\ & - g\lambda_-\chi_m\sqrt{\gamma_m}\big(F_{th} + F_{ext}\big) + gG'\chi_m\lambda_-\hat{X}_d(\omega) \\ & + \lambda_-\sqrt{\kappa}\,\hat{P}_a^{in},\end{aligned} \tag{2.30}$$

$$\hat{X}_d(\omega) = \Delta_q\chi_d\hat{P}_d(\omega) + \chi_d\sqrt{\Gamma}\,\hat{x}_d^{in}(\omega), \tag{2.31}$$

$$\begin{aligned}\hat{P}_d(\omega) = {} & \zeta\chi_d\Omega'\sqrt{\Gamma}\,\hat{X}_d^{in} + 2\zeta gG'\chi_m\sqrt{\kappa}\lambda_+\hat{X}_a^{in} \\ & - 2\zeta G'\sqrt{\gamma_m}\chi_m\big[F_{th}(\omega) + F_{ext}(\omega)\big] \\ & + \zeta G'^2\chi_m\chi_d\sqrt{\Gamma}\hat{X}_d^{in}(\omega) + \zeta\sqrt{\Gamma}\hat{P}_d^{in}.\end{aligned} \tag{2.32}$$

Here, the relevant susceptibilities and effective couplings are

$$\chi_d = \frac{1}{i\omega + \Gamma/2}, \tag{2.33}$$

$$\chi_m = \frac{\Omega}{\Omega^2 - \omega^2 + i\gamma_m\omega}, \tag{2.34}$$

$$\zeta = \frac{1}{i\omega + \Gamma/2 + \Delta_q^2\chi_d}, \tag{2.35}$$

$$G' = \sqrt{2}G\bar{d}, \tag{2.36}$$

$$g = \sqrt{2}g_0\alpha, \tag{2.37}$$

$$\lambda_+ = \frac{1}{\chi_a^{-1} - 2\mathcal{G}}, \tag{2.38}$$

$$\lambda_- = \frac{1}{\chi_a^{-1} + 2\mathcal{G}}, \qquad \chi_a = \frac{1}{i\omega + \kappa/2}. \tag{2.39}$$

The scaled external force and thermal noise are defined as [3]

$$F_{ext} = \frac{f_{ext}}{\sqrt{\hbar m\omega_m\gamma_m}}, \qquad F_{th} = \frac{f_{th}}{\sqrt{\hbar m\omega_m\gamma_m}}, \tag{2.40}$$

and the scaled Brownian thermal noise satisfies

$$\langle F_T(t)F_T(t')\rangle = \bar{n}\,\delta(t - t'), \tag{2.41}$$

where

$$\bar{n} = \frac{K_B T}{\hbar\Omega}. \tag{2.42}$$

These frequency-domain expressions make explicit how the external signal, thermal fluctuations, optical vacuum noise, and qubit noise contribute to the optical output. In the next section, we use them to construct the force estimator and derive the condition for coherent quantum noise cancellation.

2.4 Force sensing with coherent quantum noise cancellation

When the external force F_{ext} acts on the movable mirror, the mechanical displacement changes the cavity length and thereby modulates the phase of the output cavity field. Solving the linearized Langevin equations in the frequency domain, the output phase quadrature can be obtained from the standard input–output relation

$$P_a^{out} = \sqrt{\kappa}\, P_a - P_a^{in}. \tag{2.43}$$

This gives

$$\begin{aligned} P_a^{out} =& \lambda_+\lambda_-\,\kappa\left(g^2\chi_m + G'^2\chi_d'\right)\hat{x}_a^{in} \\ &+ \sqrt{\kappa}\left(-\Omega\chi_d\chi_d'\sqrt{\Gamma}\lambda_- + \chi_d\sqrt{\Gamma}gG'\chi_m\lambda_-\right)\hat{x}_d^{in} \\ &+ \sqrt{\kappa}\left(-\Omega\chi_d\right)\left(gG'\chi_m\lambda_-\right)\left(\sqrt{\Gamma}\zeta\right)\hat{p}_d^{in} \\ &+ \left(-g\chi_m\lambda_-\sqrt{\gamma_m\kappa}\right)\left(F_{ext} + F_{th}\right) \\ &+ \left(\lambda_-\kappa - 1\right)\hat{p}_a^{in}. \end{aligned} \tag{2.44}$$

Here,

$$\chi_d' = -\Omega\chi_d\zeta = \frac{\Omega}{\Omega^2 - \omega^2 + i\omega\Gamma + \Gamma^2/4}, \tag{2.45}$$

$$\chi_d = \frac{1}{i\omega + \Gamma/2}, \tag{2.46}$$

$$\chi_m = \frac{\Omega}{\Omega^2 - \omega^2 + i\gamma_m\omega}. \tag{2.47}$$

The first term of Eq. (2.44) corresponds to the backaction noise [3, 44]. For significant noise reduction, our aim is to eliminate this term completely [64, 70]. In the present hybrid system, the additional contribution proportional to $G'^2\chi_d'$ arises from the electromechanical subsystem. Under suitable conditions, this term can cancel the ordinary optomechanical backaction term $g^2\chi_m$, resulting in complete elimination of the backaction contribution.

The CQNC condition is therefore

$$g^2\chi_m + G'^2\chi_d' = 0. \tag{2.48}$$

The derivation of this condition is given in Appendix B. Equation (2.48) shows that the cancellation can be achieved when the effective couplings and susceptibilities satisfy

$$g = G', \qquad \chi_m = -\chi_d'. \tag{2.49}$$

This implies that: (i) the response of the mechanical oscillator to the backaction noise is exactly equal and opposite to that of the superconducting qubit, and (ii) the optomechanical coupling is equal to the electromechanical coupling of the hybrid system.

To satisfy Eq. (2.48), the susceptibilities of the mechanical oscillator and the qubit must also obey the following matching conditions:

1. the qubit is detuned from the cavity by $\Delta_q = \Omega$,
2. the qubit dephasing rate matches the mechanical damping rate, $\Gamma = \gamma_m$,
3. $|\Delta_q| \gg \Gamma$, which together with condition (1) implies $\Omega \gg \Gamma$.

These are the requirements for perfect backaction cancellation in the present model.

Under the CQNC condition, the output phase quadrature simplifies to

$$\begin{aligned}
P_a^{out} = &+ \sqrt{\kappa}\left(-\Omega\chi_d\chi_d'\sqrt{\Gamma}\lambda_- + \chi_d\sqrt{\Gamma}gG'\chi_m\lambda_-\right)\hat{x}_d^{in} \\
&+ \sqrt{\kappa}\left(-\Omega\chi_d\right)\left(gG'\chi_m\lambda_-\right)\left(\sqrt{\Gamma}\zeta\right)\hat{p}_d^{in} \\
&+ \left(-g\chi_m\lambda_-\sqrt{\gamma_m\kappa}\right)\left(F_{ext} + F_{th}\right) \\
&+ \left(\lambda_-\kappa - 1\right)\hat{p}_a^{in}.
\end{aligned} \tag{2.50}$$

Dividing Eq. (2.50) by the signal transduction factor gives

$$\frac{P_a^{out}}{\left(-g\chi_m\lambda_-\sqrt{\gamma_m\kappa}\right)} = F_{ext} + \frac{(\lambda_-\kappa - 1)\,\hat{p}_a^{in}}{\left(-g\chi_m\lambda_-\sqrt{\gamma_m\kappa}\right)} + \frac{\sqrt{\kappa}\left(-\Omega\chi_d\chi_d'\sqrt{\Gamma}\lambda_- + \chi_d\sqrt{\Gamma}gG'\chi_m\lambda_-\right)\hat{x}_d^{in}}{\left(-g\chi_m\lambda_-\sqrt{\gamma_m\kappa}\right)} + \frac{\sqrt{\kappa}\left(-\Omega\chi_d\right)\left(gG'\chi_m\lambda_-\right)\left(\sqrt{\Gamma}\zeta\right)\hat{p}_d^{in}}{\left(-g\chi_m\lambda_-\sqrt{\gamma_m\kappa}\right)}.$$

We estimate the impressed force on the mechanical oscillator from the output phase quadrature. Based on Eq. (2.50), the force estimator can be written as

$$\hat{F} = \frac{P_a^{out}}{\left(-g\chi_m\lambda_-\sqrt{\gamma_m\kappa}\right)} = F_{ext} + F_{add}, \tag{2.51}$$

where the added noise is

$$F_{add} = F_{th} - \frac{\kappa\lambda_- - 1}{g\chi_m\lambda_-\sqrt{\gamma_m\kappa}}\hat{P}_a^{in} + \frac{\sqrt{\Gamma}}{\gamma_m}\hat{P}_d^{in} - \left(\frac{i\omega + \Gamma/2}{\Omega}\right)\hat{x}_d^{in}. \tag{2.52}$$

The force sensitivity is characterized by the power spectral density of the added noise, defined by [70]

$$S_F^{add}(\omega)\delta(\omega-\omega') = \frac{1}{2}\left(\langle\hat{F}_{add}(\omega)\hat{F}_{add}(-\omega)\rangle + c.c.\right). \tag{2.53}$$

Using this expression, one obtains

$$S_F^{add} = \frac{K_BT}{\hbar\Omega} + \frac{1}{2}\frac{1}{g^2|\chi_m(\omega)|^2(\gamma_m\kappa)}\left(\frac{\lambda_-(\omega)\kappa - 1}{\lambda_-(\omega)}\right)^2 + \frac{1}{2}\frac{\omega^2+\Omega^2+\Gamma^2/4}{\Omega^2}. \tag{2.54}$$

To focus on the measurement-added noise reduction, the Brownian thermal background may be neglected [44]. Minimizing the spectral density then yields the minimum noise spectral density for the proposed CQNC scheme in the hybrid electro-optomechanical model,

$$S_{F,CQNC} = \frac{1}{2}\frac{\omega^2+\Omega^2+\Gamma^2/4}{\Omega^2}. \tag{2.55}$$

For comparison, the spectral density of a standard optomechanical system is [4]

$$S_F(\omega) = \frac{K_BT}{\hbar\Omega} + \frac{1}{2}\frac{\kappa}{\gamma_m}\frac{1}{g^2|\chi|^2}\frac{1}{4} + 4g^2\frac{1}{\kappa\gamma_m}, \tag{2.56}$$

where the first term corresponds to thermal noise, the second to shot noise, and the third to radiation-pressure backaction. Neglecting thermal noise and minimizing with respect to the laser power gives the SQL value

$$S_{F,SQL} = \frac{1}{\gamma_m |\chi_m|}. \tag{2.57}$$

The corresponding optimum occurs at the optomechanical coupling

$$g_{SQL} = \frac{\sqrt{\kappa}}{2\sqrt{|\chi_m|}}. \tag{2.58}$$

These expressions will be used in the next section to compare the hybrid CQNC scheme with the standard optomechanical limit.

2.5 Results and Discussion

We now turn to the numerical analysis of the spectral density of the added-force noise, which provides a direct measure of the sensitivity to force of the device [44]. The added-noise spectral density is defined as [70]

$$S_F^{add}(\omega)\delta(\omega - \omega') = \frac{1}{2}\left(\langle \hat{F}_{add}(\omega)\hat{F}_{add}(-\omega)\rangle + c.c.\right). \tag{2.59}$$

Using the force estimator derived in the previous section, the corresponding spectral density of the added noise is obtained as

$$\begin{aligned} S_F^{add} =& \frac{K_B T}{\hbar\Omega} + \frac{1}{2}\frac{1}{g^2|\chi_m(\omega)|^2(\gamma_m\kappa)}\left(\frac{\lambda_-(\omega)\kappa - 1}{\lambda_-(\omega)}\right)^2 \\ &+ \frac{1}{2}\frac{\omega^2 + \Omega^2 + \Gamma^2/4}{\Omega^2}. \end{aligned} \tag{2.60}$$

To isolate the measurement-added contribution, the Brownian thermal background may be neglected [44]. Minimizing the above expression then gives the minimum noise spectral density for the proposed hybrid electro-optomechanical CQNC scheme,

$$S_{F,CQNC} = \frac{1}{2}\frac{\omega^2 + \Omega^2 + \Gamma^2/4}{\Omega^2}. \tag{2.61}$$

For comparison, the spectral density of a standard optomechanical system is [4]

$$S_F(\omega) = \frac{K_B T}{\hbar\Omega} + \frac{1}{2}\frac{\kappa}{\gamma_m}\frac{1}{g^2|\chi|^2}\frac{1}{4} + 4g^2\frac{1}{\kappa\gamma_m}. \tag{2.62}$$

where the first term is the thermal contribution, the second corresponds to shot noise, and the third represents radiation-pressure backaction. Neglecting the thermal contribution and minimizing with respect to the laser power gives the Standard Quantum Limit

$$S_{F,SQL} = \frac{1}{\gamma_m |\chi_m|}. \tag{2.63}$$

The corresponding optimum is reached at the optomechanical coupling strength

$$g_{SQL} = \frac{\sqrt{\kappa}}{2\sqrt{|\chi_m|}}. \tag{2.64}$$

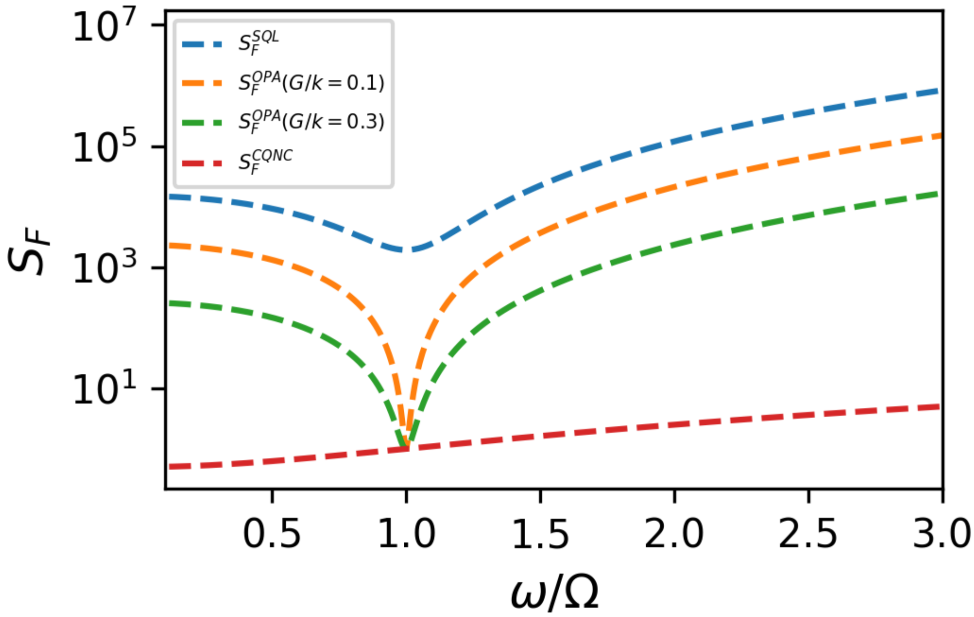

Figure 2.2: Added-force noise power spectral density for the standard optomechanical system, the hybrid electro-optomechanical system with OPA gain $G/\kappa = 0.1$ and 0.3, and the hybrid system under the CQNC condition. The spectral densities are normalized by $\hbar m \omega_m \gamma_m$ and are therefore expressed in units of $\mathrm{N}^2\,\mathrm{Hz}^{-1}$. The parameters are [70, 58]: $g_0 = 300 \times 2\pi$ Hz, $\Omega = 300 \times 2\pi$ kHz, $\gamma_m = 30 \times 2\pi$ Hz, $\kappa = 2\pi$ MHz, $P = 100$ mW, and $\omega_L = 384 \times 2\pi$ THz.

Figure 2.2 shows the frequency dependence of the added-force noise spectral density. As expected, the spectral density exhibits a dip near the mechanical resonance frequency $\omega = \Omega$, where the mechanical response is strongest. For the standard optomechanical system, this minimum is determined by the usual competition between shot noise and radiation-pressure backaction. In the hybrid electro-optomechanical platform, however, the additional electromechanical pathway modifies this balance.

A first important observation is the role of the OPA. When the OPA gain is increased from $G/\kappa = 0.1$ to 0.3, the added-force noise is reduced more strongly at off-resonant frequencies, as seen from the orange and green curves. This shows that parametric amplification provides an additional handle for suppressing the overall measurement-added noise in the hybrid platform.

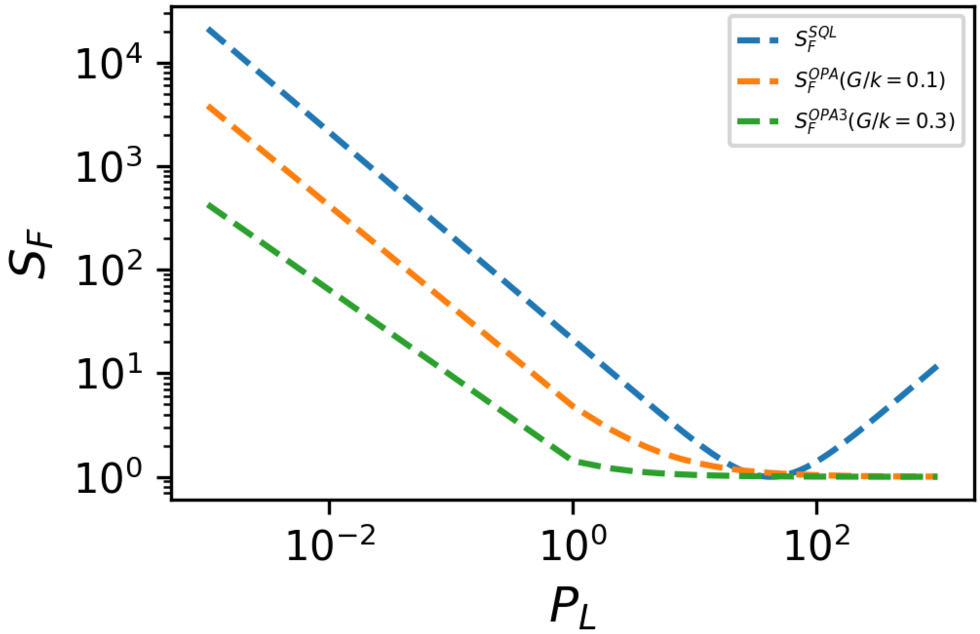

Figure 2.3: Added-force noise power spectral density at resonance, i.e. $\omega = \Omega$, as a function of the input laser power for the standard optomechanical system and the hybrid electro-optomechanical system with the CQNC scheme. The blue curve corresponds to the standard optomechanical system, while the orange and green curves represent the hybrid system with OPA gain $G/\kappa = 0.1$ and 0.3, respectively. The remaining parameters are the same as in Fig. 2.2.

The most significant effect is obtained under the CQNC condition. In this regime, the added-force noise is suppressed by several orders of magnitude at frequencies away from resonance compared with the standard optomechanical case. This strong reduction reflects the cancellation of the radiation-pressure backaction contribution by the electromechanical auxiliary pathway. Although the CQNC protocol does not necessarily improve the sensitivity exactly at the resonant point, it leads to substantial noise suppression over a broad off-resonant frequency range, which is particularly valuable for broadband sensing applications.

The dependence of the spectral density on the input laser power is shown in Fig. 2.3. Since the laser driving power is proportional to the square of the effective optomechanical coupling,

$$P_L = 2\hbar\omega_L\kappa\left(\frac{g}{g_0}\right)^2, \tag{2.65}$$

the spectral density may be expressed directly as a function of P_L. For the standard optomechanical system, represented by the blue curve, the noise spectral density initially decreases with increasing laser power due to the reduction of shot-noise imprecision. However, after reaching its minimum, it rises again because radiation-pressure backaction becomes dominant at high power. This is the familiar SQL tradeoff.

By contrast, for the hybrid CQNC scheme, shown by the orange and green curves, the added-force noise decreases with increasing laser power and does not show the pronounced upturn characteristic of the standard optomechanical case. This behavior reflects the cancellation of the backaction contribution at large drive strengths. Moreover, increasing the OPA gain shifts the minimum of the spectral density to lower laser powers. This indicates that in the present framework, the inclusion of the OPA allows the device to achieve optimal sensitivity in a lower-power operating regime.

Taken together, these results show that the hybrid electro-optomechanical architecture combines two useful mechanisms for sensitivity enhancement where the electromechanical subsystem provides the auxiliary pathway needed for coherent backaction cancellation, while the OPA improves the optical noise properties and lowers the power required to reach the optimal operating point.

2.6 Conclusion

In this chapter, we investigated force sensing in a hybrid electro-optomechanical system consisting of an optical cavity, a mechanical resonator, and a superconducting qubit, with additional intracavity optical parametric amplification. The central goal was to determine whether this hybrid architecture can realize coherent quantum noise cancellation and thereby suppress the radiation-pressure backaction that limits standard optomechanical force detection.

Our analysis showed that the electromechanical subsystem introduces an additional response pathway that can be arranged to counteract the ordinary optomechanical backaction. When the effective electromechanical and optomechanical responses are matched with opposite sign, the backaction contribution is canceled, leading to strong suppression of the added-force noise. In this CQNC regime, the force sensitivity can surpass the Standard Quantum Limit over a broad off-resonant frequency range.

We further found that the inclusion of an intracavity OPA improves the sensing performance by reducing the measurement-added noise and shifting the optimal operating point to lower input laser power. This low-power operation is particularly attractive from the viewpoint of practical implementations, since it reduces the need for strong optical driving while maintaining high sensitivity.

Overall, the results establish the hybrid electro-optomechanical system as a promising platform for backaction-suppressed force sensing. More broadly, they illustrate how auxiliary hybrid degrees of freedom can be used to engineer interference-based noise cancellation in optomechanical detectors, with possible applications in quantum metrology, weak-force sensing, quantum information processing, and related quantum technologies.

Chapter 3

Force Sensing Beyond the Standard Quantum Limit in an Optomechanical System coupled to an ensemble of Quantum Dots[1]

3.1 Introduction

In the previous chapters, coherent quantum noise cancellation (CQNC) was introduced as a route to overcome the Standard Quantum Limit by engineering destructive interference between radiation-pressure backaction and an auxiliary response pathway. An important question is how this idea can be implemented in solid-state hybrid systems with physically distinct auxiliary degrees of freedom. In this context, cavity quantum electrodynamics with quantum-dot (QD) ensembles offers a particularly interesting setting, since collective light–matter interactions in such systems can strongly modify the optical response of the cavity and create additional interference pathways that are useful for controlling quantum noise.

Recent progress in solid-state cavity QED, especially in QD ensembles embedded in high-finesse optical cavities, has made such platforms increasingly attractive for quantum sensing

[1]This work is accepted in JOSA B.

applications [50, 73, 32, 42, 22, 55]. Experiments have demonstrated robust optical coupling of QDs to microcavities [25], while strong light–matter coupling has been observed in photonic-crystal and high-Q microcavities [34, 28]. These developments suggest that hybrid cavity–QD systems can serve not only as platforms for controlling optical nonlinearities and dissipation, but also as promising auxiliary subsystems for implementing CQNC in a solid-state environment.

Motivated by these developments, in this chapter we investigate weak-force sensing in a hybrid optomechanical system consisting of an optomechanical cavity coupled to an ensemble of quantum dots [53]. The central idea is that the QD ensemble modifies the cavity response in a way that enables an interference pathway capable of suppressing radiation-pressure backaction at the detector output.

To analyze this mechanism, we employ the quantum Langevin formalism and solve the linearized dynamics in the frequency domain. From these solutions, we evaluate the output noise spectra and identify the regime in which radiation-pressure-noise cancellation can be achieved through suitable tuning of the cavity detuning and the effective exciton-mechanical coupling. We also examine the effect of imperfect matching, in particular the influence of decay-rate and coupling mismatches, in order to assess how robust the cancellation remains under realistic nonideal conditions. In addition, we show that the inclusion of an intracavity optical parametric amplifier (OPA) [48, 58] improves the low-frequency response and allows high sensitivity to be reached at lower drive power, which is advantageous for reducing heating and related technical limitations.

The results presented in this chapter show that the hybrid cavity–QD platform provides a promising route to force sensing beyond the Standard Quantum Limit. More broadly, they show that collective solid state light-matter systems can play the role of effective auxiliary channels for backaction cancellation, thereby extending the scope of CQNC-based sensing to a new class of hybrid optomechanical architectures.

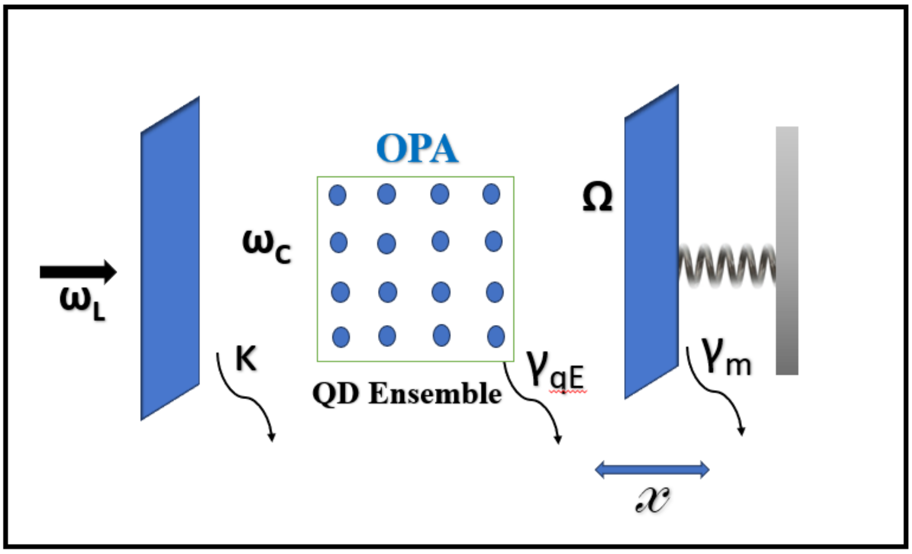

Figure 3.1: Schematic diagram of a hybrid optomechanical system equipped with an ensemble of quantum dots and an optical parametric amplifier (OPA).

3.2 System

This work analyzes a hybrid optomechanical system consisting of an optical cavity with resonance frequency ω_c, a mechanical oscillator of frequency Ω, and an ensemble of quantum dots (QDs) coupled to the cavity mode. The system is engineered such that the QD ensemble interacts only with the optical field and remains decoupled from the mechanical oscillator. The optomechanical cavity is coherently driven by a laser with frequency ω_L and input power P_L. A schematic representation of the full system configuration is shown in Fig. 3.1.

The total Hamiltonian of the system can be written as

$$H = H_{\mathrm{OM}} + H_{\mathrm{OPA}} + H_{\mathrm{L}} + H_{\mathrm{QD}}, \tag{3.1}$$

where each term represents a different subsystem or interaction within the hybrid platform.

The optomechanical Hamiltonian is given by

$$H_{\mathrm{OM}} = \hbar\Omega\hat{b}^{\dagger}\hat{b} + \hbar\Delta_c\hat{a}^{\dagger}\hat{a} - \hbar g_0\hat{a}^{\dagger}\hat{a}(\hat{b}^{\dagger} + \hat{b}), \tag{3.2}$$

where Ω is the frequency of the mechanical oscillator. This Hamiltonian describes the standard interaction between the mechanical and optical modes. The first term corresponds to the mechanical mode energy, the second to the optical cavity field, and the third term represents the radiation-pressure coupling with strength g_0. Here, the detuning between the laser and cavity frequencies is $\Delta_c = \omega_L - \omega_c$. The operators $\hat{a}$ ($\hat{a}^\dagger$) and $\hat{b}$ ($\hat{b}^\dagger$) are the annihilation (creation) operators for the cavity and mechanical modes, respectively.

The contribution of the optical parametric amplifier (OPA) is expressed as,

$$H_{\text{OPA}} = i\hbar\mathcal{G}\,(\hat{a}^{\dagger 2}e^{i\theta} - \hat{a}^2 e^{-i\theta}), \tag{3.3}$$

where $\mathcal{G}$ is the gain of the OPA and θ denotes the pump phase. Setting $\theta = 0$ simplifies the term to

$$H_{\text{OPA}} = i\hbar\mathcal{G}\,(\hat{a}^{\dagger 2} - \hat{a}^2). \tag{3.4}$$

It is important to emphasize that the OPA does not itself generate the CQNC pathway. The role of the OPA is instead shift the optimal force-sensing regime toward lower input power.

The Hamiltonian describing the laser drive is given by,

$$H_{\text{L}} = i\hbar E_L(\hat{a}^\dagger - \hat{a}), \tag{3.5}$$

where E_L represents the amplitude of the external driving field applied to the optical cavity.

Finally, the quantum-dot ensemble Hamiltonian can be expressed as (see Appendix C for details)

$$H_{\text{QD}} = \hbar\omega_{qe}\,\hat{S}^\dagger\hat{S} + \frac{1}{2}\hbar G_{cs}\,(\hat{a}^\dagger + \hat{a})(\hat{S}^\dagger + \hat{S}), \tag{3.6}$$

where $\hat{S}$ ($\hat{S}^\dagger$) are the collective annihilation (creation) operators representing the excitation mode of the quantum-dot ensemble. The first term describes the free energy of the QD ensemble with transition frequency ω_{qe}, while the second term captures the dipole interaction between the optical field and the collective QD mode, characterized by the coupling strength G_{cs}.

Moving to the frame rotating at the drive frequency ω_L and dropping the constants, the total Hamiltonian becomes

$$\begin{aligned} H = &-\hbar\Delta_c\,\hat{a}^\dagger\hat{a} + \hbar\Omega\,\hat{b}^\dagger\hat{b} - \hbar\Delta_{qe}\,\hat{S}^\dagger\hat{S} + i\hbar\mathcal{G}\,(\hat{a}^{\dagger 2}e^{i\theta} - \hat{a}^2 e^{-i\theta}) \\ &+ \hbar g_0\hat{a}^\dagger\hat{a}\,(\hat{b} + \hat{b}^\dagger) + \frac{\hbar G_{cs}}{2}\,(\hat{a} + \hat{a}^\dagger)(\hat{S} + \hat{S}^\dagger) \\ &+ i\hbar E_L(\hat{a}^\dagger - \hat{a}), \end{aligned} \tag{3.7}$$

with detunings $\Delta_c = \omega_L - \omega_c$ and $\Delta_{qe} = \omega_L - \omega_{qe}$.

with detunings $\Delta_c = \omega_L - \omega_c$ and $\Delta_{qe} = \omega_L - \omega_{qe}$. Here, Δ_c, the detuning between the laser frequency and cavity resonance frequency, is treated as an experimentally tunable control parameter. This plays an important role in establishing the CQNC matching condition. In order to simplify the analytical expressions and focus on the CQNC mechanism, we assumed $\Delta_c = 0$. As in other CQNC-based hybrid systems, the required phase matching between the mechanical and auxiliary responses can only be achieved over a finite frequency range around the operating point [64, 5, 44].

We note that $\Delta_{qe} = \omega_L - \omega_{qe}$ is considered to be the detuning, which corresponds to the difference between the laser frequency and the transition frequency of the quantum dots. This detuning parameter characterizes the frequency mismatch between the driving field and the QD ensemble.

In the linearized description, each system operator is expressed as a steady-state mean value plus a small quantum fluctuation, $\hat{A}(t) = \bar{A} + \delta\hat{A}(t)$. Terms higher than first order in the fluctuations can be neglected. The amplitude and phase quadratures of the optical, mechanical, and qubit modes can be defined as $\hat{x}_A = \frac{\hat{A}+\hat{A}^\dagger}{\sqrt{2}}$, $\hat{p}_A = i\,\frac{\hat{A}^\dagger-\hat{A}}{\sqrt{2}}$, with $\hat{A} = \hat{a}, \hat{b}, \hat{S}$ and $\bar{A} = \alpha, \beta, \alpha_S$. The corresponding input noise operators are denoted by $\hat{A}^{\rm in} = \hat{a}^{\rm in}, \hat{b}^{\rm in}, \hat{S}^{\rm in}$ and the amplitude and phase of noise terms are introduced as $\hat{x}_A^{\rm in} = \frac{\hat{A}^{\rm in}+\hat{A}^{\rm in\dagger}}{\sqrt{2}}$, $\hat{p}_A^{\rm in} = i\,\frac{\hat{A}^{\rm in\dagger}-\hat{A}^{\rm in}}{\sqrt{2}}$. They satisfy the usual Markovian correlations [66, 7, 23, 70] as follows

$$\langle \hat{a}_{\rm in}(t)\, \hat{a}_{\rm in}^\dagger(t')\rangle = \langle \hat{b}_{\rm in}(t)\, \hat{b}_{\rm in}^\dagger(t')\rangle = \langle \hat{S}_{\rm in}(t)\, \hat{S}_{\rm in}^\dagger(t')\rangle = \delta(t-t').$$

In terms of these fluctuation and noise quadratures, the linearized quantum Langevin equations can be written as

$$\dot{\hat{x}}_b = \Omega \hat{p}_b, \tag{3.8}$$

$$\dot{\hat{p}}_b = -\Omega \hat{x}_b - \gamma_m \hat{p}_b - g\hat{x}_a + \sqrt{2\gamma_m}\,(\hat{f}_{\rm th} + f_{\rm ext}), \tag{3.9}$$

$$\dot{\hat{x}}_a = \left(-\frac{\kappa}{2} + 2\mathcal{G}\right)\hat{x}_a + \sqrt{\kappa}\,\hat{x}_{a,\rm in}, \tag{3.10}$$

$$\dot{\hat{p}}_a = -g\hat{x}_b + \left(-\frac{\kappa}{2} - 2\mathcal{G}\right)\hat{p}_a - G_{cs}\hat{x}_S + \sqrt{\kappa}\,\hat{p}_{a,\rm in}, \tag{3.11}$$

$$\dot{\hat{x}}_S = -\frac{\gamma_{qE}}{2}\hat{x}_S - \Delta_{qe}\hat{p}_S + \sqrt{\gamma_{qE}}\,\hat{x}_{S,\rm in}, \tag{3.12}$$

$$\dot{\hat{p}}_S = -G_{cs}\hat{x}_a + \Delta_{qe}\hat{x}_S - \frac{\gamma_{qE}}{2}\hat{p}_S + \sqrt{\gamma_{qE}}\,\hat{p}_{S,\rm in}. \tag{3.13}$$

Here, $g = \sqrt{2} g_0 \alpha$, with α denoting the steady-state mean value of the cavity field operator $\hat{a}$. f_{th} represents the Brownian thermal noise and f_{ext} denotes the external force acting on the mechanical oscillator. The mechanical damping rate, cavity decay rate, and dephasing rate of the QD ensemble are given by γ_m, κ, and γ_{qE}, respectively.

Here γ_{qE} denotes the effective damping of the collective QD mode, which can differ from individual QD linewidths. The parameters correspond to low-decoherence conditions, with γ_{qE} chosen to approximately satisfy the CQNC matching condition. In our model, γ_{qE} should be interpreted as an effective decoherence rate of the cavity-coupled collective excitonic bright mode, rather than the bare linewidth of an individual quantum dot or of an unfiltered room-temperature QD ensemble. The smallest values considered here are therefore intended to represent an idealized low-decoherence regime, potentially achievable only under optimized conditions such as reduced-temperature operation, spectral selection of a narrow cavity-coupled subset, and favorable cavity engineering. In this sense, the present analysis should be viewed primarily as a theoretical study of CQNC-enabled force sensing in a hybrid QD–optomechanical platform. A detailed experimental assessment of achievable γ_{qE} values in specific semiconductor implementations is beyond the scope of the present work.

The linear response of the system is obtained by moving from the time domain to the frequency domain [4]. Using the Fourier transform $\hat{X}(\omega) = \frac{1}{\sqrt{2\pi}} \int dt\, \hat{x}(t)\, e^{-i\omega t}$, the Langevin equations in the Fourier domain take the following form:

$$\hat{X}_b(\omega) = \chi_m(\omega)\Big[-g\,\hat{X}_a(\omega) + \sqrt{2\gamma_m}\,\big(\hat{F}_{\rm th}(\omega) + F_{\rm ext}(\omega)\big)\Big]\,, \tag{3.14}$$

$$\hat{P}_b(\omega) = \frac{i\omega}{\Omega}\,\hat{X}_b(\omega), \tag{3.15}$$

$$\hat{X}_a(\omega) = \sqrt{\kappa}\,\lambda_+(\omega)\,\hat{X}_{a,\rm in}(\omega), \tag{3.16}$$

$$\begin{aligned}\hat{P}_a(\omega) = {}& g^2\chi_m(\omega)\lambda_-(\omega)\lambda_+(\omega)\sqrt{\kappa}\,\hat{X}_{a,\rm in}(\omega)\\ &- g\,\chi_m(\omega)\lambda_-(\omega)\sqrt{2\gamma_m}\,\big(\hat{F}_{\rm th}(\omega) + F_{\rm ext}(\omega)\big)\\ &- G_{cs}\lambda_-(\omega)\,\hat{X}_S(\omega) + \lambda_-(\omega)\sqrt{\kappa}\,\hat{P}_{a,\rm in}(\omega),\end{aligned} \tag{3.17}$$

$$\hat{X}_S(\omega) = -\,\Delta_{qe}\,\chi_S(\omega)\,\hat{P}_S(\omega) + \chi_S(\omega)\sqrt{\gamma_{qE}}\,\hat{X}_{S,\rm in}(\omega), \tag{3.18}$$

$$\begin{aligned}\hat{P}_S(\omega) = {}& -\,G_{cs}\,\xi(\omega)\lambda_+(\omega)\sqrt{\kappa}\,\hat{X}_{a,\rm in}(\omega) -\\ &- \chi'_S(\omega)\sqrt{\gamma_{qE}}\,\hat{X}_{S,\rm in}(\omega) + \xi(\omega)\sqrt{\gamma_{qE}}\,\hat{P}_{S,\rm in}(\omega).\end{aligned} \tag{3.19}$$

where,

$$\begin{aligned}&\chi_m(\omega) = \frac{\Omega}{\Omega^2 - \omega^2 + i\gamma_m\omega}, \qquad \chi_a(\omega) = \frac{1}{i\omega + \kappa/2},\\ &\chi_S(\omega) = \frac{1}{i\omega + \gamma_{qE}/2}, \quad \xi(\omega) = \Big(i\omega + \frac{\gamma_{qE}}{2} + \Delta_{qe}^2\,\chi_S\Big)^{-1},\\ &\chi'_S(\omega) = -\,\Delta_{qe}\,\xi(\omega)\,\chi_S(\omega), \lambda_\pm(\omega) = \Big(\chi_a^{-1}(\omega) \mp 2\mathcal{G}\Big)^{-1},\\ &g = \sqrt{2}\,g_0\,\alpha, \qquad G'_{cs} = \sqrt{2}\,G_{cs}\,\alpha_s.\end{aligned}$$

Here, $\Delta_{qe} = \omega_L - \omega_{qe}$ is the drive–QD detuning, γ_{qE} is the collective QD linewidth, and α (α_s) are the steady-state cavity (QD) amplitudes obtained from the linearized steady-state equations. The external and thermal forces are conveniently expressed in dimensionless form as $F_{\rm ext} = \frac{f_{\rm ext}}{\sqrt{\hbar m\Omega\gamma_m}}$, $F_{\rm th} = \frac{f_{\rm th}}{\sqrt{\hbar m\Omega\gamma_m}}$, where $f_{\rm ext}$ and $f_{\rm th}$ denote the physical external and thermal forces, respectively [3]. The rescaled thermal Brownian force obeys the correlation $\langle F_{\rm th}(t)F_{\rm th}(t')\rangle = \bar{n}\,\delta(t-t')$, with $\bar{n} = \frac{K_BT}{\hbar\Omega}$, being the mean thermal phonon number of the mechanical mode [70].

3.3 Force sensing with coherent quantum noise cancellation

When the external force F_{ext} acts on the movable mirror, it displaces the mechanical oscillator and thereby changes the cavity length. This modulation of the cavity length imprints a phase shift on the intracavity and output optical fields. To quantify this effect, we solve the linearized Langevin equations in the frequency domain and obtain the phase quadrature of the intracavity field, $P_a(\omega)$ (see Appendix D). The corresponding output phase quadrature is then given by the standard input–output relation

$$P_a^{\text{out}}(\omega) = \sqrt{\kappa}\, P_a(\omega) - P_a^{\text{in}}(\omega), \tag{3.20}$$

where κ is the cavity decay rate and $P_a^{\text{in}}(\omega)$ denotes the input phase quadrature. This can be expressed as,

Then

$$\begin{aligned} P_a^{\text{out}}(\omega) = & -\, g\,\chi_m(\omega)\,\lambda_-(\omega)\,\sqrt{2\gamma_m\kappa}\,\big[\hat{F}_{\text{th}}(\omega) + F_{\text{ext}}(\omega)\big] + \\ & \big[g^2\chi_m(\omega) + G_{cs}^2\chi_S'(\omega)\big]\,\lambda_+(\omega)\lambda_-(\omega)\,\kappa\,\hat{x}_{a,\text{in}}(\omega) + \\ & \big(\lambda_-(\omega)\kappa - 1\big)\hat{p}_{a,\text{in}}(\omega) - G_{cs}\lambda_-(\omega)\sqrt{\kappa\gamma_{qE}} \\ & \Big[\chi_S(\omega)\big(\Delta_{qe}\chi_S'(\omega) + 1\big)\hat{x}_{S,\text{in}}(\omega) \\ & + \chi_S'(\omega)\hat{P}_{S,\text{in}}(\omega)\Big]. \end{aligned} \tag{3.21}$$

where,

$$\chi_S' = -\Omega\chi_S\xi = \frac{\Omega}{\Omega^2 - \omega^2 + i\omega\gamma_{qE} + \gamma_{qE}^2/4} \tag{3.22}$$

$$\chi_S = \frac{1}{i\omega + \gamma_{qE}/2} \tag{3.23}$$

$$\chi_m = \frac{\Omega}{\Omega^2 - \omega^2 + i\gamma_m\omega} \tag{3.24}$$

The second term of $P_a^{out}(\omega)$ corresponds to the back-action noise [3, 44]. For significant noise reduction, we aim to eliminate the back-action noise completely [64, 70]. Thus complete back-action cancellation requires

$$g^2\chi_m(\omega) + G_{cs}^2\chi_S'(\omega) = 0, \tag{3.25}$$

This is the CQNC condition and it requires that $g = G_{cs}$ and $\chi_m(\omega) = -\chi_S'(\omega)$ (ideal matching). This implies that: (i) the response of the mechanical oscillator to the back-action noise exactly equal in magnitude and opposite in sign to that of the QD-ensemble mode in the system, and (ii) the optomechanical coupling is equal to the effective cavity–QD-ensemble coupling of the hybrid system.

Under this condition, $P_a^{out}(\omega)$ becomes,

$$\begin{aligned} P_a^{\text{out}}(\omega) = & - g\,\chi_m(\omega)\,\lambda_-(\omega)\,\sqrt{2\gamma_m\kappa}\,\big[\hat{F}_{\text{th}}(\omega) + F_{\text{ext}}(\omega)\big] \\ & + \big(\lambda_-(\omega)\kappa - 1\big)\hat{p}_{a,\text{in}}(\omega) - G_{cs}\lambda_-(\omega)\sqrt{\kappa\gamma_{qE}} \\ & \Big[\chi_S(\omega)\big(\Delta_{qe}\chi'_S(\omega) + 1\big)\hat{x}_{S,\text{in}}(\omega) \\ & + \chi'_S(\omega)\hat{P}_{S,\text{in}}(\omega)\Big]. \end{aligned} \tag{3.26}$$

With re-arranging the terms we can write this as follows

$$F_{\text{ext}}(\omega) + \hat{F}_{\text{add}}(\omega) = \frac{-1}{g\,\chi_m(\omega)\,\lambda_-(\omega)\,\sqrt{2\gamma_m\kappa}}\,\hat{p}_a^{\text{out}}(\omega), \tag{3.27}$$

with the added force as

$$\begin{aligned} \hat{F}_{\text{add}}(\omega) = & \hat{F}_{\text{th}}(\omega) - \frac{\lambda_-(\omega)\kappa - 1}{g\,\chi_m(\omega)\,\lambda_-(\omega)\,\sqrt{2\gamma_m\kappa}}\hat{p}_{a,\text{in}}(\omega) \\ & + \frac{G_{cs}\chi'_S(\omega)\sqrt{\kappa\gamma_{qE}}}{g\,\chi_m(\omega)\,\sqrt{2\gamma_m\kappa}}\,\Big[\tfrac{\chi_S(\omega)}{\chi'_S(\omega)}\big(\Delta_{qe}\chi'_S(\omega) + 1\big)\hat{x}_{S,\text{in}}(\omega) \\ & + \hat{p}_{S,\text{in}}(\omega)\Big]. \end{aligned} \tag{3.28}$$

Examining the spectral density of the added force provides information about the sensitivity and overall performance of the system under the CQNC condition.

3.4 Results and Discussions

We now proceed to the numerical analysis of the power spectral density which provides a measure of the force sensitivity [44]. To evaluate the performance of the proposed CQNC-based hybrid system, we compare its noise spectral density with that of a standard optomechanical system, which serves as a natural baseline. Since conventional optomechanical force sensing is fundamentally limited by radiation-pressure back-action near the SQL, this comparison provides a direct and physically meaningful way to quantify the noise-suppression advantage of the present scheme.

The force sensitivity can be defined as, $s_F(\omega) = \sqrt{\hbar m_s \gamma_m}\, S_F(\omega)$, where, $S_F(\omega)$ quantifies the noise spectral density for an equivalent input force, F. Thus, a lower value of $S_F(\omega)$ corresponds directly to an improved force sensitivity.

Following Ref. [70], the spectral density of the added noise for our setup (see Equation (3.28)) is defined as follows.

$$S_F^{add}(\omega)\delta(\omega-\omega') = \frac{1}{2}(\langle \hat{F}_{add}(\omega)\hat{F}_{add}(-\omega)\rangle + c.c.) \tag{3.29}$$

Using this we obtain the expression of spectral density of the added noise as

$$\begin{aligned} S_F^{add} =& \frac{K_B T}{\hbar\Omega} + \frac{1}{2}\frac{1}{g^2|\chi_m(\omega)|^2(2\gamma_m\kappa)}\left|\frac{\lambda_-(\omega)\kappa - 1}{\lambda_-(\omega)}\right|^2 \\ &+ \frac{1}{2}\frac{\omega^2+\Omega^2+\gamma_{qE}^2/4}{\Omega^2} \end{aligned} \tag{3.30}$$

To study the CQNC-induced reduction of the quantum measurement noise, we neglect the Brownian thermal-force background in the main spectral comparison, following the standard practice in conceptual CQNC analyses [44, 5]. However, we stress that this approximation is justified only when the effective thermal occupation of the mechanical mode is sufficiently suppressed, for example by cryogenic operation and sideband or feedback cooling such that $n_{\text{eff}} \lesssim 1$ [20, 4, 62, 17, 65, 49]. Furthermore, it has been shown that coupling a cavity to a two-level quantum system can open additional damping channels that supplement radiation-pressure sideband cooling [65]. Since the QD ensemble can be modeled as a collection of two-level systems, analogous mechanisms can contribute to effective phonon suppression in cavity–QD systems [49], although a quantitative estimate for the specific QD platform proposed here remains a subject of future experimental investigation. The present work therefore focuses on the quantum-noise-limited regime as a theoretical illustration of the CQNC mechanism, assuming that $n_{\text{eff}} \lesssim 1$ has been achieved by the above means. By minimizing the spectral density, we obtain the minimum noise spectral density for our proposed scheme in hybrid optomechanical model as,

$$S_{F,CQNC} = \frac{1}{2}\frac{\omega^2+\Omega^2+\gamma_{qE}^2/4}{\Omega^2} \tag{3.31}$$

We compare the efficiency of our hybrid system under CQNC condition by comparison with the standard optomechanical system. For such standard optomechanical system, the noise spectral density can be written as [4],

$$S_F(\omega) = \frac{K_B T}{\hbar\Omega} + \frac{1}{2}\frac{\kappa}{\gamma_m}\frac{1}{g^2|\chi|^2}\frac{1}{4} + 4g^2\frac{1}{\kappa\gamma_m} \tag{3.32}$$

The first term indicates the contribution of the thermal noise, second term represents shot noise and the third term corresponds to the back-action noise. Minimizing this with respect to the laser power, we can get the SQL value,

$$S_{F,SQL} = \frac{1}{\gamma_m|\chi_m|} \tag{3.33}$$

Here, the thermal force is considered to be negligibly small. The dip of the noise spectral density occurs at an optomechanical coupling strength,

$$g_{SQL} = \frac{\sqrt{\kappa}}{2\sqrt{|\chi_m|}} \tag{3.34}$$

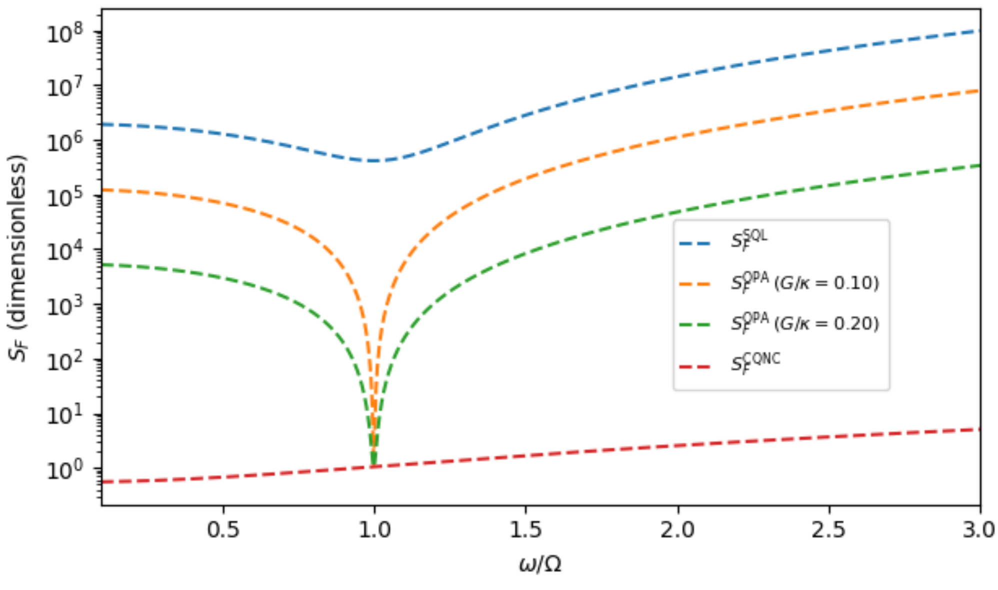

Figure 3.2: Noise Power Spectral Density for standard optomechanical system, optomechanical system with OPA for parametric gain $G/\kappa = 0, 0.1$ and 0.2 and optomechanical hybrid system with CQNC scheme. The spectral densities are normalized by $\hbar m\omega_m\gamma_m$ in order to be represented in units of N^2Hz^{-1}. The different lines in the plot represent the standard optomechanical system (blue curve), the hybrid electro-optomechanical system with OPA (orange and green curves), and the hybrid system with the CQNC scheme (the red line at the bottom). The parameters used : $g_0 = 10 \times 2\pi$ Hz, $\Omega = 10 \times 2\pi$ MHz, $\gamma_m = 100 \times 2\pi$ Hz, $\kappa = 1 \times 2\pi$ MHz, $P_L = 10^6$ pW, $\omega_L = 384 \times 2\pi$ THz

.

We first evaluate the noise spectral density at the mechanical resonance, $\omega = \Omega$, where

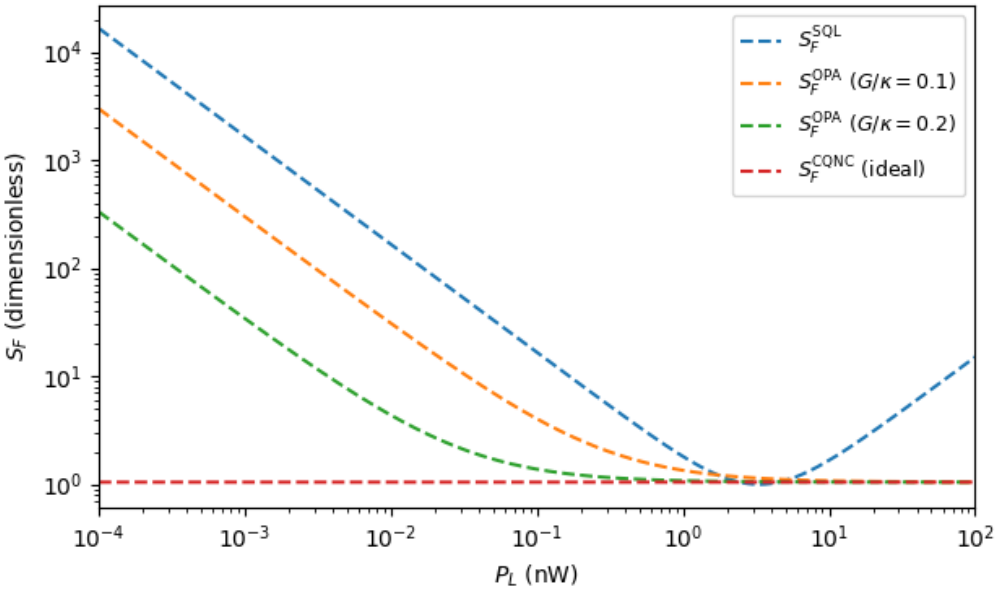

Figure 3.3: Noise Power Spectral Density at resonance (i.e., $\omega = \Omega$) as a function of laser driving power for the standard optomechanical system and the electro-optomechanical hybrid system with the CQNC scheme. The blue line represents the standard optomechanical system, whereas, the orange and green curve indicate hybrid system with OPA gain $G/\kappa = 0.1$ and 0.2 respectively. (Parameters are the same as in Fig. 3.2.)

a pronounced dip is observed (Fig. 3.2). At resonance, the hybrid system yields nearly the same sensitivity for both OPA gain values, whether CQNC condition is absent or included. By contrast, the behavior changes remarkably away from resonance. Increasing the OPA gain from $G = 0.1$ to $G = 0.3$ leads to a clear reduction of the noise spectral density at off-resonant frequencies when compared with the standard optomechanical system, as reflected in the corresponding curves. In the presence of CQNC, the suppression becomes even more prominent and S_F is reduced by several orders of magnitude for frequencies both below and above $\omega = \Omega$. Thus it provides a strong noise reduction over a broad range of off-resonant frequencies beyond SQL.

We note that while the CQNC condition $\chi_m(\omega) = -\chi'_S(\omega)$ formally enables complete cancelation of the back-action in the ideal limit [70, 5], in practice this matching is achieved only over a finite frequency range due to the frequency dependence of the susceptibilities of the system.

We next examine how the noise power spectral density (PSD) depends on the input laser power, as shown in Fig. 3.3. The laser power is related to the optomechanical coupling via

Table 3.1: Parameters used in the numerical simulations of the hybrid optomechanical CQNC scheme.

Parameter	Description	Value
g_0	Single-photon optomechanical coupling	$10 \times 2\pi$ Hz
Ω	Mechanical resonance frequency	$10 \times 2\pi$ MHz
γ_m	Mechanical damping rate	$100 \times 2\pi$ Hz
κ	Cavity linewidth (decay rate)	$1 \times 2\pi$ MHz
P_L	Input laser power	10^6 μW
ω_L	Laser frequency	$384 \times 2\pi$ THz
$\mathcal{G}$	OPA gain parameter	$0,\ 0.1\kappa,\ 0.2\kappa$
g	Linearized optomechanical coupling	$5.6 \times 2\pi$ kHz
G_{cs}	Cavity–QD ensemble coupling	$5.6 \times 2\pi$ kHz
γ_{qE}	QD ensemble linewidth	$100 \times 2\pi$ Hz
Δ_{qe}	QD detuning	$10 \times 2\pi$ MHz

$P_L = 2\hbar\omega_L\kappa\left(\frac{g}{g_0}\right)^2$, so that the noise spectral density can be viewed directly as a function of P_L. For the standard optomechanical system (blue curve), the PSD initially decreases with increasing laser power, reaches an optimum minimum, and then increases again. In contrast, for the hybrid system incorporating the OPA (orange and green curves, corresponding to OPA gains $G = 0.1$ and $G = 0.3$, respectively), the PSD decreases with increasing laser power and, after attaining its minimum value, does not increase again. This behavior is a direct consequence of the CQNC mechanism, which cancels the back-action contribution even at relatively high driving powers and thereby prevents the PSD from rising.

Moreover, increasing the OPA gain from $G = 0.1$ to $G = 0.3$, shifts the minimum of the PSD to a lower value of P_L. Thus, within our framework, the use of an OPA with higher gain allows one to reach the minimal spectral density at reduced input power. We note that the role of the OPA in these figures is not to create the CQNC pathway itself, but rather to reduce the imprecision contribution and shift the optimum operating point to lower laser power. This is evident in the power-dependent plots, where increasing the OPA gain moves the minimum of the added-noise spectrum to smaller P_L, thereby allowing the CQNC-enhanced sensitivity to be reached in a more experimentally favourable low-power regime.

In contrast to conventional optomechanical force sensors, whose performance is ultimately constrained by measurement back-action near the standard quantum limit (SQL), the present QD–OPA hybrid platform combines CQNC-based back-action cancellation with OPA-assisted quadrature control, thereby enabling enhanced force sensitivity at reduced input laser power [64, 24]. Existing hybrid CQNC-based sensing schemes, such as those reported in the hybrid optomechanical systems equipped with atomic ensemble [58, 44] and superconducting qubit [52] have demonstrated substantial suppression of the added-noise spectral density. In the present work, we obtain a pronounced reduction of the added noise, together with the advantage that the optimum sensitivity can be reached in a lower-power operating regime.

To assess the feasibility of the proposed scheme, we note that the parameter regime considered in our analysis is consistent with existing experimental platforms. In particular, the values of the cavity linewidth, mechanical frequency and damping, and effective coupling strengths used in our calculations fall within the typical ranges reported in cavity optomechanics experiments. Semiconductor quantum-dot ensembles strongly coupled to optical cavities have been demonstrated in photonic crystal and microcavity systems, while high-quality optomechanical resonators are routinely realized using nanomechanical membranes or optomechanical crystals. Intracavity optical parametric amplification can also be implemented via nonlinear optical processes within the cavity.

Although these elements are typically realized separately, their combination within a hybrid platform is compatible with current experimental capabilities. The present work focuses on a theoretical analysis of such a configuration, assuming experimentally achievable parameter regimes. This indicates that the predicted CQNC-based noise suppression and enhanced force sensitivity can, in principle, be realized in current hybrid optomechanical systems (see, e.g., [4, 62, 17]).

3.5 Imperfect Matching

Ideally, perfect back-action noise cancellation requires accurate matching of both the coupling strengths and the susceptibilities of the relevant modes, as discussed in Sec 3.4. In practice, however, achieving exact equality of the decay rates and therefore of the susceptibilities is extremely challenging, and the coupling strengths can only be tuned with finite precision. Since some degree of mismatch in both couplings and decay rates is unavoidable, it is essential to investigate the performance of the system under imperfect CQNC conditions as well.

(i) $\gamma_{qE} \neq \gamma_m$

We first consider the situation in which all CQNC conditions are satisfied except for the matching of the decay rates. A small relative mismatch δ between the decay rates of the QD ensemble and the mechanical mode can be introduced as

$$\delta = \frac{\gamma_{qE} - \gamma_m}{\gamma_m}, \tag{3.35}$$

so that $\gamma_{qE} \neq \gamma_m$ when $\delta \neq 0$. In the presence of this mismatch, the noise spectral density modifies to

$$S_{F,\mathrm{CQNC}} = \frac{1}{2}\frac{\omega^2 + \Omega^2 + \gamma_{qE}^2/4}{\Omega^2} + \frac{\lambda_+^2 \kappa g^2}{\gamma_m}\left|1 + \frac{\chi_S'}{\chi_m}\right|^2. \tag{3.36}$$

In this expression, the first term typically dominates over the second. The corresponding noise spectral densities are plotted in Fig. 3.4. As seen there, the curves for perfect CQNC (red line) and for the decay-rate–mismatched case (black dashed curve) are almost indistinguishable. Thus, even for a moderate mismatch of the decay rates (here, $\delta = 0.3$), the spectral density remains very close to the ideal CQNC limit.

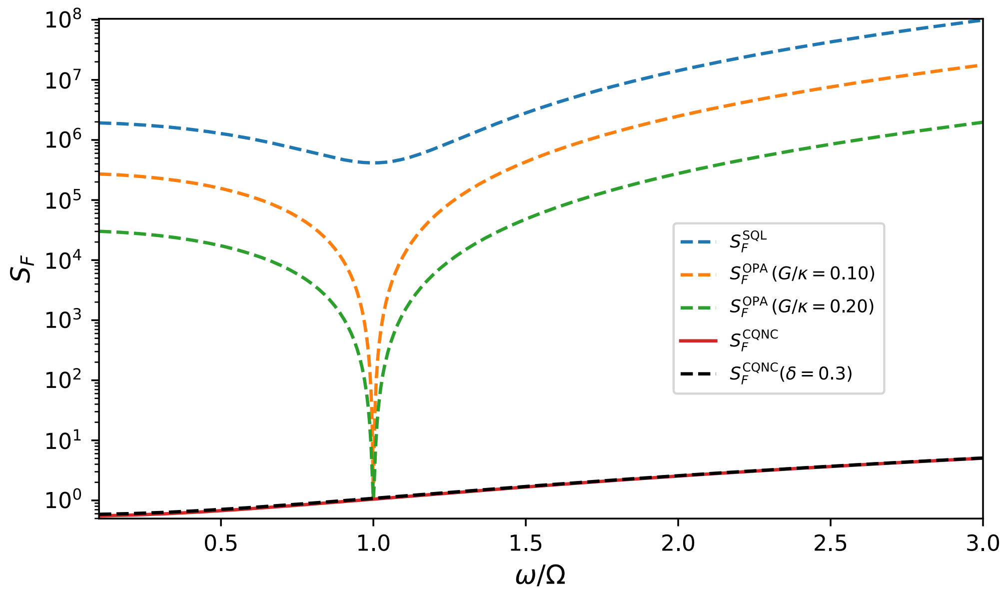

Figure 3.4: Variation of noise spectral density with frequency. The blue solid line represents SQL, the orange and green dashed lines indicates the noise spectral densities with the hybrid model with OPA gain 0.1 and 0.2 respectively. The red line is for perfect CQNC and the black dashed line represents the mismatched CQNC with $\delta = 0.3$.

(ii) $G' \neq g$

We now consider the case in which all CQNC conditions are satisfied except for the matching of the coupling strengths. A small relative mismatch ϵ between the effective coupling G' and the optomechanical coupling g is defined as

$$\epsilon = \frac{G' - g}{g}, \tag{3.37}$$

so that $G' \neq g$ when $\epsilon \neq 0$. In the presence of this coupling mismatch, the noise spectral density takes the form

$$S_{F,\text{CQNC}} = \frac{1}{2}\frac{\omega^2 + \Omega^2 + \gamma_{qE}^2/4}{\Omega^2} + \frac{\lambda_+^2 \kappa g^2}{\gamma_m}\left|1 - \frac{G'^2}{g^2}\right|^2. \tag{3.38}$$

The corresponding spectra are shown in Fig. 3.5. As illustrated there, the noise spectral density for perfect CQNC (purple curve) lies below that of the coupling-mismatched case (red curve), reflecting the presence of a small residual back-action term. Nonetheless, even under this imperfect condition, the noise level still surpasses the SQL by approximately five orders of magnitude.

Therefore from Fig. 3.4 and Fig. 3.5 it is evident that even with small deviation from the perfect CQNC conditions ($G' = g$ and $\gamma_{qE} = \gamma_m$), the hybrid system ensures the possibility of maintaining the advantage of CQNC scheme in hybrid electro-optomechanical system.

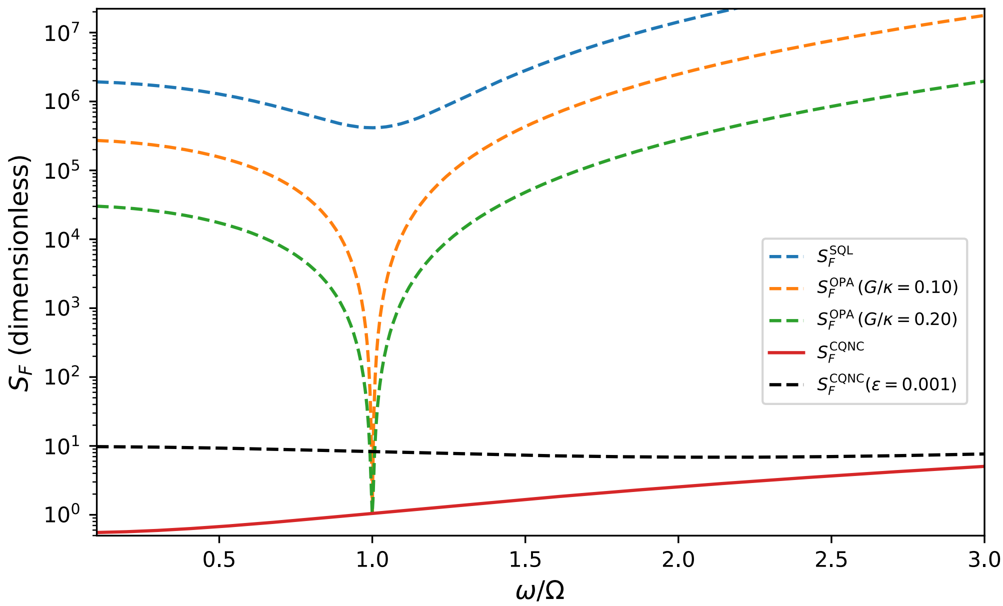

Figure 3.5: Variation of noise spectral density with frequency. The blue solid line represents SQL, the orange and green dashed lines indicates the noise spectral densities with the hybrid model with OPA gain 0.1 and 0.2 respectively. The red line is for perfect CQNC and the black line represents the mismatched CQNC with $\epsilon = 0.01$.

3.6 Conclusion

In this chapter, we have proposed and analyzed a hybrid cavity–optomechanical platform in which an ensemble of quantum dots is coupled to the intracavity optical mode, while an optical parametric amplifier (OPA) modifies the cavity quadratures. Working in the linearized regime, we derived the corresponding quantum Langevin equations and identified the conditions under which this system can implement coherent quantum noise cancellation in a solid-state hybrid setting. We showed that the CQNC scheme allows the force sensitivity to surpass the Standard Quantum Limit by up to six orders of magnitude over a broad frequency range. We further found that, as the OPA gain increases, the minimum of the added-noise spectral density is reached at progressively lower input laser power, indicating that optimal noise suppression can be achieved in a low-power operating regime.

From an experimental point of view, the realization of ideal CQNC remains challenging because it requires precise matching of the relevant coupling strengths as well as of the decay and dephasing rates. We therefore investigated the effect of imperfect parameter matching by considering both a mismatch between the optomechanical coupling and the effective cavity–QD-ensemble coupling, and unequal mechanical damping and QD-ensemble dephasing rates. In both cases, moderate deviations from the ideal matching conditions still lead to a substantial reduction of the added-noise spectral density compared to a standard optomechanical system without CQNC, while the SQL remains surpassed by several orders of magnitude.

Overall, these results show that a QD-ensemble-assisted hybrid optomechanical platform, combined with an intracavity OPA, provides a robust route toward strong backaction suppression in weak-force detection. More importantly, they show that a collective solid-state light–matter subsystem can serve as an effective auxiliary channel for coherent noise cancellation. In this way, the present analysis extends the CQNC framework to a cavity-QED-inspired hybrid architecture and highlights the broader promise of solid-state auxiliary systems for quantum-enhanced precision sensing.

Chapter 4

Quantum Noise Suppression Beyond the Standard Quantum Limit in a Hybrid Magnon-Cavity-Mechanical System[1]

4.1 Introduction

Hybrid cavity optomechanical systems provide a natural setting for interference-based noise-cancellation strategies, since additional degrees of freedom can be introduced and engineered to generate auxiliary response pathways [6, 61, 60, 59, 72]. In this context, magnon-assisted hybrid systems are particularly attractive. Magnon excitations are bosonic collective spin modes that can act as coherent ancillary degrees of freedom in hybrid quantum platforms [33, 31]. Their spectral selectivity and tunability make them promising candidates for interference-based control of measurement back-action. Recent progress in cavity optomagnonics has demonstrated photon–magnon coupling in whispering-gallery-mode and integrated photonic platforms, while related studies have explored microdisk geometries and mode engineering for enhancing cavity optomagnonic interactions [74, 16, 71, 68]. These developments make magnon modes particularly appealing as auxiliary channels for coherent quantum noise cancellation in force-sensing architectures.

[1]This work is under consideration for Phys. Rev. A (arXiv:2604.16136).

In this chapter, we study a hybrid cavity magnomechanical system in which a single optical cavity is coupled simultaneously to a mechanical oscillator through radiation pressure and to a magnon mode, while an intracavity optical parametric amplifier (OPA) is used to further tailor the measurement-noise spectrum. This system is interesting for two main reasons. First, the magnon mode provides an additional coherent pathway that can be engineered to interfere destructively with the usual radiation-pressure back-action channel. Second, the OPA modifies the cavity quadratures in a phase-sensitive way and can therefore improve sensing performance in experimentally relevant regimes. Together, these ingredients provide a natural platform for investigating how CQNC can be implemented in a magnonic hybrid setting and how such a realization compares with the existing hybrid schemes fo such system.

We show that, by appropriately tuning the cavity detuning, the effective linearized couplings, and the magnon linewidth, the system can realize coherent quantum noise cancellation [54]. In this regime, the magnon-mediated pathway contributes an equal-and-opposite response to the measurement back-action, thereby suppressing the added force noise and enabling below-SQL sensitivity near the mechanical resonance [44, 5, 58, 3, 70]. In this way, the present system provides a route beyond the more restrictive single-quadrature setting of conventional backaction-evading strategies.

To analyze this mechanism, we employ a linearized quantum-Langevin treatment and study the system response in the frequency domain. We derive analytical expressions for the output field quadratures and for the corresponding added-force noise spectrum, identify the matching conditions required for ideal CQNC, and examine the effect of realistic imperfections in coupling strengths and dissipation rates. We also analyze the role of the intracavity OPA and show that phase-sensitive gain reduces the imprecision background and shifts the optimal sensing regime toward lower input laser power [48, 44, 58]. Such low-power operation is experimentally attractive because it helps mitigate practical limitations associated with heating, instability, and technical noise in precision optomechanical measurements [13, 52].

Overall, the results presented in this chapter show that the combined action of a magnon ancilla and intracavity parametric amplification provides a promising route toward back-action-suppressed, low-power force sensing in hybrid quantum platforms. Compared with the more restrictive single-quadrature setting of conventional backaction-evading methods, the present CQNC-based architecture offers a broader route to force sensing beyond the SQL through direct suppression of radiation-pressure back-action. More broadly, this analysis shows that magnon modes can serve as tunable auxiliary channels for coherent noise cancellation, thereby extending the scope of CQNC-based sensing to a physically distinct and experimentally relevant class of hybrid systems.

4.2 System

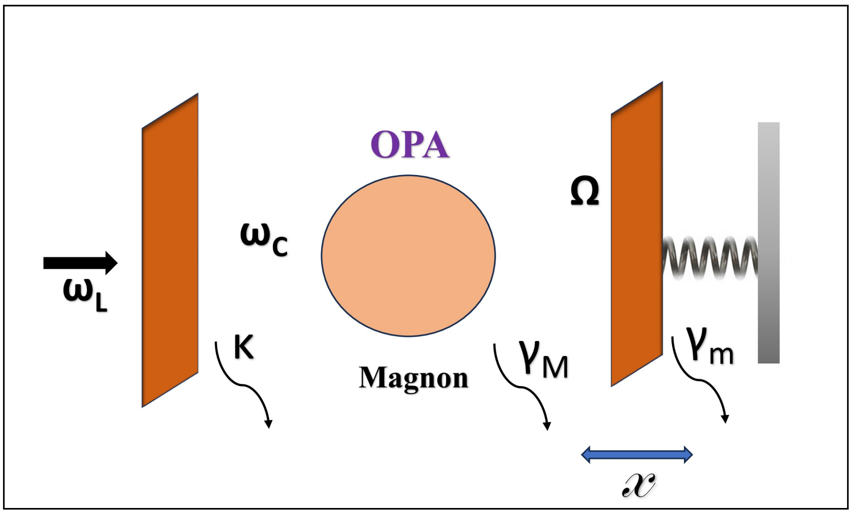

Figure 4.1: Schematic diagram of the hybrid cavity magnomechanical platform equipped with a magnon mode and an optical parametric amplifier (OPA).

We consider a hybrid cavity magnomechanical system consisting of a single cavity mode of resonance frequency ω_c, a mechanical oscillator of frequency Ω, and a magnon mode of frequency ω_M. The cavity field couples to the mechanical oscillator through the standard radiation-pressure interaction and to the magnon mode through a linearized cavity-magnon interaction. In addition, the cavity contains an intracavity OPA and is driven coherently by an external laser of frequency ω_L and input power P_L. A schematic of the setup is shown in Fig. 4.1.

The total Hamiltonian of the system can be written as

$$H = H_{\mathrm{OM}} + H_{\mathrm{OPA}} + H_{\mathrm{L}} + H_{\mathrm{M}}. \tag{4.1}$$

The optomechanical part is

$$H_{\mathrm{OM}} = \hbar\Omega\hat{b}^{\dagger}\hat{b} + \hbar\omega_c\hat{a}^{\dagger}\hat{a} - \hbar g_0\hat{a}^{\dagger}\hat{a}\,(\hat{b} + \hat{b}^{\dagger}), \tag{4.2}$$

where $\hat{a}$ ($\hat{a}^{\dagger}$) and $\hat{b}$ ($\hat{b}^{\dagger}$) are the annihilation (creation) operators of the cavity and mechanical modes, respectively, and g_0 denotes the single-photon optomechanical coupling strength.

The OPA contribution is

$$H_{\mathrm{OPA}} = i\hbar\mathcal{G}\left(\hat{a}^{\dagger 2}e^{i\theta} - \hat{a}^2 e^{-i\theta}\right), \tag{4.3}$$

where $\mathcal{G}$ is the parametric gain and θ is the pump phase. For simplicity, we take $\theta = 0$, so that

$$H_{\mathrm{OPA}} = i\hbar\mathcal{G}\left(\hat{a}^{\dagger 2} - \hat{a}^2\right). \tag{4.4}$$

The coherent laser drive is described by

$$H_{\mathrm{L}} = i\hbar E_L(\hat{a}^{\dagger} - \hat{a}), \tag{4.5}$$

where E_L is the amplitude of the driving field.

The magnonic part of the Hamiltonian is written as

$$H_{\mathrm{M}} = \hbar\omega_M\hat{M}^{\dagger}\hat{M} + \frac{\hbar G_{OM}}{2}(\hat{a} + \hat{a}^{\dagger})(\hat{M} + \hat{M}^{\dagger}), \tag{4.6}$$

where $\hat{M}$ ($\hat{M}^{\dagger}$) denotes the annihilation (creation) operator of the magnon mode, and G_{OM} is the cavity-magnon coupling strength.

Moving to the frame rotating at the drive frequency ω_L, and dropping constant terms, the total Hamiltonian becomes

$$\begin{aligned} H = &-\hbar\Delta_c\hat{a}^{\dagger}\hat{a} + \hbar\Omega\hat{b}^{\dagger}\hat{b} - \hbar\Delta_M\hat{M}^{\dagger}\hat{M} + i\hbar\mathcal{G}\left(\hat{a}^{\dagger 2}e^{i\theta} - \hat{a}^2 e^{-i\theta}\right) \\ &- \hbar g_0\hat{a}^{\dagger}\hat{a}(\hat{b} + \hat{b}^{\dagger}) + \frac{\hbar G_{OM}}{2}(\hat{a} + \hat{a}^{\dagger})(\hat{M} + \hat{M}^{\dagger}) \\ &+ i\hbar E_L(\hat{a}^{\dagger} - \hat{a}), \end{aligned} \tag{4.7}$$

where

$$\Delta_c = \omega_L - \omega_c, \qquad \Delta_M = \omega_L - \omega_M. \tag{4.8}$$

We now linearize the dynamics around the semiclassical steady state by writing each system operator as

$$\hat{A}(t) = \bar{A} + \delta\hat{A}(t), \tag{4.9}$$

where $\bar{A}$ denotes the steady-state mean value and $\delta\hat{A}(t)$ represents the corresponding quantum fluctuation. Retaining only terms up to first order in the fluctuations yields the linearized description of the system.

For each bosonic mode $A = a, b, M$, we define the amplitude and phase quadratures as

$$\hat{x}_A = \frac{\hat{A} + \hat{A}^\dagger}{\sqrt{2}}, \qquad \hat{p}_A = i\frac{\hat{A}^\dagger - \hat{A}}{\sqrt{2}}. \tag{4.10}$$

Similarly, for the input noise operators $\hat{A}_{\text{in}}$, we define

$$\hat{x}_{A,\text{in}} = \frac{\hat{A}_{\text{in}} + \hat{A}_{\text{in}}^\dagger}{\sqrt{2}}, \qquad \hat{p}_{A,\text{in}} = i\frac{\hat{A}_{\text{in}}^\dagger - \hat{A}_{\text{in}}}{\sqrt{2}}. \tag{4.11}$$

The input noises satisfy the Markovian correlations [66, 7, 23, 70]

$$\langle \hat{a}_{\text{in}}(t)\hat{a}_{\text{in}}^\dagger(t')\rangle = \langle \hat{b}_{\text{in}}(t)\hat{b}_{\text{in}}^\dagger(t')\rangle = \langle \hat{M}_{\text{in}}(t)\hat{M}_{\text{in}}^\dagger(t')\rangle = \delta(t - t'). \tag{4.12}$$

The resulting linearized quantum Langevin equations are

$$\dot{\hat{x}}_b = \Omega\hat{p}_b, \tag{4.13}$$

$$\dot{\hat{p}}_b = -\Omega\hat{x}_b - \gamma_m\hat{p}_b - g\hat{x}_a + \sqrt{2\gamma_m}\left(\hat{F}_{\text{th}} + F_{\text{ext}}\right), \tag{4.14}$$

$$\dot{\hat{x}}_a = \left(-\frac{\kappa}{2} + 2\mathcal{G}\right)\hat{x}_a + \sqrt{\kappa}\,\hat{x}_{a,\text{in}}, \tag{4.15}$$

$$\dot{\hat{p}}_a = -g\hat{x}_b + \left(-\frac{\kappa}{2} - 2\mathcal{G}\right)\hat{p}_a - G_{OM}\hat{x}_M + \sqrt{\kappa}\,\hat{p}_{a,\text{in}}, \tag{4.16}$$

$$\dot{\hat{x}}_M = -\frac{\gamma_M}{2}\hat{x}_M - \Delta_M\hat{p}_M + \sqrt{\gamma_M}\,\hat{x}_{M,\text{in}}, \tag{4.17}$$

$$\dot{\hat{p}}_M = -G_{OM}\hat{x}_a + \Delta_M\hat{x}_M - \frac{\gamma_M}{2}\hat{p}_M + \sqrt{\gamma_M}\,\hat{p}_{M,\text{in}}. \tag{4.18}$$

Here,

$$g = \sqrt{2}\,g_0\,\alpha, \tag{4.19}$$

with $\alpha = \langle\hat{a}\rangle$ denoting the steady-state intracavity field amplitude. The parameters γ_m, κ, and γ_M are the mechanical damping rate, cavity decay rate, and magnon damping rate, respectively. The terms $\hat{F}_{\text{th}}$ and F_{ext} denote the Brownian thermal force and the external force acting on the mechanical oscillator.

To obtain the response functions, we move to the frequency domain using the Fourier transform

$$\hat{O}(\omega) = \frac{1}{\sqrt{2\pi}}\int dt\,\hat{O}(t)e^{-i\omega t}. \tag{4.20}$$

The linearized Langevin equations then take the form

$$\hat{X}_b(\omega) = \chi_m(\omega)\left[-g\,\hat{X}_a(\omega) + \sqrt{2\gamma_m}\big(\hat{F}_{\text{th}}(\omega) + F_{\text{ext}}(\omega)\big)\right], \tag{4.21}$$

$$\hat{P}_b(\omega) = \frac{i\omega}{\Omega}\hat{X}_b(\omega), \tag{4.22}$$

$$\hat{X}_a(\omega) = \sqrt{\kappa}\,\lambda_+(\omega)\hat{X}_{a,\text{in}}(\omega), \tag{4.23}$$

$$\begin{aligned}\hat{P}_a(\omega) = {} & g^2\chi_m(\omega)\lambda_-(\omega)\lambda_+(\omega)\sqrt{\kappa}\,\hat{X}_{a,\text{in}}(\omega)\\ & - g\chi_m(\omega)\lambda_-(\omega)\sqrt{2\gamma_m}\big(\hat{F}_{\text{th}}(\omega) + F_{\text{ext}}(\omega)\big)\\ & - G_{OM}\lambda_-(\omega)\hat{X}_M(\omega) + \lambda_-(\omega)\sqrt{\kappa}\,\hat{P}_{a,\text{in}}(\omega),\end{aligned} \tag{4.24}$$

$$\hat{X}_M(\omega) = -\Delta_M\chi_M(\omega)\hat{P}_M(\omega) + \chi_M(\omega)\sqrt{\gamma_M}\,\hat{X}_{M,\text{in}}(\omega), \tag{4.25}$$

$$\begin{aligned}\hat{P}_M(\omega) = {} & -G_{OM}\,\xi_M(\omega)\lambda_+(\omega)\sqrt{\kappa}\,\hat{X}_{a,\text{in}}(\omega)\\ & - \chi'_M(\omega)\sqrt{\gamma_M}\,\hat{X}_{M,\text{in}}(\omega) + \xi_M(\omega)\sqrt{\gamma_M}\,\hat{P}_{M,\text{in}}(\omega).\end{aligned} \tag{4.26}$$

Here we have introduced the susceptibilities and auxiliary response functions

$$\chi_m(\omega) = \frac{\Omega}{\Omega^2 - \omega^2 + i\gamma_m\omega}, \tag{4.27}$$

$$\chi_a(\omega) = \frac{1}{i\omega + \kappa/2}, \tag{4.28}$$

$$\chi_M(\omega) = \frac{1}{i\omega + \gamma_M/2}, \tag{4.29}$$

$$\xi_M(\omega) = \left(i\omega + \frac{\gamma_M}{2} + \Delta_M^2\chi_M(\omega)\right)^{-1}, \tag{4.30}$$

$$\chi'_M(\omega) = -\Delta_M\xi_M(\omega)\chi_M(\omega), \tag{4.31}$$

$$\lambda_\pm(\omega) = \left(\chi_a^{-1}(\omega) \mp 2\mathcal{G}\right)^{-1}. \tag{4.32}$$

For later convenience, we also define the effective linearized cavity-magnon coupling

$$G'_{OM} = \sqrt{2}\,G_{OM}\,\alpha_M, \tag{4.33}$$

where $\alpha_M = \langle\hat{M}\rangle$ denotes the steady-state magnon amplitude.

The dimensionless external and thermal forces are defined as

$$F_{\text{ext}} = \frac{f_{\text{ext}}}{\sqrt{\hbar m\Omega\gamma_m}}, \qquad F_{\text{th}} = \frac{f_{\text{th}}}{\sqrt{\hbar m\Omega\gamma_m}}, \tag{4.34}$$

where f_{ext} and f_{th} are the corresponding physical forces [3]. The rescaled Brownian force satisfies

$$\langle F_{\rm th}(t)F_{\rm th}(t')\rangle = \bar{n}\,\delta(t-t'), \tag{4.35}$$

with

$$\bar{n} = \frac{k_B T}{\hbar\Omega}, \tag{4.36}$$

which is the mean thermal phonon number of the mechanical mode in the high-temperature limit [70].

The above set of equations forms the starting point for our analysis of force transduction, added-noise spectra, and the conditions required for coherent quantum noise cancellation in the hybrid cavity magnomechanical system.

4.3 Force sensing with coherent quantum noise cancellation

When a weak external force $F_{\rm ext}$ acts on the mechanical resonator, it displaces the movable mirror and thereby modulates the cavity length. This modulation is imprinted onto the phase quadrature of the intracavity field and can therefore be detected through the phase quadrature of the output field. To analyze this transduction process, we solve the linearized quantum Langevin equations in the frequency domain and obtain the intracavity phase quadrature $\hat{P}_a(\omega)$ (see Appendix E). The corresponding output phase quadrature follows from the standard input-output relation,

$$\hat{P}_a^{\rm out}(\omega) = \sqrt{\kappa}\,\hat{P}_a(\omega) - \hat{P}_{a,\rm in}(\omega), \tag{4.37}$$

where κ is the cavity decay rate and $\hat{P}_{a,\rm in}(\omega)$ denotes the input phase quadrature.

Substituting the frequency-domain solution for $\hat{P}_a(\omega)$ into Eq. (4.37), we obtain

$$\begin{aligned}
\hat{P}_a^{\rm out}(\omega) &= -g\,\chi_m(\omega)\,\lambda_-(\omega)\,\sqrt{2\gamma_m\kappa}\,\left[\hat{F}_{\rm th}(\omega) + F_{\rm ext}(\omega)\right] \\
&+ \left[g^2\chi_m(\omega) + G_{OM}^2\chi_M'(\omega)\right]\lambda_+(\omega)\lambda_-(\omega)\,\kappa\,\hat{X}_{a,\rm in}(\omega) \\
&+ \left[\lambda_-(\omega)\kappa - 1\right]\hat{P}_{a,\rm in}(\omega) \\
&- G_{OM}\lambda_-(\omega)\sqrt{\kappa\gamma_M}\Big[\chi_M(\omega)\big(\Delta_M\chi_M'(\omega)+1\big)\hat{X}_{M,\rm in}(\omega) \\
&+ \chi_M'(\omega)\hat{P}_{M,\rm in}(\omega)\Big].
\end{aligned} \tag{4.38}$$

Here,

$$\chi_M(\omega) = \frac{1}{i\omega + \gamma_M/2}, \qquad \chi'_M(\omega) = -\Delta_M\, \xi_M(\omega)\chi_M(\omega), \tag{4.39}$$

with $\xi_M(\omega)$ defined in Sec. 4.2. The first term in Eq. (4.38) contains the transduced signal and thermal force contribution, the second term represents the back-action contribution of the cavity mode, the third term corresponds to the input phase noise, and the final term arises from the magnon input noise.

The back-action term can be cancelled through destructive interference between the mechanical and magnon-mediated pathways. This is the essence of coherent quantum noise cancellation (CQNC) [64, 70, 3, 44]. The condition for complete cancellation of the back-action contribution is therefore

$$g^2\chi_m(\omega) + G_{OM}^2\chi'_M(\omega) = 0. \tag{4.40}$$

This condition implies that the mechanical response to radiation-pressure back-action is exactly compensated by the magnon-induced contribution. Physically, it requires both a matching of susceptibilities and an appropriate balance between the effective optomechanical and cavity-magnon couplings.

Under the CQNC condition, Eq. (4.38) reduces to

$$\begin{aligned}\hat{P}_a^{\mathrm{out}}(\omega) &= -g\,\chi_m(\omega)\,\lambda_-(\omega)\,\sqrt{2\gamma_m\kappa}\,\left[\hat{F}_{\mathrm{th}}(\omega) + F_{\mathrm{ext}}(\omega)\right] \\ &\quad + \left[\lambda_-(\omega)\kappa - 1\right]\hat{P}_{a,\mathrm{in}}(\omega) \\ &\quad - G_{OM}\lambda_-(\omega)\sqrt{\kappa\gamma_M}\Big[\chi_M(\omega)\big(\Delta_M\chi'_M(\omega) + 1\big)\hat{X}_{M,\mathrm{in}}(\omega) \\ &+ \chi'_M(\omega)\hat{P}_{M,\mathrm{in}}(\omega)\Big].\end{aligned} \tag{4.41}$$

It is then convenient to rewrite the output signal in terms of an equivalent added-force operator. Rearranging Eq. (4.41), we obtain

$$F_{\mathrm{ext}}(\omega) + \hat{F}_{\mathrm{add}}(\omega) = -\frac{\hat{P}_a^{\mathrm{out}}(\omega)}{g\,\chi_m(\omega)\,\lambda_-(\omega)\,\sqrt{2\gamma_m\kappa}}, \tag{4.42}$$

where the added force noise is given by

$$\begin{aligned}\hat{F}_{\text{add}}(\omega) = \hat{F}_{\text{th}}(\omega) &- \frac{\lambda_-(\omega)\kappa - 1}{g\,\chi_m(\omega)\,\lambda_-(\omega)\,\sqrt{2\gamma_m\kappa}}\,\hat{P}_{a,\text{in}}(\omega) \\ &+ \frac{G_{OM}\sqrt{\kappa\gamma_M}}{g\,\chi_m(\omega)\,\sqrt{2\gamma_m\kappa}}\Big[\chi_M(\omega)\big(\Delta_M\chi'_M(\omega)+1\big)\hat{X}_{M,\text{in}}(\omega) \\ &+ \chi'_M(\omega)\hat{P}_{M,\text{in}}(\omega)\Big].\end{aligned} \tag{4.43}$$

The spectral density associated with $\hat{F}_{\text{add}}(\omega)$ provides a direct measure of the force sensitivity of the system under CQNC conditions [44]. In the following section, we evaluate this added-force spectrum and compare the sensitivity of the present hybrid cavity magnomechanical scheme with that of conventional optomechanical sensing.

4.4 Results and Discussion

We now turn to a quantitative analysis of the force sensitivity of the proposed hybrid system through its added-force spectral density [44]. As a force-sensitivity measure, we use the force-referred noise

$$s_F(\omega) = \sqrt{\hbar m\Omega\gamma_m\, S_F(\omega)}, \tag{4.44}$$

where $S_F(\omega)$ denotes the dimensionless force-noise spectrum referred to the input force. A lower value of $S_F(\omega)$ therefore corresponds to better force sensitivity.

To assess the performance of the present scheme, we compare its force-noise spectrum with that of a standard optomechanical sensor. The added-force spectrum of the hybrid system is defined as [70]

$$S_F^{\text{add}}(\omega)\,\delta(\omega-\omega') = \frac{1}{2}\left[\langle\hat{F}_{\text{add}}(\omega)\hat{F}_{\text{add}}(-\omega)\rangle + \text{c.c.}\right]. \tag{4.45}$$

Using Eq. (4.43), the corresponding added-noise power spectral density takes the form

$$\begin{aligned}S_F^{\text{add}}(\omega) =&\frac{k_BT}{\hbar\Omega} + \frac{1}{2}\,\frac{1}{g^2|\chi_m(\omega)|^2(2\gamma_m\kappa)}\left|\frac{\lambda_-(\omega)\kappa-1}{\lambda_-(\omega)}\right|^2 \\ &+ \frac{1}{2}\,\frac{\omega^2+\Omega^2+\gamma_M^2/4}{\Omega^2}.\end{aligned} \tag{4.46}$$

The first term represents the Brownian thermal contribution, the second term corresponds to optical imprecision noise, and the last term is the residual contribution associated with the magnon-assisted CQNC channel.

Table 4.1: Representative experimentally accessible parameters for the hybrid cavity magnomechanical platform with a magnon ancilla.

Parameter	**Symbol**	**Typical value**
Cavity decay rate	κ	$2\pi \times 1$ MHz
Mechanical frequency	Ω	$2\pi \times 10$ MHz
Mechanical damping rate	γ_m	$2\pi \times 100$ Hz
Magnon linewidth	γ_M	$2\pi \times 200$ Hz
Single-photon optomechanical coupling	g_0	$2\pi \times 10$ Hz
Cavity-magnon coupling	G_{OM}	$2\pi \times 10$ Hz
OPA nonlinear gain	$\mathcal{G}$	$0.3\,\kappa$
OPA phase	θ	$0 - \pi$
Laser wavelength	λ_L	1064 nm
Input power	P_L	$10^{-3} - 10^{6}$ pW

In the following, we focus primarily on the measurement-induced contribution and neglect the Brownian term, as is commonly done in CQNC analyses when assessing the intrinsic quantum-limited sensitivity of the scheme [44, 5]. Under this approximation, minimizing Eq. (4.46) yields the CQNC-limited noise floor

$$S_{F,\mathrm{CQNC}}(\omega) = \frac{1}{2}\,\frac{\omega^2 + \Omega^2 + \gamma_M^2/4}{\Omega^2}. \tag{4.47}$$

For comparison, the force-noise spectrum of a standard cavity optomechanical sensor is given by [4]

$$S_F^{(\mathrm{std})}(\omega) = \frac{k_B T}{\hbar\Omega} + \frac{1}{2}\,\frac{\kappa}{\gamma_m}\,\frac{1}{g^2|\chi_m(\omega)|^2}\,\frac{1}{4} + \frac{4g^2}{\kappa\gamma_m}, \tag{4.48}$$

where the three terms arise from thermal noise, imprecision noise, and radiation-pressure backaction, respectively. Neglecting thermal noise and optimizing with respect to the drive strength gives the familiar SQL limit,

$$S_{F,\mathrm{SQL}}(\omega) = \frac{1}{\gamma_m|\chi_m(\omega)|}, \tag{4.49}$$

which is attained for

$$g_{\mathrm{SQL}} = \frac{\sqrt{\kappa}}{2\sqrt{|\chi_m(\omega)|}}. \tag{4.50}$$

Figure 4.2 compares the spectral densities of the standard optomechanical sensor, the OPA-assisted hybrid configuration, and the CQNC-enabled hybrid system. Around the mechanical resonance $\omega = \Omega$, all spectra exhibit a pronounced minimum. Near resonance, the OPA-assisted hybrid system already improves the sensitivity relative to the standard optomechanical

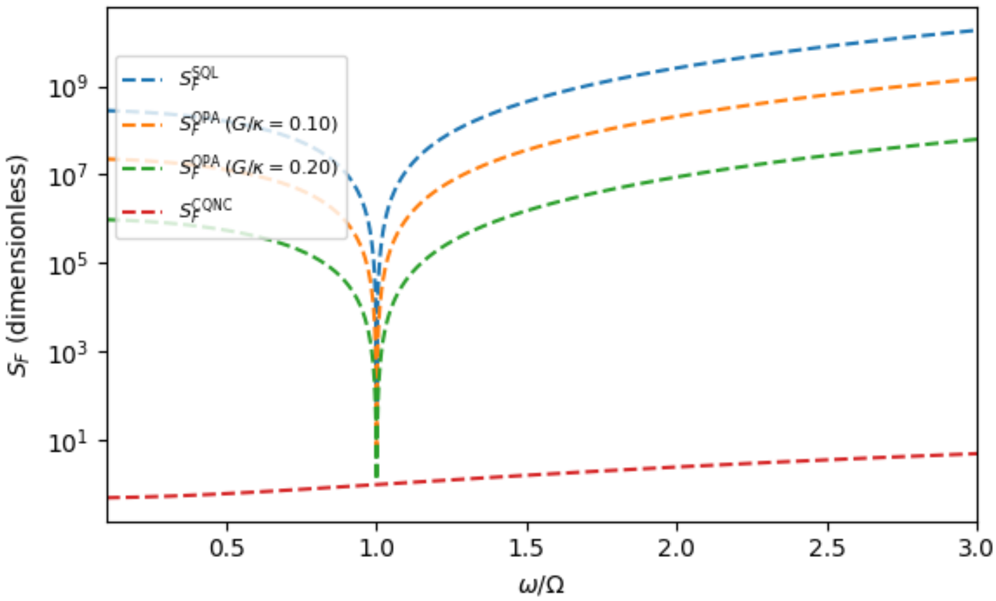

Figure 4.2: Force-referred noise PSD for (i) a standard optomechanical sensor (blue), (ii) an OPA-assisted hybrid sensor with $\mathcal{G}/\kappa = 0.1$ and 0.3 (orange and green), and (iii) the hybrid CQNC architecture (red). Spectra are normalized by $\hbar m\Omega\gamma_m$, so that the plotted quantity is expressed in units of $\mathrm{N}^2\,\mathrm{Hz}^{-1}$. Parameters are taken from Refs. [70, 58]: $g_0 = 300 \times 2\pi$ Hz, $\Omega = 300 \times 2\pi$ kHz, $\gamma_m = 30 \times 2\pi$ Hz, $\kappa = 2\pi$ MHz, $P = 100$ mW, and $\omega_L = 384 \times 2\pi$ THz.

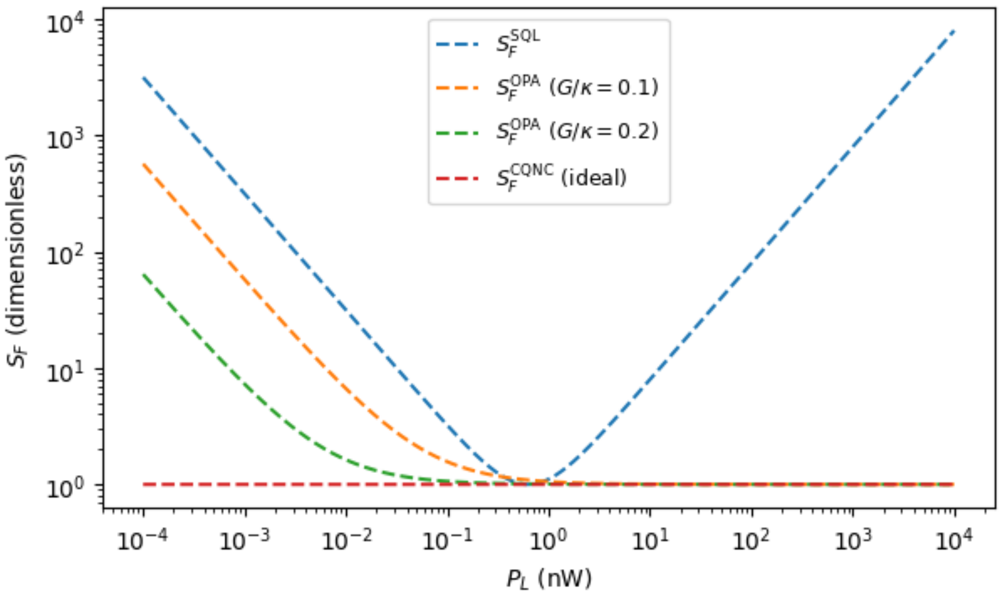

Figure 4.3: Resonant force-noise PSD at $\omega = \Omega$ as a function of laser power for the standard optomechanical sensor (blue) and the OPA-assisted hybrid scheme for $\mathcal{G}/\kappa = 0.1$ and 0.3 (orange and green). The remaining parameters are the same as in Fig. 4.2.

case. Once the CQNC condition is imposed, the suppression of radiation-pressure back-action becomes much more pronounced, and the resulting noise spectrum lies well below the standard SQL reference over a broad off-resonant frequency range. This demonstrates that the magnon-assisted CQNC channel can significantly extend the beloew-SQL operating bandwidth.

The role of the OPA is further illustrated in Fig. 4.3, which shows the resonant force-noise PSD as a function of laser power. For the standard optomechanical sensor, the noise initially decreases with increasing power because of the reduction of imprecision noise, reaches an optimum, and then rises again as radiation-pressure back-action becomes dominant. In contrast, the OPA-assisted hybrid configuration with CQNC maintains a decreasing trend up to its optimal operating point, without exhibiting the same pronounced back-action-induced upturn. Moreover, increasing the OPA gain shifts the minimum of the noise curve toward lower input power. This indicates that strong force sensitivity can be achieved in a lower-power regime, which is advantageous from an experimental perspective because it reduces the impact of heating and other power-related limitations [24].

Taken together, these results show that the combined action of the magnon ancilla and intracavity OPA yields a substantial reduction of the force-noise spectral density compared with a conventional optomechanical sensor. The proposed hybrid scheme therefore provides a viable route toward broadband and low-power below-SQL force sensing.

4.5 Imperfect Matching

The ideal CQNC condition requires precise matching of both the relevant susceptibilities and the effective coupling strengths. In practice, however, exact matching is difficult to achieve experimentally. The dissipation rates of the mechanical and magnon modes generally cannot be tuned independently with arbitrary precision, and the effective couplings are likewise subject to finite control accuracy. It is therefore important to examine the robustness of the scheme against realistic parameter mismatch.

(i) Decay-rate mismatch: $\gamma_M \neq \gamma_m$

We first consider the case in which all CQNC conditions are satisfied except for the matching of the decay rates. To quantify the deviation from the ideal case, we introduce the relative mismatch parameter

$$\delta = \frac{\gamma_M - \gamma_m}{\gamma_m}. \tag{4.51}$$

When $\delta \neq 0$, the magnon linewidth differs from the mechanical damping rate, and the noise floor is limited by the CQNC,

$$S_{F,\text{CQNC}}(\omega) = \frac{1}{2}\frac{\omega^2 + \Omega^2 + \gamma_M^2/4}{\Omega^2} \tag{4.52}$$

$$+ \frac{\kappa g^2}{\gamma_m}\left|\lambda_+(\omega)\right|^2 \left|1 + \frac{\chi_M'(\omega)}{\chi_m(\omega)}\right|^2. \tag{4.53}$$

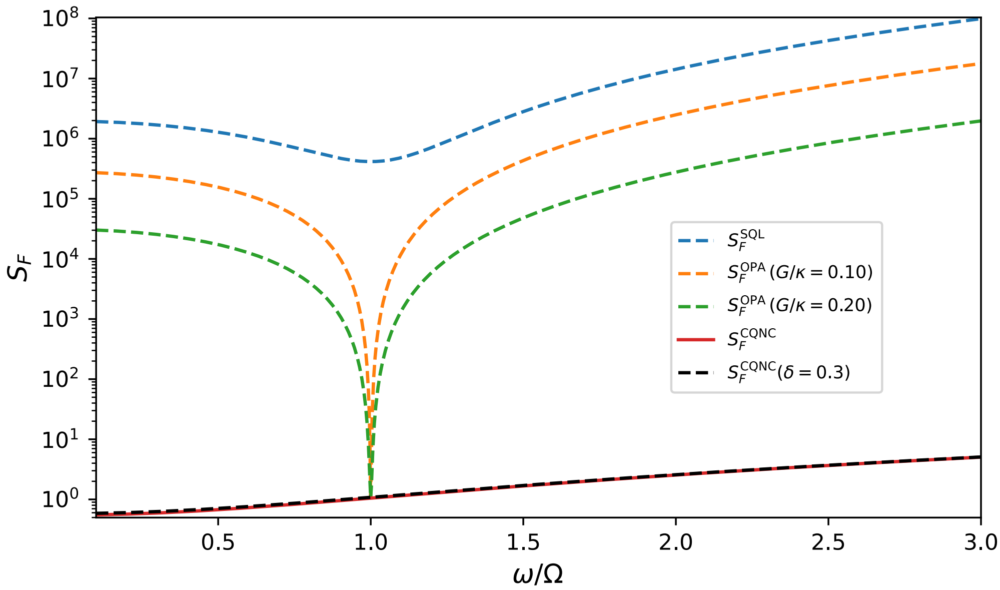

Figure 4.4: Variation of the force-noise spectral density with frequency in the presence of decay-rate mismatch. The blue solid line denotes the SQL, the orange and green dashed lines show the hybrid model with OPA gains $\mathcal{G}/\kappa = 0.1$ and 0.2, respectively, the red solid line corresponds to ideal CQNC, and the black dashed line represents the mismatched CQNC case with $\delta = 0.3$.

The corresponding spectra are shown in Fig. 4.4. The ideal CQNC curve and the spectrum obtained in the presence of a moderate decay-rate mismatch remain very close to one another, indicating that the performance degradation is weak. Even for $\delta = 0.3$, the added-force noise remains near the ideal CQNC benchmark and stays substantially below the SQL over the relevant frequency range. This shows that the proposed scheme is relatively insensitive to moderate mismatch in the dissipation rates.

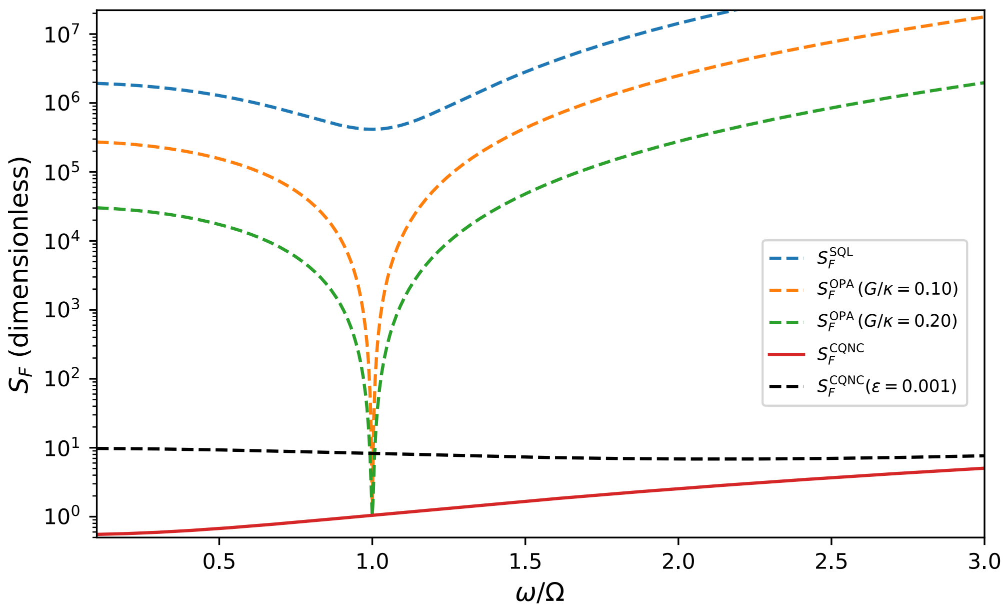

Figure 4.5: Variation of the force-noise spectral density with frequency in the presence of coupling mismatch. The blue solid line denotes the SQL, the orange and green dashed lines show the hybrid model with OPA gains $\mathcal{G}/\kappa = 0.1$ and 0.2, respectively, the red solid line corresponds to ideal CQNC, and the black solid line represents the mismatched CQNC case with $\epsilon = 0.01$.

(ii) Coupling mismatch: $G'_{OM} \neq g$

We next consider imperfect matching of the effective couplings. Let

$$\epsilon = \frac{G'_{OM} - g}{g}, \tag{4.54}$$

where G'_{OM} denotes the effective cavity-magnon coupling introduced in Sec. 4.2. When $\epsilon \neq 0$, the coupling-matching condition is not exactly satisfied, and the force-noise spectrum acquires a residual back-action contribution. In this case, the CQNC-limited spectrum becomes

$$S_{F,\mathrm{CQNC}}(\omega) = \frac{1}{2}\frac{\omega^2 + \Omega^2 + \gamma_M^2/4}{\Omega^2} + \frac{\kappa g^2}{\gamma_m}|\lambda_+(\omega)|^2 \left|1 - \frac{G'^2_{OM}}{g^2}\right|^2 . \tag{4.55}$$

The spectra are plotted in Fig. 4.5. As expected, the coupling mismatch introduces a residual back-action term, so that the imperfectly matched curve lies above the ideal CQNC result. Nevertheless, even in the presence of this mismatch, the hybrid scheme continues to outperform the off-resonant SQL by several orders of magnitude. Thus, although precise coupling matching is beneficial for optimal performance, moderate deviations do not destroy the main advantage of the CQNC mechanism.

Overall, Figs. 4.4 and 4.5 show that the proposed hybrid cavity magnomechanical platform retains the principal advantages of CQNC even when the ideal matching conditions are only approximately satisfied. This robustness strengthens the practical relevance of the scheme for experimentally realistic implementations.

4.6 Conclusion

In this work, we have investigated a hybrid cavity magnomechanical system in which the intracavity optical field is coupled simultaneously to a mechanical oscillator and a magnon mode, with the cavity further assisted by an intracavity optical parametric amplifier (OPA). Within the linearized regime, we derived the quantum Langevin equations, transformed the dynamics into the frequency domain, and obtained the corresponding output-field response relevant for force detection.

Our analysis shows that the magnon-assisted pathway can be used to realize coherent quantum noise cancellation (CQNC), whereby the magnon-induced response destructively interferes with the radiation-pressure back-action of the mechanical mode. As a result, the added-force noise can be significantly suppressed, enabling force sensitivity below the Standard Quantum Limit over a broad frequency range.

We also examined the robustness of the scheme against imperfect parameter matching. In particular, we showed that moderate mismatch in effective coupling strengths and dissipation rates does not destroy the main advantage of the CQNC mechanism. Even away from the ideal matching condition, the hybrid system retains substantial back-action suppression and continues to operate below the Standard Quantum Limit over an experimentally relevant bandwidth.

Taken together, these results identify the OPA-assisted cavity magnomechanical platform as a promising setting for back-action-suppressed weak-force detection. More broadly, the present work shows that magnonic degrees of freedom and phase-sensitive optical control can be combined within a hybrid architecture to enhance precision sensing and to go beyond the more restrictive single-quadrature setting of conventional backaction-evading schemes.

Chapter 5

Conclusion and Future Scope

This thesis has investigated force sensing beyond the Standard Quantum Limit in hybrid optomechanical systems through the framework of coherent quantum noise cancellation. The main goal has been to understand how an auxiliary hybrid degree of freedom can be used to suppress radiation-pressure back-action through destructive interference and thereby improve the sensitivity of continuous force detection. Within this general picture, the thesis has developed a common theoretical framework for CQNC-based sensing and applied it to three distinct hybrid platforms.

A central result of this work is that CQNC can be formulated in a unified way in terms of the output response and the corresponding added-noise spectrum of a hybrid optomechanical detector. Starting from the linearized description of cavity optomechanics, the analysis shows how weak external forces are transduced into the measured optical output, how the Standard Quantum Limit emerges from the usual imprecision and back-action trade-off, and how this trade-off can be modified when an additional coherent pathway is introduced. In all the systems studied here, the essential requirement for CQNC is the same: the auxiliary subsystem must generate a response to the relevant optical fluctuations that matches the ordinary back-action pathway with opposite sign over the frequency range of interest. When this condition is approximately satisfied, the radiation-pressure contribution to the added-force noise is strongly reduced and the sensitivity can go beyond the conventional SQL.

The first hybrid realization considered in the thesis was the electro-optomechanical system of Chapter 2, in which a mechanical resonator is coupled simultaneously to an optical cavity and to a superconducting qubit. This system provides a natural setting for implementing CQNC because it combines optical, mechanical, and electrical degrees of freedom within a single architecture. The analysis showed that the electromechanical channel can provide the auxiliary response needed to cancel the ordinary optomechanical back-action. As a result, the force sensitivity surpasses the Standard Quantum Limit over a broad off-resonant frequency range. An important feature of this chapter is the role of the intracavity optical parametric amplifier (OPA). Although the OPA does not itself produce CQNC, it improves the sensing conditions by lowering the added-noise floor and shifting the optimal operating point toward lower input laser power.

To study the possibility of further improvement in noise reduction, another hybrid OM system has been realized in the Chapter 3, which is basically hybrid optomechanical platform assisted by an ensemble of quantum-dots. In this case, the auxiliary subsystem is provided by a quantum-dot ensemble coupled to the intracavity optical mode, placing the CQNC problem in a solid-state cavity-QED setting. The analysis showed that the collective light-matter response of the QD ensemble can act as an effective auxiliary channel for back-action cancellation. By solving the linearized quantum Langevin equations and evaluating the force-referred noise spectrum, the chapter identified the conditions under which destructive interferenc eliminates the radiation-pressure contribution. The inclusion of an intracavity OPA again improves the practical operating regime by enhancing the low-frequency response and reducing the drive power required for optimal performance. This chapter also examined the effect of unequal dissipation and coupling mismatch, showing that substantial sensitivity improvement remains possible even when the ideal CQNC condition is only approximately fulfilled.

Then in chapter 4 we extended the work by considering a cavity magnomechanical system, wherein the optical cavity, in a similar way, couples simultaneously to a mechanical mode and to a magnon mode. Since we have already seen that the presence of OPA in the intracavity field reduces the required laser drive power, we again utlize cavity mode assisted by an intracavity OPA. This extension is especially attractive because magnons are coherent bosonic collective excitations with tunable spectral properties and controllable linewidth, making them particularly useful as auxiliary modes for interference-based noise engineering. The analysis shows that the magnon-induced susceptibility can be used to construct the auxiliary response required for CQNC and that, under suitable matching conditions, the magnon-mediated pathway cancels the ordinary radiation-pressure back-action at the detector output. Among the systems studied in this thesis, this platform yields the largest sensitivity enhancement, reaching improvement by up to nine orders of magnitude beyond the SQL in the relevant regime, whereas the systems with optomechanical system coupled to superconducting qubit and to an ensemble of quantum dots show noise spectral density approximately 4 orders and 6 orders of magnitude below SQL respectively. It also provides the clearest picture of robustness under nonideal conditions, since the influence of unequal dissipation rates and coupling mismatch were examined explicitly. This clarifies that even when it is not possible to achieve the ideal cancellation perfectly, the system retains strong performance advantages over experimentally relevant bandwidths.

Taken together, these three platform-specific studies show that the physical implementation of CQNC can vary widely while the central mechanism remains the same. The electromechanical, QD-ensemble, and magnomechanical systems are therefore not just separate examples, but three realizations of a similar design principle. In such cases, hybridization of the optomechanical system with the subsystem, makes it possible to create an additional coherent pathway that modifies the detector dynamics and suppresses measurement back-action through interference. At the same time, the comparison between these platforms also shows that the practical form of the auxiliary susceptibility, the available tuning knobs, and the dominant imperfections strongly depend on the chosen hybrid architecture. Also, we have analyzed and compared the noise spectral density and therefore the force sensitivity of all three systems. We have realized that each system has its own benefit. However, the later two systems shows better sensitivity, especially the magnon cavity-mechanical system emerges out to show the highest sensitivity among all three platforms. A second broad conclusion concerns the role of intracavity OPA. In all three systems, the OPA improves the practical usefulness of CQNC by reducing the imprecision background and moving the optimal sensing regime toward lower input power. This recurring feature suggests that phase-sensitive optical control is an important companion to interference-based back-action suppression in realistic hybrid sensing schemes.

The thesis also makes clear that CQNC is a nontrivial operating condition rather than an automatic consequence of hybrid coupling. The auxiliary response must be matched to the mechanical back-action channel with sufficient accuracy, and this matching can be affected by linewidth, dissipation, detuning, and coupling mismatch. For this reason, the present work has not been limited to idealized cancellation alone, but has also examined the robustness of the predicted sensitivity improvement under realistic imperfections. The overall picture that emerges is encouraging: although perfect cancellation is sensitive to parameter matching, substantial back-action suppression and beyond-SQL sensitivity can still be retained in experimentally meaningful regimes.

Beyond the individual systems studied here, the thesis points to a broader view of quantum sensing. In the usual picture, the SQL appears as the natural consequence of the trade-off between imprecision noise and measurement back-action in coherent probing. The present work shows that, once hybrid coherent dynamics are introduced, this trade-off can be reshaped at the level of the detector itself. From this perspective, hybrid optomechanical systems are not merely more complicated sensing devices, but flexible architectures in which the flow of quantum noise can be engineered.

Several directions naturally follow from this work. One important direction is the inclusion of additional technical noise sources, such as finite detection efficiency, laser phase noise, thermal instability, and material absorption, in order to understand fully how the predicted SQL-beating performance survives under laboratory conditions. A second direction is the optimization of bandwidth, since practical sensing applications often depend not only on the minimum noise at a single frequency but on performance over a wider spectral window. A third direction is the study of time-dependent and transient protocols, where coherent cancellation may interplay in nontrivial ways with pulsed driving, switching, or feedback. It would also be interesting to extend the present framework to other hybrid platforms, including additional cavity-QED and spin-based systems that may offer favorable coherence and tunability for auxiliary-channel engineering.

Another promising direction is the combination of CQNC with other quantum-enhanced sensing techniques. Since the present thesis already shows the usefulness of OPA-assisted operation, it is natural to ask how this can be combined with squeezed input fields, frequen dependent readout, or engineered dissipative channels. Such combinations may not only further improve sensitivity, but also enlarge the parameter window in which cancellation remains stable against imperfections.

In summary, this thesis has shown that coherent quantum noise cancellation provides a consistent and versatile route toward force sensing beyond the Standard Quantum Limit in hybrid optomechanical systems. By applying a common theoretical framework to electro-optomechanical, quantum-dot-assisted, and magnomechanical platforms, the work demonstrates that auxiliary hybrid degrees of freedom can be used to engineer effective anti-noise pathways and that intracavity parametric amplification can make the resulting sensing performance more experimentally favorable. The overall message is that beyond-SQL sensing need not rely on a single universal platform. Instead, it can emerge from carefully designed hybrid architectures in which measurement noise is shaped and suppressed at the dynamical level.

Appendix A

Hamiltonian

The Hamiltonian of the system without dissipation is given by [47],

$$\begin{aligned}\hat{H} =& \frac{[\hat{Q} - Q_{xq}(x)]^2}{2C_\Sigma(x)} - E_J(\Phi_{ext})cos\theta + \hbar\Omega\hat{b}^\dagger\hat{b} \\ & - \hbar\Delta\hat{a}^\dagger\hat{a} + \hbar g_0\hat{a}^\dagger\hat{a}(\hat{b}^\dagger + \hat{b}) + \hbar\eta(\hat{a}^\dagger + \hat{a}) \end{aligned} \quad (A.1)$$

where, $Q = 2e\hat{N}$ with $\hat{N}$ being the number operator for the transferred Cooper pairs, $Q_{xq}(x)$, is the gate charge produced by the external gate voltages V_x and V_q. The total capacitance of the qubit is $C_\Sigma(x) = 2C_J + C_q + C_x(x)$. The effective energy in the two parallel junctions is $E_J(\phi_{ext})cos\theta$ with energy $E_J/2$ each. Here, θ is the phase difference between the junctions and ϕ_{ext} is the external flux.

When the qubit and the optical cavity is driven, we get

$$\begin{aligned}\hat{H} =& \frac{\hbar\omega_q}{2}\sigma_z + \hbar\Omega_R\cos(\omega_d t)(\sigma_x\cos\phi - \sigma_z\sin\phi) \\ & + \hbar g(\hat{b}^\dagger + \hat{b})(\sigma_x\cos\phi - \sigma_z\sin\phi) + \hat{b}^\dagger\hat{b}\Omega \\ & - \hbar\Delta\hat{a}^\dagger\hat{a} + \hbar g_0\hat{a}^\dagger\hat{a}(\hat{b}^\dagger + \hat{b}) + \hbar\eta(\hat{a}^\dagger + \hat{a}) \end{aligned} \quad (A.2)$$

Where, $\tan\phi = \epsilon/\mathrm{E_J}$ and $\hbar\omega_q = \sqrt{\epsilon^2 + E_J^2}$.

At symmetyric point, $\delta N \simeq 0$ which corresponds to $\sin\phi = 0$ and $\cos\phi = 1$. Therefore the above Hamiltonian after applying RWA takes the form,

$$\hat{H} = \frac{\hbar\omega_q}{2}\sigma_z + \hbar\Omega_R\sigma_x \\ + \hbar g(\hat{b}^\dagger + \hat{b})\sigma_x + \hat{b}^\dagger\hat{b}\Omega \\ - \hbar\Delta\hat{a}^\dagger\hat{a} + \hbar g_0\hat{a}^\dagger\hat{a}(\hat{b}^\dagger + \hat{b}) + \hbar\eta(\hat{a}^\dagger + \hat{a}) \tag{A.3}$$

The Hamiltonian is then further simplified after making the transformation $\hat{a} = \alpha + \delta\hat{a}$ and $\hat{b} = \beta + \delta\hat{b}$ where, α and β are the respective steady states of cavity and mechanical modes and $\delta\hat{a}$, $\delta\hat{b}$ are the fluctuations around the corresponding mean value. Subsequently the fluctuation variables are re-expressed as, $\hat{a} \implies \delta\hat{a}$ and $\hat{b} \implies \delta\hat{b}$. Also rotating wave approximation has been taken care of. The Hamiltonian takes the form [47],

$$\hat{H} = -\hbar\frac{\Delta_q}{2}\sigma_z + \frac{1}{2}\hbar\Omega'_R\sigma_x + \hbar(G\hat{b}^\dagger + G^*\hat{b})\sigma_z + \hbar\Omega\hat{b}^\dagger\hat{b} \\ - \hbar\Delta_c\hat{a}^\dagger\hat{a} + \hbar(g_0\alpha\hat{a}^\dagger + g_0\alpha^*\hat{a})(\hat{b}^\dagger + \hat{b}) \\ + H_a + H_b \tag{A.4}$$

where, $H_a = \hbar g_0(\alpha^* a + \alpha a^\dagger)(\beta + \beta^*) + \hbar\eta(a + a^\dagger) - \hbar\Delta_c(\alpha^* a + \alpha a^\dagger)$ and $H_b = \hbar g_0|\alpha|^2(b + b^\dagger) + \hbar\Omega(\beta b^\dagger + \beta^* b)$. $\Omega'_R = \Omega_R + g(\beta + \beta^*)$

Here, σ_x and σ_z are Pauli matrices. In the low excitation limit, $\sigma_z \simeq \langle\sigma_z\rangle \simeq -1$ and σ^+ and σ^- satisfy the bosonic commutation relation $[\sigma^-, \sigma^+] = 1$.The bosonic annihilation (creation) operator $\hat{d}(\hat{d}^\dagger)$ are the corresponding to the two level system (qubit). Furthermore, following the same approach the qubit mode can be written as $\hat{d} = \bar{d} + \delta\hat{d}$.

Appendix B

Derivation of the constraint

The contribution to the back-action noise in the expression of F_{add} comes from the term involving x_a^{in}. Solving the Langevin equation, we obtain the expressions for all the quadratures (X and P) out of which P_a^{out} holds the most significance in our calculation. In the expression of P_a^{out}, the coefficient of x_a^{in} is,

$$\begin{aligned}[x_a^{in}]_{Coef} =& \sqrt{\kappa}(g^2\chi_m\lambda_+\lambda_-\sqrt{\kappa} \\ &+ \Omega\chi_d\zeta g G'\chi_m\sqrt{\kappa}\lambda_+\lambda_- g\chi_m)x_a^{in}\end{aligned} \tag{B.1}$$

Here,

$$\zeta = \frac{1}{i\omega + \frac{\Gamma}{2} + (\Delta_q + 2G\bar{\chi} - 2\Omega_R\bar{d} - 2G'^2\chi_m)\Delta_q\chi_d} \tag{B.2}$$

Also, the modified susceptibility of the electro-mechanical sub-system is given by, $\chi'_d = -\Delta_q\zeta\chi_d$. To match the susceptibilities of sub-systems, we consider $\Delta_q = \Omega$ then $\chi'_d = -\Omega\zeta\chi_d$. This gets further simplified for, $2G\bar{\chi} - 2\Omega_R\bar{d} - 2G'^2\chi_m = 0$. Consequently, the expression B.2 can be re-written as,

$$\zeta = \frac{1}{i\omega + \frac{\Gamma}{2} + \Delta_q^2\chi_d} \tag{B.3}$$

Hence $\chi'_d = \frac{\Omega}{\Omega^2 - \omega^2 + i\omega\Gamma + \Gamma^2/4}$. Furthermore, for $g^2\chi^2 = 1$, B.1 finally takes the form

$$\sqrt{\kappa}(g^2\chi_m\lambda_+\lambda_-\sqrt{\kappa}+\Omega\chi_d\zeta gG'\chi_m\sqrt{\kappa}\lambda_+\lambda_-g\chi_m)x_a^{in}$$
$$=\lambda_+\lambda_-\kappa(g^2\chi_m+G'^2\chi_{d'})x_a^{in} \tag{B.4}$$

This has been used in the expression of P_a^{out} (Eq. 2.50).

The above mentioned condition, $g^2\chi^2=1$ provides the constraint equation, which can be further simplified as,

$$\frac{g^2\Omega^2}{(\Omega^2-\omega^2)^2+\omega^2\gamma_m^2}=1 \tag{B.5}$$

After solving this Eq. (B.5) symbolically, we obtain frequency,

$$\omega_{1,2}=\pm\left[\Omega^2-\gamma_m^2/2-\sqrt{(4\Omega^2g^2-4\Omega\gamma_m^2+\gamma_m^4)/2}\right]^{1/2} \tag{B.6}$$
$$\omega_{3,4}=\pm\left[\Omega^2-\gamma_m^2/2+\sqrt{(4\Omega^2g^2-4\Omega\gamma_m^2+\gamma_m^4)/2}\right]^{1/2} \tag{B.7}$$

When one of the above constraints is satisfied by the parameters $\Omega,\ \gamma,\ g$, Eq. (B.4) will hold consequently.

Appendix C

Collective description of the QD ensemble

We consider an ensemble of N identical two-level quantum dots (QDs), each with ground state $|g_i\rangle$ and excited state $|e_i\rangle$, coupled to the cavity optical mode $\hat{a}$. The lowering and raising operators of the ith QD are defined as

$$\sigma_i^- = |g_i\rangle\langle e_i|, \qquad \sigma_i^+ = |e_i\rangle\langle g_i|. \tag{C.1}$$

The Hamiltonian describing the QD ensemble and its interaction with the cavity field can be written as

$$H_{QD} = \hbar \sum_{i=1}^{N} \omega_{qe}\sigma_i^+\sigma_i^- + \hbar g_0(\hat{a}+\hat{a}^\dagger)\sum_{i=1}^{N}(\sigma_i^- + \sigma_i^+), \tag{C.2}$$

where ω_{qe} is the transition frequency of the quantum dots and g_0 denotes the single-QD coupling strength to the cavity field.

It is convenient to introduce collective spin operators for the ensemble using Holstein-Primakoff [HP] [33] transformation,

$$\hat{S}^- = \frac{1}{\sqrt{N}}\sum_{j=1}^{N}\sigma_j^-, \qquad \hat{S}^+ = \frac{1}{\sqrt{N}}\sum_{j=1}^{N}\sigma_j^+, \tag{C.3}$$

which describe the symmetric collective excitation of the QDs. In terms of these operators, the Hamiltonian in (C.2) can be rewritten as

$$H_{\mathrm{QD}} = \hbar\omega_{qe}\hat{S}^+\hat{S}^- + \hbar G_{cs}(\hat{a}+\hat{a}^\dagger)\big(\hat{S}^- + \hat{S}^+\big), \tag{C.4}$$

Appendix D

Derivation of the cavity phase quadrature $P_a(\omega)$

Starting from the linearized quantum Langevin equations in the frequency domain, the relevant quadrature relations are

$$X_a(\omega) = \sqrt{\kappa}\,\lambda_+(\omega)\,X_{a,\text{in}}(\omega), \tag{D.1}$$

$$P_a(\omega) = g^2\chi_m(\omega)\lambda_-(\omega)\lambda_+(\omega)\sqrt{\kappa}\,X_{a,\text{in}}(\omega) - g\,\chi_m(\omega)\lambda_-(\omega) \tag{D.2}$$

$$\times\,\sqrt{2\gamma_m}\,F(\omega)$$

$$-\,G_{cs}\lambda_-(\omega)\,X_S(\omega) + \lambda_-(\omega)\sqrt{\kappa}\,P_{a,\text{in}}(\omega), \tag{D.3}$$

$$X_S(\omega) = -\Delta_{qe}\chi_S(\omega)\,P_S(\omega) + \chi_S(\omega)\sqrt{\gamma_{qE}}\,X_{S,\text{in}}(\omega). \tag{D.4}$$

The remaining relation is

$$P_S(\omega) = -G_{cs}\,\xi(\omega)\lambda_+(\omega)\sqrt{\kappa}\,X_{a,\text{in}}(\omega) - \chi'_S(\omega)\sqrt{\gamma_{qE}}\,X_{S,\text{in}}(\omega)$$

$$+\,\xi(\omega)\sqrt{\gamma_{qE}}\,P_{S,\text{in}}(\omega), \tag{D.5}$$

where

$$F(\omega) = F_{\text{th}}(\omega) + F_{\text{ext}}(\omega), \tag{D.6}$$

and

$$\chi'_S(\omega) = -\Delta_{qe}\,\xi(\omega)\chi_S(\omega). \tag{D.7}$$

Substituting (D.5) into (D.4), we obtain

$$X_S(\omega) = -\Delta_{qe}\chi_S(\omega)\Big[- G_{cs}\xi(\omega)\lambda_+(\omega)\sqrt{\kappa}\, X_{a,\text{in}}(\omega) \tag{D.8}$$

$$- \chi'_S(\omega)\sqrt{\gamma_{qE}}\, X_{S,\text{in}}(\omega) + \xi(\omega)\sqrt{\gamma_{qE}}\, P_{S,\text{in}}(\omega)\Big]$$

$$+ \chi_S(\omega)\sqrt{\gamma_{qE}}\, X_{S,\text{in}}(\omega). \tag{D.9}$$

Using $\chi'_S(\omega) = -\Delta_{qe}\xi(\omega)\chi_S(\omega)$, this simplifies to

$$X_S(\omega) = -G_{cs}\chi'_S(\omega)\lambda_+(\omega)\sqrt{\kappa}\, X_{a,\text{in}}(\omega) + \chi_S(\omega)\big[\Delta_{qe}\chi'_S(\omega) + 1\big] \tag{D.10}$$

$$\times \sqrt{\gamma_{qE}}\, X_{S,\text{in}}(\omega) + \chi'_S(\omega)\sqrt{\gamma_{qE}}\, P_{S,\text{in}}(\omega). \tag{D.11}$$

Finally, substituting (D.11) into (D.3), we obtain the cavity phase quadrature in the form

$$\begin{aligned} P_a(\omega) = \Big[g^2\chi_m(\omega) + G_{cs}^2\chi'_S(\omega)\Big]\lambda_-(\omega)\lambda_+(\omega)\sqrt{\kappa}\, X_{a,\text{in}}(\omega) \\ - g\,\chi_m(\omega)\lambda_-(\omega)\sqrt{2\gamma_m}\, F(\omega) \\ - G_{cs}\lambda_-(\omega)\sqrt{\gamma_{qE}}\,\Big[\chi_S(\omega)\big(\Delta_{qe}\chi'_S(\omega) + 1\big)\, X_{S,\text{in}}(\omega) \\ + \chi'_S(\omega)\, P_{S,\text{in}}(\omega)\Big] + \lambda_-(\omega)\sqrt{\kappa}\, P_{a,\text{in}}(\omega), \end{aligned} \tag{D.12}$$

Using the standard input–output relation

$$P_a^{\text{out}}(\omega) = \sqrt{\kappa}\, P_a(\omega) - P_{a,\text{in}}(\omega), \tag{D.13}$$

(D.12) directly leads to Eq. (21) in the main text.

Appendix E

Derivation of the cavity phase quadrature $\hat{P}_a(\omega)$

In this appendix, we derive the frequency-domain expression for the intracavity phase quadrature $\hat{P}_a(\omega)$, which is used in the main text to obtain the output phase quadrature and the corresponding added-force noise spectrum.

Starting from the linearized quantum Langevin equations in the frequency domain, the relevant quadrature equations are

$$\hat{X}_b(\omega) = \chi_m(\omega)\left[-g\,\hat{X}_a(\omega) + \sqrt{2\gamma_m}\,\hat{F}(\omega)\right], \tag{E.1}$$

$$\hat{X}_a(\omega) = \sqrt{\kappa}\,\lambda_+(\omega)\,\hat{X}_{a,\text{in}}(\omega), \tag{E.2}$$

$$\hat{P}_a(\omega) = -g\,\chi_m(\omega)\lambda_-(\omega)\sqrt{2\gamma_m}\,\hat{F}(\omega) + g^2\chi_m(\omega)\lambda_-(\omega) \tag{E.3}$$

$$* \,\lambda_+(\omega)\sqrt{\kappa}\,\hat{X}_{a,\text{in}}(\omega) - G_{OM}\lambda_-(\omega)\hat{X}_M(\omega) + \lambda_-(\omega)\sqrt{\kappa}\,\hat{P}_{a,\text{in}}(\omega), \tag{E.4}$$

$$\hat{X}_M(\omega) = -\Delta_M\chi_M(\omega)\hat{P}_M(\omega) + \chi_M(\omega)\sqrt{\gamma_M}\,\hat{X}_{M,\text{in}}(\omega), \tag{E.5}$$

$$\hat{P}_M(\omega) = -G_{OM}\xi_M(\omega)\lambda_+(\omega)\sqrt{\kappa}\,\hat{X}_{a,\text{in}}(\omega) - \chi'_M(\omega)\sqrt{\gamma_M}\,\hat{X}_{M,\text{in}}(\omega) \tag{E.6}$$

$$+\,\xi_M(\omega)\sqrt{\gamma_M}\,\hat{P}_{M,\text{in}}(\omega), \tag{E.7}$$

where

$$\hat{F}(\omega) = \hat{F}_{\text{th}}(\omega) + F_{\text{ext}}(\omega). \tag{E.8}$$

The susceptibilities and auxiliary response functions are defined as

$$\chi_m(\omega) = \frac{\Omega}{\Omega^2 - \omega^2 + i\gamma_m\omega}, \tag{E.9}$$

$$\chi_M(\omega) = \frac{1}{i\omega + \gamma_M/2}, \tag{E.10}$$

$$\xi_M(\omega) = \left(i\omega + \frac{\gamma_M}{2} + \Delta_M^2\chi_M(\omega)\right)^{-1}, \tag{E.11}$$

$$\chi'_M(\omega) = -\Delta_M\,\xi_M(\omega)\chi_M(\omega), \tag{E.12}$$

$$\lambda_\pm(\omega) = \left(\chi_a^{-1}(\omega) \mp 2\mathcal{G}\right)^{-1}. \tag{E.13}$$

To obtain a closed expression for $\hat{P}_a(\omega)$, we first substitute Eq. (E.7) into Eq. (E.5). This gives

$$\hat{X}_M(\omega) = -\Delta_M\chi_M(\omega)\begin{bmatrix} -G_{OM}\xi_M(\omega)\lambda_+(\omega)\sqrt{\kappa}\,\hat{X}_{a,\text{in}}(\omega) \\ -\chi'_M(\omega)\sqrt{\gamma_M}\,\hat{X}_{M,\text{in}}(\omega) \\ +\xi_M(\omega)\sqrt{\gamma_M}\,\hat{P}_{M,\text{in}}(\omega) \end{bmatrix}$$
$$+\chi_M(\omega)\sqrt{\gamma_M}\,\hat{X}_{M,\text{in}}(\omega). \tag{E.14}$$

Using the definition

$$\chi'_M(\omega) = -\Delta_M\xi_M(\omega)\chi_M(\omega),$$

this simplifies to

$$\begin{aligned}\hat{X}_M(\omega) = {} & G_{OM}\chi'_M(\omega)\lambda_+(\omega)\sqrt{\kappa}\,\hat{X}_{a,\text{in}}(\omega) \\ & + \chi_M(\omega)\left[1 + \Delta_M\chi'_M(\omega)\right]\sqrt{\gamma_M}\,\hat{X}_{M,\text{in}}(\omega) \\ & - \chi'_M(\omega)\sqrt{\gamma_M}\,\hat{P}_{M,\text{in}}(\omega).\end{aligned} \tag{E.15}$$

Substituting Eq. (E.15) into Eq. (E.4), we obtain

$$\hat{P}_a(\omega) = g^2\chi_m(\omega)\lambda_-(\omega)\lambda_+(\omega)\sqrt{\kappa}\,\hat{X}_{a,\text{in}}(\omega) \tag{E.16}$$

$$\begin{aligned}& - g\,\chi_m(\omega)\lambda_-(\omega)\sqrt{2\gamma_m}\,\hat{F}(\omega) \\ & - G_{OM}\lambda_-(\omega)\Big[G_{OM}\chi'_M(\omega)\lambda_+(\omega)\sqrt{\kappa}\,\hat{X}_{a,\text{in}}(\omega) \\ & + \chi_M(\omega)\big(1 + \Delta_M\chi'_M(\omega)\big)\sqrt{\gamma_M}\,\hat{X}_{M,\text{in}}(\omega) \\ & - \chi'_M(\omega)\sqrt{\gamma_M}\,\hat{P}_{M,\text{in}}(\omega)\Big] + \lambda_-(\omega)\sqrt{\kappa}\,\hat{P}_{a,\text{in}}(\omega).\end{aligned} \tag{E.17}$$

Collecting terms finally yields

$$\begin{aligned}\hat{P}_a(\omega) = &\left[g^2\chi_m(\omega) + G_{OM}^2\chi_M'(\omega)\right]\lambda_-(\omega)\lambda_+(\omega)\sqrt{\kappa}\,\hat{X}_{a,\text{in}}(\omega)\\ &- g\,\chi_m(\omega)\lambda_-(\omega)\sqrt{2\gamma_m}\,\hat{F}(\omega) + \lambda_-(\omega)\sqrt{\kappa}\,\hat{P}_{a,\text{in}}(\omega)\\ &- G_{OM}\lambda_-(\omega)\sqrt{\gamma_M}\left[\chi_M(\omega)\big(1 + \Delta_M\chi_M'(\omega)\big)\hat{X}_{M,\text{in}}(\omega) - \chi_M'(\omega)\hat{P}_{M,\text{in}}(\omega)\right].\end{aligned} \tag{E.18}$$

Equation (E.18) is the required expression for the intracavity phase quadrature in terms of the input noise operators and the total force. Using the standard input-output relation,

$$\hat{P}_a^{\text{out}}(\omega) = \sqrt{\kappa}\,\hat{P}_a(\omega) - \hat{P}_{a,\text{in}}(\omega), \tag{E.19}$$

one then obtains the output phase quadrature used in the main text to derive the added-force noise spectrum and the corresponding force-sensing sensitivity.

Bibliography

[1] J. Aasi et al. “Enhanced Sensitivity of the LIGO Gravitational Wave Detector by Using Squeezed States of Light”. In: Nature Photonics 7 (2013), pp. 613–619. DOI: 10.1038/nphoton.2013.177.

[2] B. P. Abbott et al. “Observation of Gravitational Waves from a Binary Black Hole Merger”. In: Physical Review Letters 116 (2016), p. 061102. DOI: 10.1103/PhysRevLett.116.061102.

[3] H Allahverdi et al. “Homodyne coherent quantum noise cancellation in a hybrid optomechanical force sensor”. In: Physical Review A 106.2 (2022), p. 023107.

[4] Markus Aspelmeyer, Tobias J. Kippenberg, and Florian Marquardt. “Cavity optomechanics”. In: Rev. Mod. Phys. 86 (4 Dec. 2014), pp. 1391–1452. DOI: 10.1103/RevModPhys.86.1391. URL: https://link.aps.org/doi/10.1103/RevModPhys.86.1391.

[5] F Bariani et al. “Atom-based coherent quantum-noise cancellation in optomechanics”. In: Physical Review A 92.4 (2015), p. 043817. DOI: 10.1103/PhysRevA.92.043817. URL: https://doi.org/10.1103/PhysRevA.92.043817.

[6] Sh Barzanjeh et al. “Entangling optical and microwave cavity modes by means of a nanomechanical resonator”. In: Physical Review A 84.4 (2011), p. 042342. DOI: 10.1103/PhysRevA.84.042342. URL: https://doi.org/10.1103/PhysRevA.84.042342.

[7] Rafael Benguria and Mark Kac. "Quantum langevin equation". In: Physical Review Letters 46.1 (1981), pp. 1–4. DOI: 10.1103/PhysRevLett.46.1. URL: https://doi.org/10.1103/PhysRevLett.46.1.

[8] Roy S Bondurant and Jeffrey H Shapiro. "Squeezed states in phase-sensing interferometers". In: Physical Review D 30.12 (1984), pp. 2548–2556. DOI: 10.1103/PhysRevD.30.2548. URL: https://doi.org/10.1103/PhysRevD.30.2548.

[9] K Børkje et al. "Observability of radiation-pressure shot noise in optomechanical systems". In: Physical Review A—Atomic, Molecular, and Optical Physics 82.1 (2010), p. 013818.

[10] Warwick P. Bowen and Gerard J. Milburn. Quantum Optomechanics. CRC Press, 2015.

[11] VB Braginsky. "Classical and quantum restrictions on the detection of weak disturbances of a macroscopic oscillator". In: Zh. Eksp. Teor. Fiz 53 (1967), pp. 1434–1441.

[12] Vladimir B. Braginsky and Farid Ya. Khalili. Quantum Measurement. Cambridge University Press, 1992.

[13] Tal Carmon et al. "Temporal Behavior of Radiation-Pressure-Induced Vibrations of an Optical Microcavity Phonon Mode". In: Physical Review Letters 94 (22 June 2005), p. 223902. DOI: 10.1103/PhysRevLett.94.223902. URL: https://doi.org/10.1103/PhysRevLett.94.223902.

[14] Daniel Carney et al. "Ultralight dark matter detection with mechanical quantum sensors". In: New Journal of Physics 23.2 (Mar. 2021), p. 023041. DOI: 10.1088/1367-2630/abd9e7. URL: https://dx.doi.org/10.1088/1367-2630/abd9e7.

[15] Carlton M. Caves. "Quantum-Mechanical Noise in an Interferometer". In: Physical Review D 23 (1981), pp. 1693–1708. DOI: 10.1103/PhysRevD.23.1693.

[16] C. Z. Chai et al. "Single-sideband microwave-to-optical conversion in high-Q magneto-optical whispering-gallery-mode microcavities". In: Photonics Research 10.3 (2022), pp. 820–826. DOI: 10.1364/PRJ.446335.

[17] Jasper Chan et al. "Laser Cooling of a Nanomechanical Oscillator into Its Quantum Ground State". In: Nature 478 (2011), pp. 89–92. DOI: 10.1038/nature10461.

[18] Yue Chang et al. "Multistability of electromagnetically induced transparency in atom-assisted optomechanical cavities". In: Physical Review A 83.6 (2011), p. 063826. DOI: 10.1103/PhysRevA.83.063826. URL: https://doi.org/10.1103/PhysRevA.83.063826.

[19] Simon Chelkowski et al. "Experimental characterization of frequency-dependent squeezed light". In: Physical Review A 71.1 (2005), p. 013806. DOI: 10.1103/PhysRevA.71.013806. URL: https://doi.org/10.1103/PhysRevA.71.013806.

[20] A. A. Clerk et al. "Introduction to Quantum Noise, Measurement, and Amplification". In: Reviews of Modern Physics 82 (2010), pp. 1155–1208. DOI: 10.1103/RevModPhys.82.1155.

[21] Stefan L. Danilishin and Farid Ya. Khalili. "Quantum Measurement Theory in Gravitational-Wave Detectors". In: Living Reviews in Relativity 15.5 (2012). DOI: 10.12942/lrr-2012-5.

[22] A. Mark Fox. "Solid-State Quantum Emitters". In: Advanced Quantum Technologies 8.2 (2025), p. 2300390. DOI: https://doi.org/10.1002/qute.202300390. eprint: https://advanced.onlinelibrary.wiley.com/doi/pdf/10.1002/qute.202300390. URL: https://advanced.onlinelibrary.wiley.com/doi/abs/10.1002/qute.202300390.

[23] Crispin W Gardiner and Matthew J Collett. "Input and output in damped quantum systems: Quantum stochastic differential equations and the master equation". In: Physical Review A 31.6 (1985), pp. 3761–3774. DOI: 10.1103/PhysRevA.31.3761. URL: https://doi.org/10.1103/PhysRevA.31.3761.

[24] Emanuel Gavartin, Pierre Verlot, and Tobias J Kippenberg. "A hybrid on-chip optomechanical transducer for ultrasensitive force measurements". In: Nature nanotechnology 7.8 (2012), pp. 509–514.

[25] B. Gayral and J. M. Gérard. "Photoluminescence experiment on quantum dots embedded in a large Purcell-factor microcavity". In: Phys. Rev. B 78 (23 Dec. 2008), p. 235306.

DOI: 10.1103/PhysRevB.78.235306. URL: https://link.aps.org/doi/10.1103/PhysRevB.78.235306.

[26] Claudiu Genes, David Vitali, and Paolo Tombesi. "Emergence of atom-light-mirror entanglement inside an optical cavity". In: Physical Review A 77.5 (2008), p. 050307. DOI: 10.1103/PhysRevA.77.050307. URL: https://doi.org/10.1103/PhysRevA.77.050307.

[27] Sohitri Ghosh et al. "Back-action evading impulse measurement with mechanical quantum sensors". In: arXiv preprint arXiv:1910.11892 (2019).

[28] Noel C. Giebink, Gary P. Wiederrecht, and Michael R. Wasielewski. "Strong exciton-photon coupling with colloidal quantum dots in a high-Q bilayer microcavity". In: Applied Physics Lette 98.8 (Feb. 2011), p. 081103. ISSN: 0003-6951. DOI: 10.1063/1.3558731. URL: https://doi.org/10.1063/1.3558731.

[29] Vittorio Giovannetti, Seth Lloyd, and Lorenzo Maccone. "Quantum-Enhanced Measurements: Beating the Standard Quantum Limit". In: Science 306.5700 (2004), pp. 1330–1336. DOI: 10.1126/science.1104149.

[30] H. Grote et al. "First Long-Term Application of Squeezed States of Light in a Gravitational-Wave Observatory". In: Physical Review Letters 110 (2013), p. 181101. DOI: 10.1103/PhysRevLett.110.181101.

[31] Pooja Kumari Gupta, Sampreet Kalita, and Amarendra K. Sarma. "Quantum-interference-induced magnon blockade and antibunching in a hybrid quantum system". In: J. Opt. Soc. Am. B 41.2 (Feb. 2024), pp. 447–455. DOI: 10.1364/JOSAB.507012. URL: https://opg.optica.org/josab/abstract.cfm?URI=josab-41-2-447.

[32] Tobias Heindel et al. "Quantum dots for photonic quantum information technology". In: Adv. Opt. Photon. 15.3 (Sept. 2023), pp. 613–738. DOI: 10.1364/AOP.490091. URL: https://opg.optica.org/aop/abstract.cfm?URI=aop-15-3-613.

[33] T. Holstein and H. Primakoff. "Field Dependence of the Intrinsic Domain Magneti[illegible]tion of a Ferromagnet". In: Phys. Rev. 58 (12 Dec. 1940), pp. 1098–1113. DOI: 10.1103/PhysRev.58.1098. URL: https://link.aps.org/doi/10.1103/PhysRev.58.1098.

[34] Hyochul Kim et al. "Strong coupling between two quantum dots and a photonic crystal cavity using magnetic field tuning". In: Opt. Express 19.3 (Jan. 2011), pp. 2589–2598. DOI: 10.1364/OE.19.002589. URL: https://opg.optica.org/oe/abstract.cfm?URI=oe-19-3-2589.

[35] H. J. Kimble et al. "Conversion of Conventional Gravitational-Wave Interferometers into Quantum Nondemolition Interferometers by Modifying Their Input and/or Output Optics". In: Physical Review D 65 (2001), p. 022002. DOI: 10.1103/PhysRevD.65.022002.

[36] Tobias J. Kippenberg and Kerry J. Vahala. "Cavity Optomechanics: Back-Action at the Mesoscale". In: Science 321.5893 (2008), pp. 1172–1176. DOI: 10.1126/science.1156032.

[37] Benjamin J Lawrie et al. "Quantum sensing with squeezed light". In: Acs Photonics 6.6 (2019), pp. 1307–1318.

[38] Bei-Bei Li et al. "Cavity Optomechanical Sensing". In: Nanophotonics 10.11 (2021), pp. 2799–2832. DOI: 10.1515/nanoph-2021-0256.

[39] Ming-Cui Li and Ai-Xi Chen. "Enhanced Entanglement in Hybrid Cavity Mediated by a Two-way Coupled Quantum Dot". In: Open Physics 18.1 (2020), pp. 14–23. DOI: 10.1515/phys-2020-0003. URL: https://doi.org/10.1515/phys-2020-0003.

[40] T Li, W Wang, and Xuexi Yi. "Enhancing the sensitivity of optomechanical mass sensors with a laser in a squeezed state". In: Physical Review A 104.1 (2021), p. 013521.

[41] Zeng-Xing Liu et al. "Quantum sensing with cavity optomechanics". In: Applied Physics Reviews 13.1 (2026).

[42] Peter Lodahl, Sahand Mahmoodian, and Søren Stobbe. "Interfacing single photons and single quantum dots with photonic nanostructures". In: Rev. Mod. Phys. 87 (2 May 2015), pp. 347–400. DOI: 10.1103/RevModPhys.87.347. URL: https://link.aps.org/doi/10.1103/RevModPhys.87.347.

[43] Florian Marquardt et al. "Quantum Theory of Cavity-Assisted Sideband Cooling of Mechanical Motion". In: Physical Review Letters 99 (2007), p. 093902. DOI: 10.1103/PhysRevLett.99.093902.

[44] Ali Motazedifard et al. "Force sensing based on coherent quantum noise cancellation in a hybrid optomechanical cavity with squeezed-vacuum injection". In: New Journal of Physics 18.7 (July 2016), p. 073040. DOI: 10.1088/1367-2630/18/7/073040. URL: https://dx.doi.org/10.1088/1367-2630/18/7/073040.

[45] C M Mow-Lowry et al. "Experimental demonstration of a classical analog to quantum noise cancellation for use in gravitational wave detection". In: Physical Review Letters 92.16 (2004), p. 161102. DOI: 10.1103/PhysRevLett.92.161102. URL: https://doi.org/10.1103/PhysRevLett.92.161102.

[46] Yohei Nishino et al. "Quantum backaction evasion with reservoir engineering". In: Physical Review A 112.2 (2025), p. 023512.

[47] Roson Nongthombam, Ambaresh Sahoo, and Amarendra K Sarma. "Ground-state cooling of a mechanical oscillator via a hybrid electro-optomechanical system". In: Physical Review A 104 (2 Aug. 2021), p. 023509. DOI: 10.1103/PhysRevA.104.023509. URL: https://doi.org/10.1103/PhysRevA.104.023509.

[48] V Peano et al. "Intracavity squeezing can enhance quantum-limited optomechanical position detection through deamplification". In: Physical Review Letters 115.24 (2015), p. 243603. DOI: 10.1103/PhysRevLett.115.243603. URL: https://doi.org/10.1103/PhysRevLett.115.243603.

[49] J-M Pirkkalainen et al. "Cavity optomechanics mediated by a quantum two-level system". In: Nature communications 6.1 (2015), p. 6981.

[50] J. P. Reithmaier et al. "Strong coupling in a single quantum dot–semiconductor microcavity system". In: Nature 432.7014 (2004), pp. 197–200. ISSN: 1476-4687. DOI: 10.1038/nature02969. URL: https://doi.org/10.1038/nature02969.

[51] Brittany Richman et al. "Backaction-evading receivers with magnetomechanical and electromechanical sensors". In: Physical Review Research 6.2 (2024), p. 023141.

[52] Alolika Roy and Amarendra K Sarma. "Overcoming the standard quantum limit with an electro-optomechanical hybrid system for enhanced force sensing". In: Physical Review A 111.1 (2025), p. 013509.

[53] Alolika Roy and Amarendra K. Sarma. "Force Sensing Beyond the Standard Quantum Limit in a Hybrid Optomechanical Platform". In: (Dec. 2025). arXiv: 2512.20081 [quant-ph].

[54] Alolika Roy and Amarendra K. Sarma. "Quantum Noise Suppression Beyond the Standard Quantum Limit in a Hybrid Magnonic Optomechanical System". In: (Apr. 2026). arXiv: 2604.16136 [quant-ph].

[55] Bijita Sarma and Amarendra K. Sarma. "Controllable optical bistability in a hybrid optomechanical system". In: J. Opt. Soc. Am. B 33.7 (July 2016), pp. 1335–1340. DOI: 10.1364/JOSAB.33.001335. URL: https://opg.optica.org/josab/abstract.cfm?URI=josab-33-7-1335.

[56] Jakob Schweer et al. "All-optical coherent quantum-noise cancellation in cascaded optomechanical systems". In: Physical Review A 106.3 (2022), p. 033520.

[57] Eyob A Sete and Hichem Eleuch. "Controllable nonlinear effects in an optomechanical resonator containing a quantum well". In: Physical Review A 85.4 (2012), p. 043824. DOI: 10.1103/PhysRevA.85.043824. URL: https://doi.org/10.1103/PhysRevA.85.043824.

[58] S K Singh et al. "Enhanced weak force sensing based on atom-based coherent quantum noise cancellation in a hybrid cavity optomechanical system". In: Frontiers in Physics 11 (2023), p. 1142452. DOI: 10.3389/fphy.2023.1142452.

[59] K Stannigel et al. “Optomechanical quantum information processing with photons and phonons”. In: Physical Review Letters 109.1 (2012), p. 013603. DOI: 10.1103/PhysRevLett.109.013603. URL: https://doi.org/10.1103/PhysRevLett.109.013603.

[60] K Stannigel et al. “Optomechanical transducers for quantum-information processing”. In: Physical Review A 84.4 (2011), p. 042341. DOI: 10.1103/PhysRevA.84.042341. URL: https://doi.org/10.1103/PhysRevA.84.042341.

[61] Kai Stannigel et al. “Optomechanical transducers for long-distance quantum communication”. In: Physical Review Letters 105.22 (2010), p. 220501. DOI: 10.1103/PhysRevLett.105.220501. URL: https://doi.org/10.1103/PhysRevLett.105.220501.

[62] J. D. Teufel et al. “Sideband Cooling of Micromechanical Motion to the Quantum Ground State”. In: Nature 475 (2011), pp. 359–363. DOI: 10.1038/nature10261.

[63] C Troullinou et al. “Squeezed-light enhancement and backaction evasion in a high sensitivity optically pumped magnetometer”. In: Physical Review Letters 127.19 (2021), p. 193601.

[64] Mankei Tsang and Carlton M. Caves. “Coherent Quantum-Noise Cancellation for Optomechanical Sensors”. In: Physical Review Letters 105 (2010), p. 123601. DOI: 10.1103/PhysRevLett.105.123601.

[65] Koji Usami et al. “Optical cavity cooling of mechanical modes of a semiconductor nanomembrane”. In: Nature Physics 8.2 (2012), pp. 168–172.

[66] D F Walls. GJ Milburn, Quantum Optics (Springer, Berlin. 1994.

[67] Doudou Wang et al. “Ultrasensitive displacement measurement with nonlinear optomechanical coupling and squeezed light injection”. In: Journal of the Optical Society of America B 40.3 (2023), pp. 604–611.

[68] Kai Wang et al. “Recent progress on optomagnetic coupling and optical manipulation based on cavity-optomagnonics”. In: Frontiers of Physics 17.4 (2022), p. 42501. DOI: 10.1007/s11467-022-1165-2.

[69] I. Wilson-Rae et al. "Theory of Ground State Cooling of a Mechanical Oscillator Using Dynamical Backaction". In: Physical Review Letters 99 (2007), p. 093901. DOI: 10.1103/PhysRevLett.99.093901.

[70] Maximilian H Wimmer et al. "Coherent cancellation of backaction noise in optomechanical force measurements". In: Physical Review A 89.5 (2014), p. 053836. DOI: 10.1103/PhysRevA.89.053836. URL: https://doi.org/10.1103/PhysRevA.89.053836.

[71] X. Y. Wu et al. "Optimal photon-magnon mode matching in whispering-gallery microdisk resonator systems". In: Optics Express 29.24 (2021), pp. 40061–40073. DOI: 10.1364/OE.440058.

[72] Ze-Liang Xiang et al. "Hybrid quantum circuits: Superconducting circuits interacting with other quantum systems". In: Reviews of Modern Physics 85.2 (2013), pp. 623–653. DOI: 10.1103/RevModPhys.85.623. URL: https://doi.org/10.1103/RevModPhys.85.623.

[73] Surabhi Yadav et al. "Optical bistability and entanglement in two optically coupled cavities under the effect of a nonlinear medium". In: Journal of Modern Optics 70.11 (2023), pp. 731–741.

[74] Nan Zhu et al. "Waveguide cavity optomagnonics for microwave-to-optics conversion". In: Optica 7.10 (2020), pp. 1291–1297. DOI: 10.1364/OPTICA.401474.